UNIVERSITY OF TURIN
DOCTORAL SCHOOL OF SCIENCES AND INNOVATIVE TECHNOLOGIES
DEPARTMENT OF EARTH SCIENCES

PhD Degree in Earth Sciences (XXXIII Cycle)

William Hideki Ito

THERMOELASTIC ANALYSIS DUE TO DAILY VARIATION OF TEMPERATURE IN MARBLE SLABS

Thesis approved in its final version by:

Supervisor

Prof. Dr.	Anna Maria Ferrero	Supervisor	-	UNITO

Co-supervisors:

Dr.	Federico Vagnon	Co-supervisor	-	UNITO
Prof. Dr.	Paulo Ivo Braga de Queiroz	Co-supervisor	-	ITA

Committee members:

Prof. Dr.	Maria Rita Migliazza	Member	-	POLITO
Prof. Dr.	Andrea Spagnoli	Member	-	UNIPR
Prof. Dr.	Eliseu Lucena Neto	Member	-	ITA
Prof. Dr.	Dimas Bertioli Ribeiro	Chair	-	ITA

Academic field: **ICAR/07 Geotechnics**

Turin, Piedmont – Italy
2021

THERMOELASTIC ANALYSIS DUE TO DAILY VARIATION OF TEMPERATURE IN MARBLE SLABS

William Hideki Ito

Thesis Committee Composition:

Prof. Dr.	Anna Maria Ferrero	Supervisor	-	UNITO
Dr.	Federico Vagnon	Co-supervisor	-	UNITO
Prof. Dr.	Paulo Ivo Braga de Queiroz	Co-supervisor	-	ITA
Prof. Dr.	Andrea Spagnoli	Member	-	UNIPR
Prof. Dr.	Maria Rita Migliazza	Member	-	POLITO
Prof. Dr.	Eliseu Lucena Neto	Member	-	ITA
Prof. Dr.	Dimas Bertioli Ribeiro	Chair	-	ITA

UNITO

To my wife and my lovely daughter who faced this amazing journey on my side.

Declaration of originality

I hereby declare that all work presented in this dissertation is my own work, and all else is appropriately referenced.

Declaration of copyright

THIS PAGE INTENTIONALLY LEFT BLANK

Acknowledgments

This dissertation is the result of a cotutelle agreement for double PhD degree between the Università degli studi di Torino (UniTO), in Turin/Italy, and the Instituto Tecnológico de Aeronáutica (ITA), in São Jose dos Campos/Brazil, which unified both fields of the Geotechnical Engineering: an Earth Science department and a Division of Civil Engineering.

The author would like to thank everyone who contributed directly or indirectly to this work, but, in special, to:

- Prof Dr. Marilena Cardu, for referring and forwarding my application to Prof Ferrero;
- Prof Dr. Maria Rita Migliazza for the support with the data used in the papers;
- Dr. Federico Vagnon and Dr. Gessica Umili for the support during all my PhD.

Special thanks for:

- Prof Dr. Anna Maria Ferrero for her trust in my work, all the support during my PhD, friendship, and for providing me the scholarship to financially support this work;
- Prof Dr. Paulo Ivo Braga de Queiroz for his essential support on the mathematical formulation and friendship.

Finally, thanks must be driven to Damiano and Beatriz, friends who shared the office with me providing pleasant talks, and to my wife and my lovely daughter who shared this PhD journey with me and the numerous packing, unpacking, and long flights between Brazil and Italy.

"The most beautiful feeling that someone can experience is the mystery. It is the source of all true art and science. The one to whom this emotion is not stranger, who can no longer pause to wonder and stand wrapped in awe, is as good as dead; his eyes are closed."

ALBERT EINSTEIN

Riassunto

I processi di termodegradazione sono noti come meccanismi chiave responsabili del degrado dei materiali da costruzione utilizzati nell'ambiente esterno. Per affrontare questo problema è stato fatto un grande sforzo sia per sviluppare nuovi materiali, sia per proteggere quelli già esistenti. I materiali lapidei sono un esempio di materiali naturali che soddisfano le esigenze di durabilità e che sono stati ampiamente utilizzati fin dall'antichità. Inoltre, grazie alle loro caratteristiche estetiche uniche e alla bassa emissione di CO2 nella loro catena di sfruttamento, particolarmente importante al giorno d'oggi, questi materiali rivestono tutt'ora una grande importanza nel settore delle costruzioni. Mentre le interazioni chimiche, come l'ossidazione o l'idrolisi, sono processi da tempo ampiamente studiati nelle pietre naturali, l'alterazione fisica dovuta alla variazione giornaliera della temperatura in alcuni tipi di rocce metamorfiche è stata considerata un meccanismo chiave per il loro degrado e incorporato negli standard solo pochi decenni fa. Un fenomeno, noto come *bowing*, causa la perdita di coesione intergranulare della calcite che potrebbe indurre grandi deformazioni delle lastre di marmo e significative perdite di resistenza in intervalli temporali che variano da anni a decenni dopo l'esposizione nell'ambiente esterno. In questa tesi sono state condotte analisi termoelastiche sulle lastre utilizzate nelle facciate ventilate. In primo luogo viene presentato un approccio numerico per valutare l'influenza dei sistemi di ancoraggio sulle condizioni di vincolo delle lastre. Successivamente viene discusso lo sviluppo di sollecitazioni interne dovute all'espansione termica con flusso di calore variabile e stazionario in condizioni di contorno fisse. Infine, viene presentato un modello basato su una soluzione esatta per valutare le sollecitazioni termiche considerando la variazione giornaliera della temperatura sulla facciata del Tribunale di Pescara. I risultati indicano come la maggiore influenza sugli stress indotti sia ascrivibile alla variazione del gradiente termico sulla larghezza della lastra piuttosto che il valore assoluto del gradiente termico tra le superfici a diverse profondità nella lastra. Inoltre, la rapida diminuzione della temperatura sulla superficie esposta di un sistema di rivestimento esterno può di indurre un livello più elevato di sollecitazione a trazione.

Resumo

Intemperismo é considerado um dos principais mecanismos de degradação de materiais utilizados em construção quando estes encontram-se em ambiente externo. Um grande esforço tem sido feito para desenvolver novos materiais e novos procedimentos para proteger aqueles já existentes a fim de se defrontar este desafio. Rochas ornamentais são exemplos de materiais naturais amplamente usados desde a antiguidade que atendem esses requisitos de durabilidade. Além disso, devido às suas características estéticas únicas e a baixa emissão de CO2 em sua cadeia de produção, particularmente importante atualmente, esses materiais ainda mantem grande relevância no mercado de construção. Enquanto alterações químicas, como a oxidação e hidrólise, tem sido amplamente estudadas em rochas ornamentais há muito tempo, degradações físicas devido à variação térmica diária de temperature em alguns tipos de rocha metamórfica tem sido considerado um mecanismo importante de degradação e incorporado em normas internacionais apenas há algumas décadas. Um fenômeno, conhecido como bowing, causa decoesão intergranular da calcita que pode induzir grandes deformações em placas de mármore e perda significativa da resistência após períodos de exposição que variam de anos a décadas. Nesta tese, análises termoelásticas de placas usadas em revestimento de fachada são apresentadas. Inicialmente, um estudo numérico sobre a influência dos sistemas de ancoragem e das condições de contorno é apresentado. Posteriormente, a evolução de tensões internas devido à expansão térmica em fluxos transiente e estacionário são discutidas considerando condições de contorno fixas. Finalmente, um modelo baseado na solução exata para calcular as tensões térmicas considerando a variação diária da temperatura medida na fachada externa do Tribunal de Justiça de Pescara é apresentado. Os resultados indicam uma maior influência da variação do gradiente térmico através da espessura do que do valor absoluto do gradiente de temperatura entre as superfícies nas tensões induzidas por ações térmicas. Ademais, o rebaixamento rápido de temperatura na face exposta de um revestimento externo pode ser responsável por induzir os maiores níveis de tensão de tração na estrutura.

Abstract

Natural weathering is known as one of the key mechanisms responsible to cause degradation in building materials used in the external environment. Great effort has been done to develop new materials and new processes for protecting those already existent in order to face this challenge. Natural stones are an example of natural materials extensively used, since ancient times, that fit the durability need. Moreover, due to their unique aesthetic feature and the low CO2 emission in their exploitation chain, particularly important nowadays, these materials still have great importance in the construction business. While chemical interactions in natural stones, such as oxidation or hydrolyses, have been widely studied for a long time, the physical weathering due to daily variation of temperature in some kinds of metamorphic rocks has been considered as a key mechanism of degradation and incorporated in international standards just a few decades ago. A phenomenon, known as bowing, causes intergranular decohesion of calcite that might induce large warping of marble slabs and significant loss of strength in periods that vary from years to decades after exposition in the external environment. In this dissertation, thermoelastic analyses of slabs used in ventilated façades were explored. Firstly, a numerical approach to evaluate the influence of the anchoring systems and the restraint conditions of the slabs is presented. Afterward, the development of internal stresses due to thermal expansion in the transient and stationary heat flux is discussed for fixed boundary conditions. Finally, a model based on an exact solution to evaluate the thermal stresses considering the daily variation of temperature at the Pescara Justice Court's façade is presented. The outcomes indicate a greater influence of the changing in the thermal gradient through slab width rather than the absolute value of the thermal gradient between the surfaces on the induced stresses due to thermal actions. Furthermore, the rapid decrease of temperature on the exposed surface of an external covering system can be responsible to induce a higher level of tensile stress.

List of Figures

Chapter 2

Chapter 3

Chapter 4

Chapter 5

Chapter 6

Appendix A

List of Tables

Abbreviations and Acronyms

AGA	Adjacent Grain Analysis - a method based on petrographic analysis to enhance the identification of marble susceptible to bowing
BS	British standard
CEN	European committee for standardization
FDT	Finite Displacement Theory
FEM	Finite Element Method
Finlandia City Hall	A building in Helsinki, Finland, covered by Carrara marble in which the slabs in the façade presented one of the largest deformation ever reported
ITA	Instituto Tecnológico de Aeronáutica
MARA	The European research Project: Developing Long-Term Durability of Marble Façades
Sol-air temperature	An equivalent external temperature that would give the same temperature distribution through a wall if all the contributions of the thermal exchanges were considered
TEAM	The European research Project: Testing and Assessment of Marble and Limestone
UNI	Italian standardization committee
UNITO	Università degli studi di Torino

List of Symbols

$(\mathbf{u}, \mathbf{v})$	displacement vectors of a (X,Y) position
(x, y)	coordinates in the current configuration
(X, Y)	coordinates in the reference configuration
a_0, a_1, b_0, b_1, c_0, c_1, d_0, d_1,	coefficients of the polynomial function
a	crack length
A	components of the nonlinear part of Green-Lagrange strain tensor
C	Paris constant
$\mathbb{C}$	constitutive elastic matrix
c	constant
C	cosine function
Ch	hyperbolic cosine function
c_p	specific heat capacity
D	displacement gradient
E	Young elastic modulus
F	deformation gradient
$\boldsymbol{f}^b$	body forces
$\boldsymbol{f}^s$	surface forces
G	matrix of derivative shape function in relation to reference coordinate
H	components of the linear part of Green-Lagrange strain tensor
h_e	convection heat-transfer coefficient for outside surface
h_i	convection heat-transfer coefficient for inside surface
I	identity matrix
j	Jacobian matrix
$\mathbf{K}_{NL}$	nonlinear stiffness matrix

$\mathbf{K}_\sigma$	geometric stiffness matrix
L_0	distance between the supports under the specimen
m	Paris constant
M	constant
n	number of cycles
N	shape function
N	constant
O	constant
P	constant
q	heat flux
S	sine function
Sh	hyperbolic sine function
$\mathbf{S}_{\mathrm{PK2}}$	Second Piola-Kirchhoff stress tensor
t	time
$\mathbf{U}_{\mathrm{R}}$	real displacement
$\mathbf{U}_{\mathrm{v}}$	virtual displacement
W_{ext}	external virtual work
$W_{external,eq}$	equivalent external virtual work
W_{int}	internal virtual work
$W_{internal,eq}$	equivalent internal virtual work
(ξ, η)	local coordinate system
α_{a_i}	thermal expansion coefficienty in ‘a’ direcion;
α_c	thermal expansion coefficienty in ‘c’ direcion;
α_t	thermal diffusivity
Γ	surface of the body in the current configuration
Γ_0	surface of the body in the reference configuration
γ_{ig}	fracture resistance energy for the grain boundaries

γ_{xtal}	fracture surface energy of crystals
$\boldsymbol{\delta}$	directional derivative of . In the direction ..
ΔH	deflection
$\boldsymbol{\varepsilon}$	small (engineering) stress tensor
θ	temperature function
Θ	dimensionless temperature function
κ_I	stress intensity factor
κ_t	thermal conductivity
$\boldsymbol{\Lambda}$	vectorized form of the matrix D
ν	Poisson ratio
Π	Total potential energy
ρ	density
$\boldsymbol{\sigma}$	Cauchy stress tensor
χ	dimensionless position function
Ω	volume of the body in the current configuration
Ω_0	volume of the body in the reference configuration
ω_0	fundamental angular frequency
$\boldsymbol{\epsilon}$	Green-Lagrange strain tensor
$\boldsymbol{\epsilon}_{\mathrm{mec}}$	mechanical part of the Green-Lagrange strain tensor
$\boldsymbol{\epsilon}_{\theta}$	thermal part of the Green-Lagrange strain tensor

Contents

1 Introduction

Ornamental stones are one of the oldest building materials ever used in civilization. Durability against weathering can be cited as a key feature and help us to understand the widespread use of these materials. For hundreds of years these materials have been used in bridges, castles, aqueducts, etc (BENJELLOUN *et al*, 2018; CHEN *et al*, 2021; ORTLOFF, 2018; WILCZEK, 2020 and others), and, nowadays, they still have great importance in engineering, especially as covering systems of internal and external surfaces of buildings. Even facing competition with new artificial materials, created to supply the market requirements for durability or self-cleaning, ornamental stones still maintain high market value due to their unique aesthetic appeals and environmental requirements, such as the low CO_2 emission in their exploitation chain (esteemed requisite nowadays).

Besides the great durability against natural weathering, a pathology known as bowing has caused problems in facades covered by ornamental stones in the last few decades. Bowing is a phenomenon that affects rock materials, particularly in some kinds of calcitic marbles, causing deformation due to decohesion of grains due to physical interaction with the environment. Numerous occurrences have been reported in the literature (TEAM, 2005) and one of the most known cases is the Finlandia City Hall in which bowing affected the marble panels twice at the cost of several million dollars (GRELK *et al*, 2006). This occurrence rose many questions about bowing and it was responsible to foster several research activities on this theme.

Similar to the iconic Finlandia City Hall occurrence, several other problems analogous to that one were reported worldwide. These events and the lack of reliability of some kinds of ornamental stones have caused restrictive rules of the uses for the external environment in new architectural designs in many countries, affecting an important branch of this economical activity. To enhance the knowledge and the uses of local ornamental stones, the European Committee funded some research projects focused on the characterization of this *new* phenomenon.

The major research projects were the Developing long-term durability of marble facades (MARA, 2001) and the Testing and assessment of marbles and limestone (TEAM, 2005). Lack of information about bowing was the starting point; thus, the understanding of this *new* phenomenon was the main objective of these research projects. Several European

universities and institutes composed the research teams to explore different areas, such as field monitoring, laboratory tests as far as quarry exploitation and long-term durability.

The influence of microstructure was found as one of the fundamental properties that were responsible to lead to this degradation. For this reason, the majority of the models proposed by previous authors were focused on the microstructural behavior of calcite grain at the micro-scale. On the other hand, the macro-mechanical effect was not deeply exploited and will be the theme of this dissertation as an attempt to get the full picture and to fill this gap in the literature on bowing.

1.1 Objectives

This dissertation approaches the distribution of stresses induced in thermoelastic problems of ventilated façades used in the external environment. The effect of nonlinearity in the stress-strain relationship is discussed in problems of bowing considering parametric analysis using the finite element method.

An additional formulation was developed to calculate the thermal stresses considering an exact solution and the variation of temperature on both sides of the slab. In this analysis, the analytical formulation is implemented using the experimental tests on the Pescara Justice Court's façade in which the temperatures on both surfaces (internal and external) were measured in loco.

1.2 Contributions

A great number of studies have been conducted on bowing focused on laboratory and in situ tests trying to understand the key mechanisms responsible for leading to this degradation. Just in the TEAM project, a budget of 5 million dollars was available to understand and to prevent bowing on limestone and marble (GRELK *et al*, 2007), so, it was possible to perform numerous tests and field inspections. Many papers were published about bowing, but the great majority of them were driven on laboratory tests (ALENKA; TADEJA; ANA, 2009; GRELK *et al*, 2007; KOCH; SIEGESMUND, 2002; MALAGA; SCHOUENBORG; MARINI; BELLOPEDE, 2009; ROYER-CARFAGNI, 1999a and others). Several of them correspond to numerical analyses trying to correlate the stress-strain relationship and constitutive models to predict them (FERRERO; MIGLIAZZA; SPAGNOLI,

2014; ROYER-CARFAGNI, 1999b; WEISS; SIEGESMUND; FULLER JR, 2003). Among these, it was verified a gap in theoretical thermoelastic approaches considering transient heat flux which seems a niche to be fitted.

Two different approaches are considered. The first one is related to a numerical formulation and comparison between linear and nonlinear models in parametric analysis; the other considers an exact solution to evaluate the thermal stresses induced by daily variation of temperature in a slab. The case of the Pescara Justice Court's façade, in Central Italy, was used to present the results because in situ measures and laboratory tests were available and published by other contributors of the same research group that this dissertation belongs.

The numerical and analytical formulations in this study aim to provide a better understanding of the distribution of thermal stresses in external panels induced by daily variation of temperature. The influence of transient heat flux in bowing might clarify the evaluation of some results of field inspections accomplished by previous authors.

1.3 Organization of the dissertation

a) Chapter 1: *Introduction*

   Introductory thoughts on the natural weathering of building materials are addressed in this section as well as the main objectives discussed in the dissertation. The concepts of physical degradation of bowing and previous research projects are also introduced.

b) Chapter 2: *Bowing – state of art*

   A literature survey on bowing is presented in this chapter. It starts presenting the pathology and the key mechanisms responsible to lead to this degradation. Theoretical models to explain the macro and micromechanical behavior are discussed and the idealization of the internal stress distribution proposed in this dissertation is addressed.

c) Chapter 3: *Numerical approach of thermal stresses in façades*

   Concepts of nonlinear stress-strain measures are presented at the beginning of this section because they will be used in the numerical formulation. Then, the numerical model is described and the discretization via FEM is presented.

d) Chapter 4: *Thermal stresses in façades based on an exact solution*

An exact solution was developed to compute the thermal stresses induced by the variation of temperature measured at both sides of a slab in an external façade.

e) Chapter 5: *Results and discussion*

In this section, the discussion on the numerical and exact solutions is presented. The measures acquired on both sides of a slab at the external façade of the Pescara Justice Court were used as input data.

f) Chapter 6: *Final remarks*

The last part of the dissertation summarizes the outcomes developed during the PhD course. Final remarks and suggestions for future researches are also discussed.

g) *Appendix A*

The theoretical functions, which interpolates the discrete measures of temperature, are presented in Appendix A.

h) *Appendix B*

The list of publications is presented in Appendix B.

2 Bowing – state of art

Abrasion resistance, durability, and thermal comfort are some useful characteristics that help the understanding of the widespread uses of natural stones in civilization. Resistance to degradation processes, especially against natural weathering, is an important attribute desired in building materials and it can be verified in a great part of the natural stones, as proven by numerous historical monuments and buildings spread worldwide. However, in the past decades, bowing has affected some kinds of marble raising questions about their uses in the external environment.

Gambino *et al* (2019) registered the main historical monuments and palaces in Turin, northern Italy, where ornamental stones were used and now symbolize a part of their history and cultural heritage. *Piazza San Carlo* (1637-1642), *Palazzo di Città* (1659-1665), and *Basilica Mauriziana* (1718-1730) can be cited as these places in which Carrara marble was used.

Carrara marble is an example of valued ornamental stone used in architecture that carries this cultural heritage. It became worldwide known due to Michelangelo, the Italian artist who promoted the Carrara marble through some of his masterpieces: *The Pietà*, *Madonna of Bruges*, *David,* and many others. Due to this promotion, Carrara marble was mainly demanded in upscale architecture projects, such as the Finlandia City Hall (Finland), Amoco building (US), Nyköping building (Sweden), Grande Arch de la Défense (France), among others. Nonetheless, due to the problems identified decades ago, there are some restriction rules for the use of marble as an external coating material in many countries.

Marble is a type of metamorphic rock that is the product of the alteration of sedimentary limestone basins due to high temperature and low to moderate pressure. The Carrara marble comes from the Apuan Alps, in Tuscany/IT, and belongs to the Northern Apennines. The Northern Apennines were formed by the collision between Apulia (African plate) and Briançonnais (European plate), known as the Apennine orogeny (CARMIGNANI et al, 2004). According to Maccheri *et al* (2007), there are some commercial varieties of Carrara marble, such as:

- Ordinary marble (*marmo ordinario*) is obviously the most abundant in Carrara basins. It presents a pearl-white to a light grey color almost homogeneous with shaded short veins;

- Veined marble (*marmo venato*) presents milk and pearl-white to a very light grey color. The commercial name is linked with some geological features, the orientation, persistence, spacing, and thickness of veins (*Venatino* or *Venato forte*);
- Cloudy-like marble (*marmo nuvolato*) is a highly heterogeneous rock with grey to light grey color and numerous whitish veins;
- Arabesque-like marble (*marmo arabescato*) is grey-colored with highly irregular veins. The name came from Arabian origin (irregular decoration that recalls arabesque fashion).

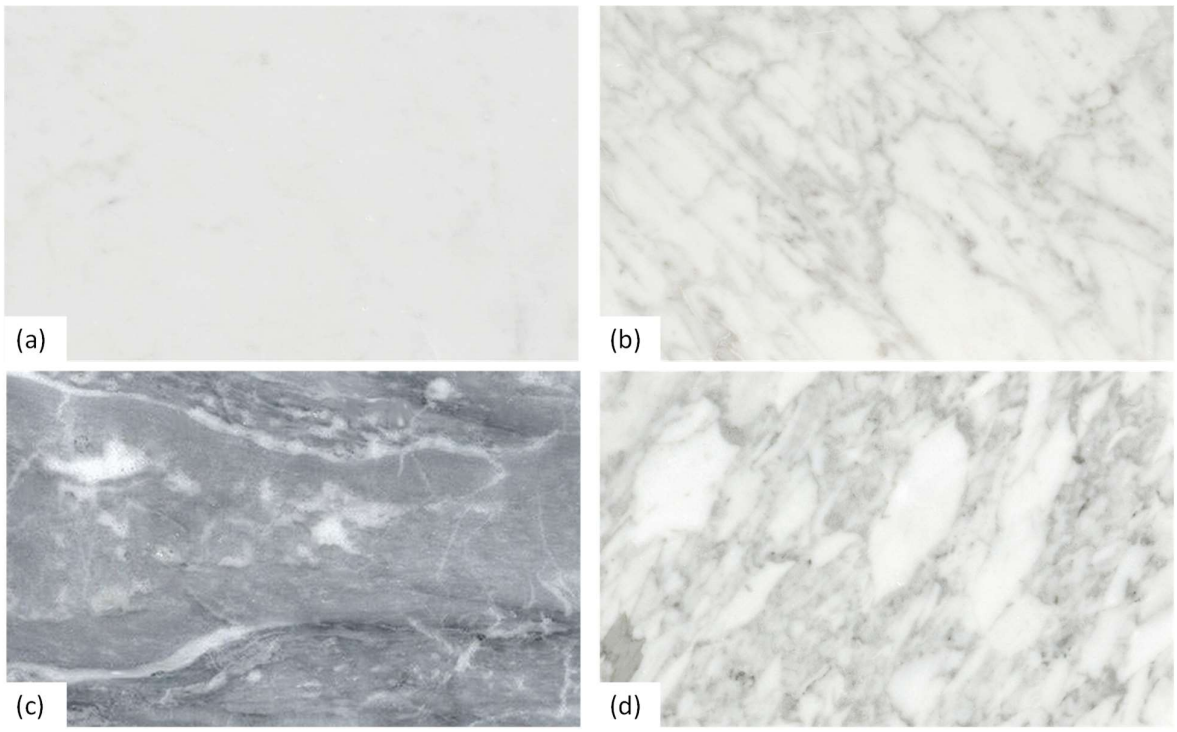

Figure 2.1 – Carrara marbles (MARMI-CARRARA, 2020)

(a) ordinary (b) veined (c) cloudy (d) arabescato

According to Grelk *et al* (2007), evidence of bowing has been reported since the early 20th century in isolated cases affecting different types of ornamental stones. Reported occurrences in limestones are also known, but the great majority of them affected calcitic marbles.

Inspection on building façades accomplished in several countries revealed the occurrence toward concave and convex sides, as indicated in Figure 2.2. One must be aware

that bowing problems were also reported in other types of marble, such as the Hove (Norwegian marble), Verde Viana (Portuguese marble), and many others but the Carrara marble is the most frequent in literature.

Large deformation presented by the bowed slabs in external façades is a key feature that quickly helps the identification of this pathology. Nonetheless, it worthwhile to point out that the effects of decohesion of grains and loss of resistance might not cause so evident deformations such as those indicated in the figures, and, in this case, the degradation can be even harmful because the expansion concentrates loads at the anchorage which is already damaged by the loss of strength. Schouenborg, Grelk, and Malaga (2007) discussed cases in which the free clearance to allow thermal dilatation is too small and the expansion due to bowing causes failure by spalling at the anchorage.

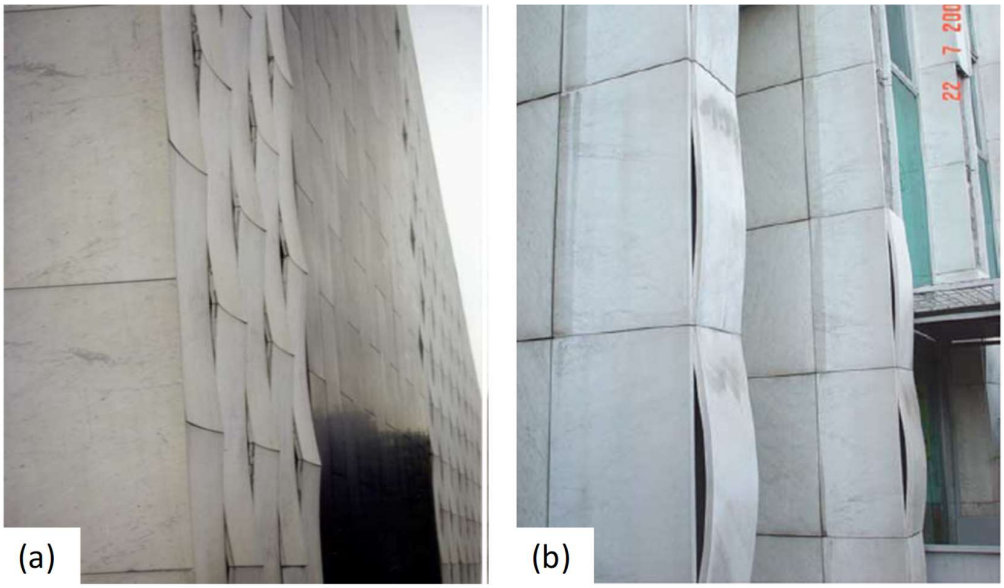

Figure 2.2 - Bowing in marble panels (GELK et al, 2007)

(a) Finland Hall façade in Helsinki (b) Zagrepcanka business tower façade in Zagreb

2.1 Finlandia City Hall

One of the most known cases of bowing occurred at the Finlandia City Hall, built in Helsinki between 1967 to 1972 according to Alvar Aalto's design. Besides the architectural features, the whiteness of Carrara marble was required by the Finnish architect because it would

symbolize a link between the introduction of Mediterranean culture (South Europe) in Finland (MARA, 2001).

In the original project, the panels were fixed at vertical joints by dowels whose largest ones were 140 cm in length and 3 cm in thickness. However, after some years, the deformation of those panels was easily noticed; in 1983, the deflection of bowed panels reached up to 5 cm inward relative to the façade (concave) (GELK *et al*, 2007).

In 1997, a process to restore the original conception started, and the whole façade was completely replaced with Carrara marble in 1999 in order to keep the original guidelines. Design requirements, such as the anchoring system and the dimension of the slabs, were previously reviewed to minimize the problem, such as:

- a requirement of minimum flexural strength (at least 9 MPa) of marble specimens;
- improvement of thermal exchange (insulation and ventilation);
- reduction of the panel sizes by 20% of the original size;
- moving the anchorage system from vertical to horizontal joints.

Nonetheless, just some months after the restoration, the new covering started to bow, but outward (convex). Figure 2.3 presents the *new* façade with the slabs slightly bowed. According to Gelk *et al* (2007), no explanation had been established for this unpredictable behavior by then.

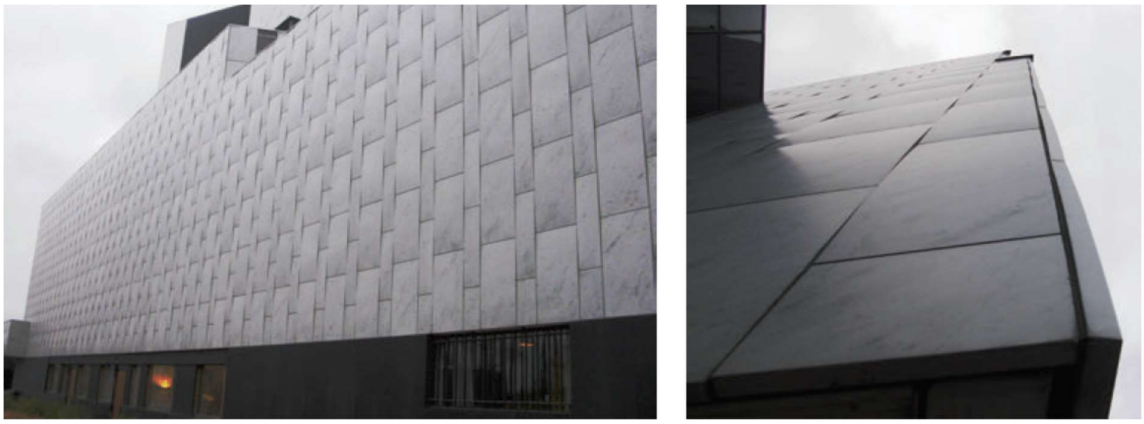

Figure 2.3 – Bowed panels at the *new* Finland Hall's façade (HUDSON and COSGROVE, 2019)

2.2 Key Mechanisms

Several hypotheses were proposed by Garzonio *et al* (1995), Winkler (1996), Erlin (1999), and Siegesmund, Ruedrich, and Koch (2008) to explain bowing in some kinds of calcitic marble. Some of them were corroborated by laboratory tests, but others were not plainly proven. The thermal anisotropy of calcite, the influence of microfabrics, and moisture are some common points widely accepted by experts (ROYER-CARFAGNI, 1999a, 1999b; WEISS; SIEGESMUND; FULLER, 2003; FERRERO; MIGLIAZZA; SPAGNOLI, 2014 and others). On the other hand, dissolution of grain boundaries by acid rain, proposed by Winkler (1996), is a barely consistent guess. Even knowing that chemical attack might induce intergranular decohesion (LIVINGSTON, 2016), it could not explain why specimens bow in laboratory tests using distilled water under heating-cooling cycles. Moreover, assuming the harmful effect of acid rain on marble, it could not be used to enlighten the bowing phenomenon because the chemical attack would cause erosive processes on the marble's surface, since the acid rain should not distinguish between the chemical dissolution of boundaries and granular disintegration, and it is not what occurs in bowing.

The next subsections go into the key mechanisms assumed to be correlated with bowing and which were verified by laboratory tests or in situ measurements whose were mainly accomplished during the MARA and TEAM research projects.

2.2.1 Geological stresses

Given that bowing causes intergranular decohesion, locked-in stresses must be an important factor in this phenomenon because marble is the result of tectono-metamorphic deformations of limestone, as discussed by Hudson and Cosgrove (2019). In fact, when the crystals of calcite are rearranged due to metamorphic processes, the new configuration should be taken as the reference condition and all the further deformation would induce stresses considering this new configuration as the reference.

Following this thought, the exploitation of marble from the quarries would cause stress releases that would induce additional intergranular stresses in these structures. In situ stress measurements at one of the Carrara's quarries, accomplished by the TEAM research group, verified horizontal stresses up to 18 MPa; in Gioia quarry, the high level of stresses were found

even close to the rock surface indicating that some residual locked-in stresses should remain in marble slabs.

2.2.2 Thermal anisotropy

One of the most accepted hypotheses for explaining this degradation in calcitic marble is the anisotropic thermal expansion of grains. Since the Carrara marble is considered a monomineralic metamorphic rock composed mainly of calcite, this anisotropy should have some importance. Excellent rhombohedral cleavage and low to moderate relief are the distinguishing features of this mineral in the microscope (KLEIN; PHILPOTTS, 2016).

Calcite ($CaCO_3$) is classified in the trigonal-hexagonal crystal family, which means that it presents three crystallographic axes ***a*** forming 120° between them and one axis ***c*** perpendicular to this plane, as indicated in Figure 2.4. The extremely anisotropic behavior is caused by the antagonistic thermal expansion coefficients in ***a*** and ***c*** directions. Both heating and cooling cycles could induce intergranular stresses that may lead to this degradation.

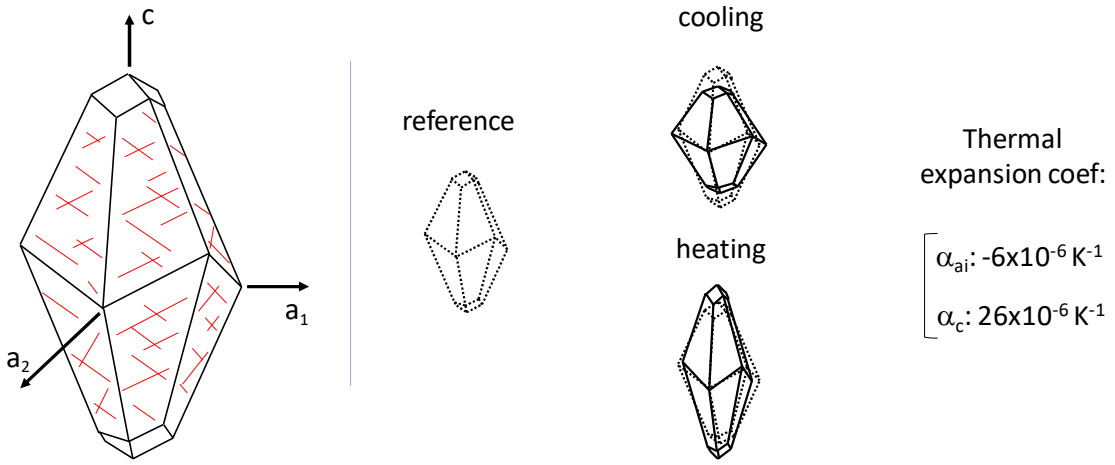

Figure 2.4 - Anisotropy of calcite grain.

The detachment of calcite grains can be identified in a micrograph presented by Royer-Carfagni (1999b), in Figure 2.5, in which the partial decohesion of calcite in a thermally treated marble is presented. Thermally weathered marble, or *marmo cotto*, can also be found in the outcrop of marble bodies, as presented by Bertagnini *et al* (1984).

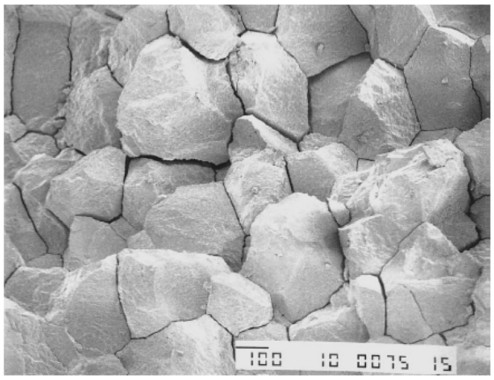

Figure 2.5 – Micrograph in thermal treated marble (ROYER-CARFAGNI, 1999b)

The elastoplastic behavior of marble under cyclic thermal loading was also studied by Koch and Siegesmund (2004). According to the authors, heating-cooling rates of 0.5°C/min were established to equalize the temperature over the specimens and they were in agreement with the values measured on the external building façades. Three cycles were performed using cylindrical specimens and the deformation was continuously measured using a pushrod dilatometer. In the first cycle, the sample was heated up to 60°C, followed by others up to 90°C. It is clear that residual strain is larger at the first cycle, but it still increases for repeated thermal loading, as presented in Figure 2.6. The results could indicate rearrangement of calcite grains after each cycle as responsible for creating internal stresses and intergranular decohesion.

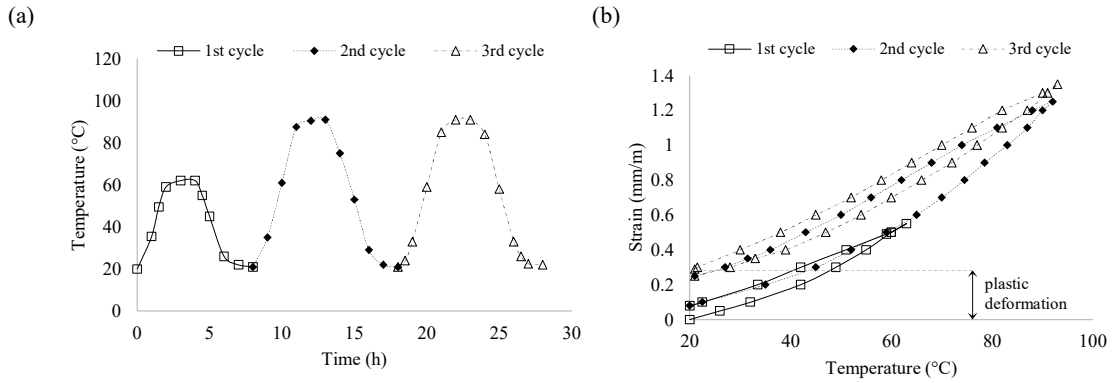

Figure 2.6 – Typical elastoplastic behavior of marble under cyclic loads (modified from KOCH; SIEGESMUND, 2004)

2.2.3 Microstructure/texture of marble

The intriguing problem in which some marble panels presented appropriate long-term durability and others were degraded in a few months/years led researchers to conclude that just the thermal anisotropy of calcite was not sufficient to explain bowing problems. Considering the decohesion of grains due to thermal action an important factor, some questions have arisen about the influence of microstructure on this phenomenon.

Extremally opposite conditions would suggest distinct behavior under thermal treatment, thus, Akesson *et al* (2005) performed tests on marble with different textures to verify the effect of this property on bowing. Laboratory tests were accomplished using a granoblastic texture with straight grain boundaries in which calcite presented regular geometric patterns and almost even size. Diverse textures, xenoblastic interlobate microstructures characterized by different grain size distribution and irregular contours, were also tested. Both microstructures are presented in Figure 2.7.

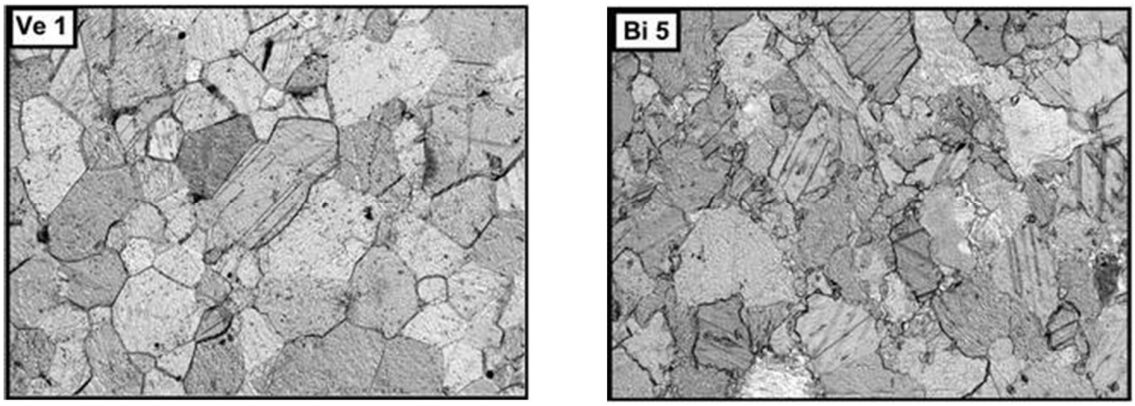

Figure 2.7 – Texture: Ve 1 - granoblastic Bi5 – xenoblastic (AKESSON *et al*, 2005)

According to the authors, granoblastic textures are more likely to bow than xenoblastic ones. However, it was verified that xenoblastic textures were not composed of grains with irregular shapes, but for eudral (well-formed) and subeudral (partially well-formed) grains smaller than the main matrix. Figure 2.8 shows the euhedral and subeuhedral grains identified in the thin section.

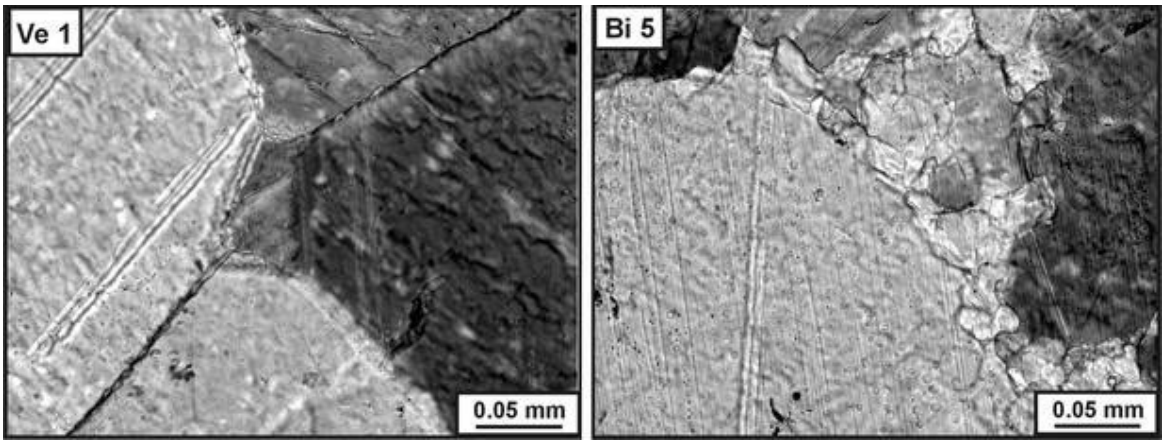

Figure 2.8 – Regular and 'irregular' contours (AKESSON *et al*, 2005)

The results led the authors to propose a new method to verify the bowing trend called Adjacent Grain Analysis (AGA). Considering an ideal granoblastic texture, each calcite grain should be surrounded by six other grains (adjacent grains). The increasing complexity of the texture would also increase the number of adjacent grains, as presented in Figure 2.9. Due to the correlation between bowing and adjacent grains was verified thresholds in which bowing is more likely to occur. For instance, textures in which each grain is surrounded by six other adjacent grains indicate a high trend to bow, while others, in which the number is eight or higher, the probability is reduced.

The efficacy of AGA was confirmed by TEAM (2005) and afterward by Bellopede *et al* (2016). The methodology was adopted in European standards, such as UNI (Italian standard), BS (British Standard), and CEN (European Committee for Standardization), for enhancement of petrographical analysis in thermal and moisture tests required for marble intended for cladding of building façades.

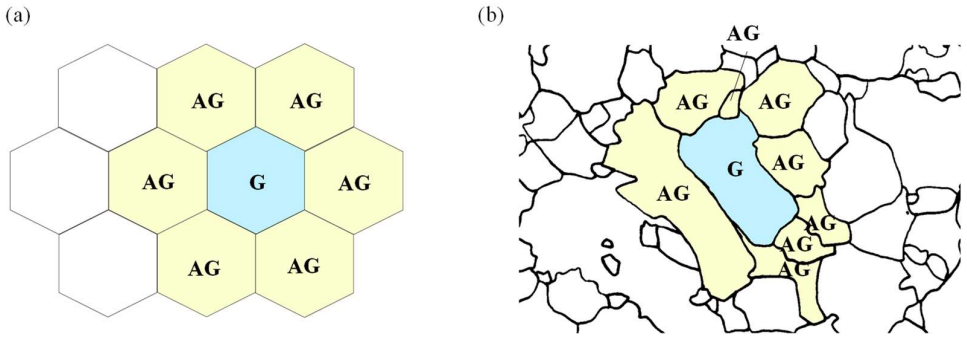

Figure 2.9 – Adjacent grain analysis – AGA (modified from EN 16306)
(a) Idealized granoblastic structure (b) xenoblastic structure

2.2.4 Moisture effect

Koch and Siegesmund (2004) verified the influence of the humidity in bowing tests and its comparison with the dry condition. According to their work, the residual deformation in marble is larger at the beginning but it should reach a plateau after some cycles of thermal loading if only the dry condition is considered. However, in a wet environment, the deformation due to bowing keeps increasing continuously. Partial and total dehydration during the thermal loading could also influence residual strain rate, as indicated in Figure 2.10.

Previous findings were confirmed by Gelk *et al* (2004) for at least 100 cycles of thermal loading in a Norwegian marble. The influence of fabric elements (foliation) was also verified in some rocks, although no great differences were found for Italian marble.

The outcomes of laboratory tests might suggest the interpretation that induced stresses can be higher in a wet environment than in a dry one, nonetheless, until now, no publication has verified this increase of the internal stresses. Impregnation and surface coating as protective barriers against humidity was also tested by the TEAM research group in order to minimize the influence of moisture on the deterioration of stone panels, but accelerated tests have not found a correlation between impregnation of marble panels and degradation of the specimens. The mechanisms that explain the influence of wet environments in bowing are not quite understood by now.

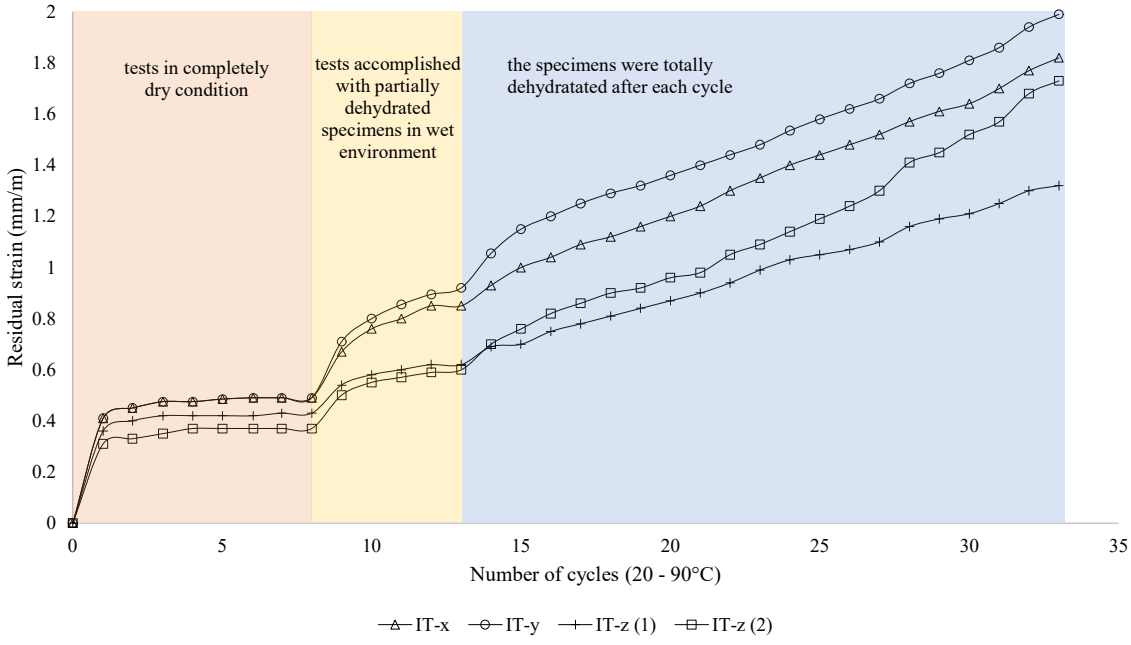

Figure 2.10 – Residual strain due to thermal loading (modified from KOCH; SIEGESMUND, 2004)

2.2.5 Influence of anchorage systems and sunlight exposure

Fixing systems for external façade must be designed as any other structural element supporting dead loads, mainly due to self-weight, and live loads, for instance, wind loads, earthquakes, and thermal actions. Different types of anchors are currently available, such as dowel, kerf, undercut, or other variations of them. BS 8298 and ASTM C1242 present guidelines to support fixing system projects using ornamental stones. These standards clearly state that the fixing system should allow articulation and take into account differential thermal strain. These assumptions are valid for the majority of ornamental stones used in external cladding, but it does not apply to some types of marble due to plastic thermal deformation.

Failure mechanisms are directly linked with forces acting by anchoring systems. According to Camposinhos and Camposinhos (2008), forces acting on the external face should induce spalling in triangular shapes in slabs fixed by dowel anchors. For similar loading conditions, continuous kerf anchors failure at kerf's legs as presented by Camposinhos and Camposinhos (2009). For undercut anchorage, the crack occurs in a conical shape.

TEAM (2005) identified 194 cases of bowing reported in the literature and they have chosen 26 for further investigation. The influence of anchoring systems was also assessed by that research group. Building inspections have shown that marble slabs fixed by mortar presented almost no deflection due to bowing, however, no fixing system could prevent the phenomenon. To verify the influence of fixing systems on bowing, a test simulating real degradation was performed from 2003 to 2005 to check the influence of each of them. Slabs were fixed using different anchorage systems and the wall was kept outdoor in Fishcherwerke, Germany. After two years the slabs fixed by mortar were those in which the bowing deflection was minimum; those slabs fixed by kerf anchors presented greater deflection as compared with dowel anchors.

Evidence of expansion leading to cracking and spalling was verified in many types of fixing systems, however, due to scattered results, no much attention was paid by TEAM (2005). Figure 2.11 presents some damage on slabs due to bowing.

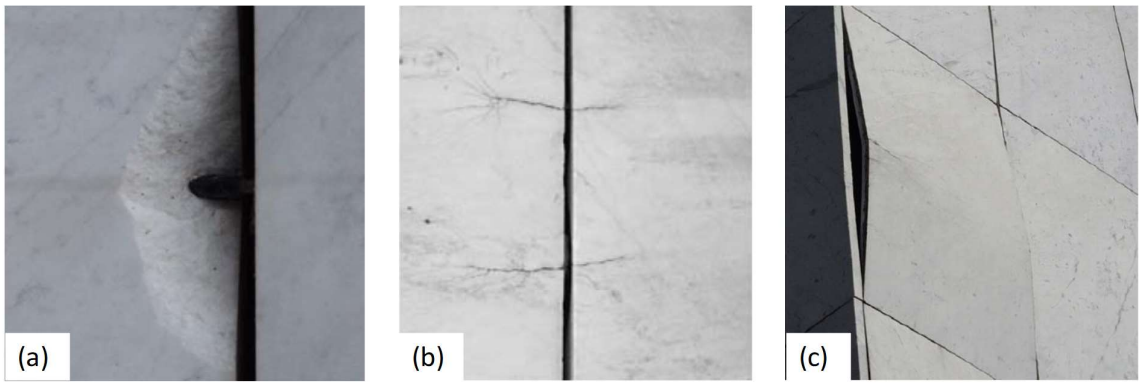

Figure 2.11 – Some damage on bowed slabs (TEAM, 2005)

Field inspections also verified some correlation between the façade orientation with bowing and flexural strength decay. In the northern hemisphere, the smaller deflections were identified in north/south rather than east/west façades due to the lower sunlight exposure and daily thermal amplitude. A similar correlation was verified connecting the height of the panels above the ground and the deflection of weathered panels.

2.3 Porosity and mechanical behavior

The decay of mechanical properties would be an expected outcome considering the weathering processes that affect the microstructure and might produce large deformation as macroscopic behavior. In fact, numerous tests in artificially and naturally weathered marble indicated a correlation between the increase in porosity and the decrease in flexural strength and elastic properties (FERRERO; MARINI, 2001; MARA, 2001; TEAM, 2005; MARINI and BELLOPEDE, 2009; BELLOPEDE; CASTELLETTO; MARINI, 2016, among others).

Bellopede, Castelletto, and Marini (2016) evaluated the differences between artificially and naturally aged marble slabs after ten years of exposure in northern Italy. Good correlation was achieved with artificial thermal degradation, *AG* analysis, and naturally aged marbles. Some types of marbles presented the same decay of mechanical strength as 10 years of naturally aged just after 60 cycles of artificial thermal loading; in others, the correlation was lower than 30, indicating that the artificial thermal treatment accelerates the degradation of natural stones susceptible to thermal degradation. The authors verified that porosity has increased in the exposed surface greater than the inner part which could explain the shape of bowed panels. Figure 2.12 presents the difference between the intergranular voids close to the exposed surface

and at the inner part (the original image has poor resolution, so, no great changes can be made to improve it without changing the original results).

A further study published by Bellopede, Zichella, and Marini (2020) not only corroborates the preceding statement, but additional and intriguing findings are presented. In the last study, the authors present the measures of porosity in three sections: one close to the exposed surface, one close to the hidden surface, and another one at the center of the specimens. A higher increase in porosity of thermally treated marbles occurred at the boundaries (hidden and exposed) while in the inner part the deterioration was lower. Then, it can be assumed that the degradation does not increase continuously from the hidden to the exposed surface, but it has a parabolic-like shape. For GI marble, the porosity at the exposed surface increased almost twice as the one close to the hidden surface, but almost a stable condition was found in the inner part. On the other hand, for CA marble, the porosity at the hidden surface was higher than the one close to the exposed side. Some reservations could be done about the critics by Bellopede, Zichella, and Marini (2020) on the AGA method because the authors state that bowing was not verified in some marble specimens with AGA of six, but they did not present a magnified picture of the subeudral grains and it is not possible to assure the AGA is really six or higher due to small grains formed at the boundaries, such as the one presented in Figure 2.8.

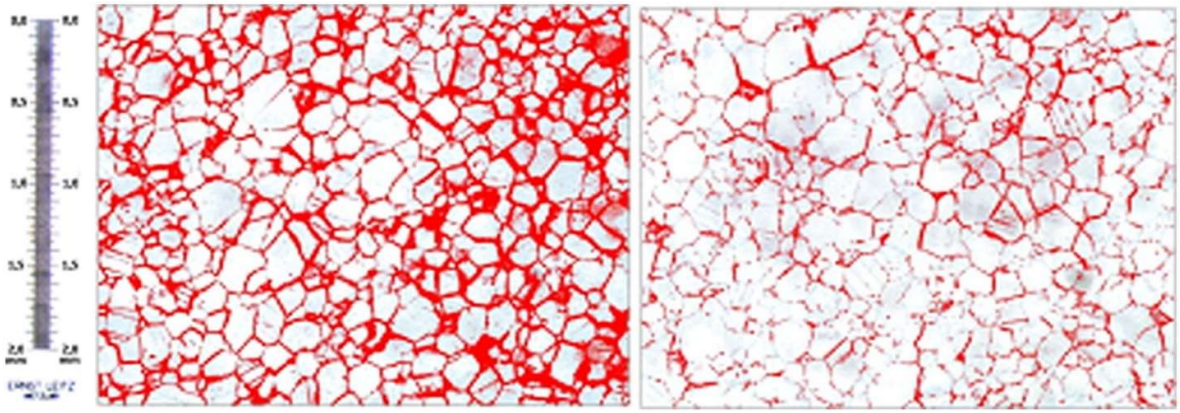

Figure 2.12 – Thin section micrograph: superficial (left) and internal (right) porosity

(BELLOPEDE; CASTELLETTO; MARINI, 2016)

Several studies have proved the correlation between decreasing in Young modulus and strength envelope with thermally treated specimens (MARINI; BELLOPEDE, 2009; RONGA *et al*, 2018; MURRU *et al*, 2018; VAGNON *et al*, 2019; and others). However, many of them

evaluated the mechanical behavior of weathered rocks after one heating-cooling cycle, because they were focused on behavior at high temperatures for oil and gas production or radioactive waste disposal purposes, and cycling thermal loads cannot be assessed.

Mustonen (1993, apud ROYER-CARFAGNI, 1999a) watched the evolution of mechanical decay of marble panels at Finland Hall from the beginning (1971) up to 1990. Almost linear correlation between flexural strength and bowing was verified over 20 years, presented in Figure 2.13. However, it must be clarified that laboratory tests based on mechanical actions cannot simulate the same degradation as the thermal treatment in bowing. For this reason, tensile strength tests, such as the diametral compression or three-point bending tests, are not reliable to simulate intergranular decohesion due to bowing because the cracks initiate at those points in which stresses reach the failure envelope and not at the boundary between grains.

Rodríguez, Arab, and Celestino (2016) and Rodriguez and Celestino (2019) evaluated the fracturing processes in different types of rocks through acoustic emission technique in diametral compression tests. Intact marble specimens with granoblastic texture and euhedral to subhedral calcite grains indicated that microcracking processes start at 75-80% of the peak load and the nucleation processes occurred randomly along the loaded axis at the cleavage planes (intragranular) and grains contour (intergranular), as presented in Figure 2.14. The microcracks distribution indicates some similarities between those zones with a high density of cleavage planes and the grain boundaries, but the physical behavior is different from the one finding in the bowing phenomenon (recall Figure 2.5).

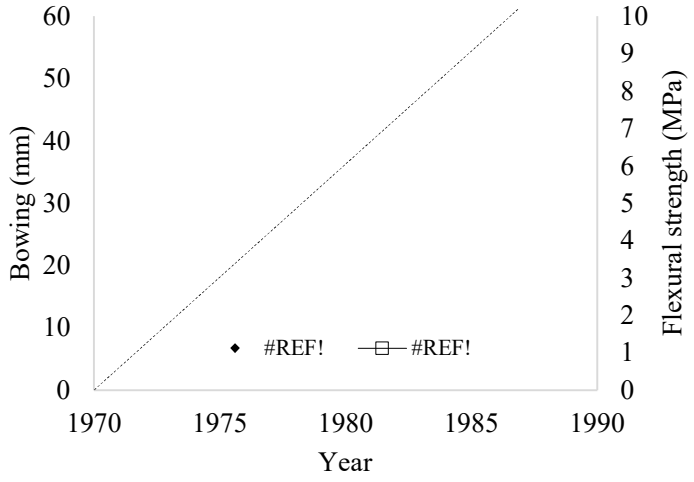

Figure 2.13 – Bowing x flexural strength at Finland Hall (modified from MUSTONEN, 1993 *apud* ROYER-CARFAGNI, 1999a, p. 454)

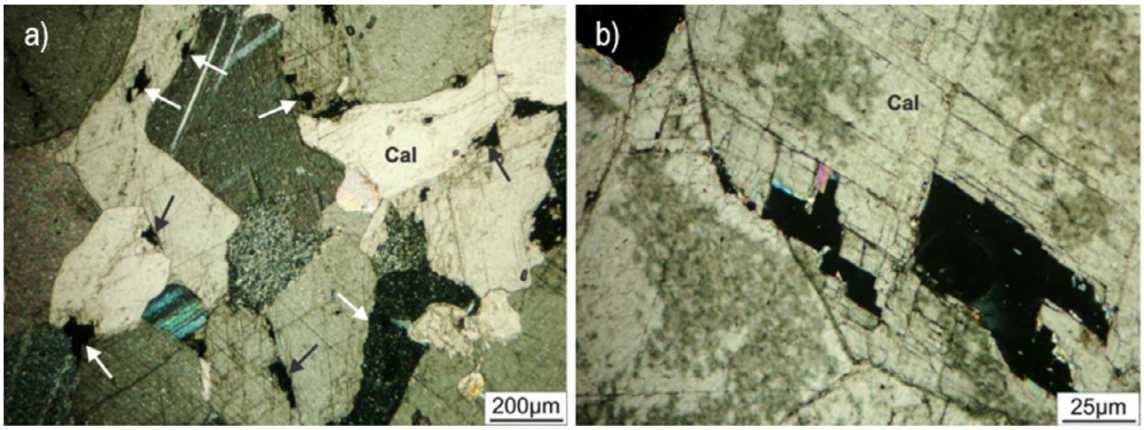

Figure 2.14 – Microcracks in marble specimens (RODRIGUEZ; CELESTINO, 2019)

2.4 Bowing test

A specific laboratory test was developed by the EU-project TEAM to evaluate the possibility of degradation in marble used in the external environment. It was standardized after some simplifications by the European standardization committee in EN 16306:2013 (BELLOPEDE et al, 2016). This test simulates the degradation suffered by marble slabs due to the combined action of cyclic thermal loading and moisture.

In this test at least six dry specimens (400 mm x 100 mm x 30 mm) are exposed to controlled heating from 20°C to 80°C at a maximum rate of 0.35°C/minute. Then, the maximum temperature is kept for one to three hours and the system is turned off to cool down naturally until 20°C. Prior to start the thermal loading, the lower part of specimens (5 mm) must be immersed in distilled water and the level should be kept constant during the cycle. The entire cycle must be repeated fifty times.

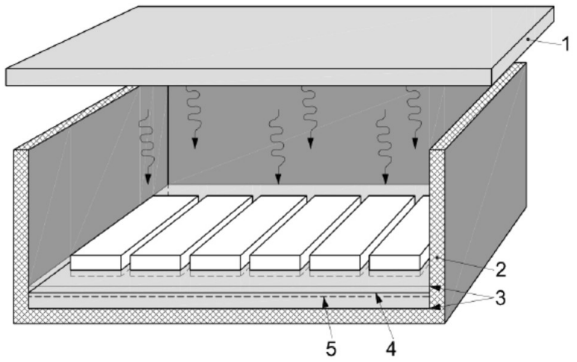

Figure 2.15 – Bowing test (modified from EN 16306)

After each cycle of thermal loading, the bowing magnitude is measured and normalized:

$$bowing\ magnitude = \frac{deflection\ (\Delta H)}{L_0}$$

Bending tests should be performed with thermally treated specimens and compared with others used as a reference. The decrease in flexural strength must also be in the test report. An informative threshold for deflection is presented to provide guidance and the decrease in flexural strength should be used for dimensioning the panels.

2.5 Bowing models

Several authors proposed models to approach the phenomenon in microscale trying to explain the decohesion in calcite grains due to thermal loading, others were focused on the macro mechanical behavior.

2.5.1 Micromechanical behavior

Royer-Carfagni (1999b) evaluated the self-equilibrated stresses due to thermal actions in a plane stresses state model. A chessboard-oriented structure was used to represent the internal stresses due to the orthotropic behavior of calcite under thermal actions. In this formulation, the self-equilibrated stresses induced by thermal actions are concentrated at the grain contours, and, for this reason, they are responsible to produce decohesion between calcite grains instead of inducing and propagate fracture in any other cleavage plane. Figure 2.16 presents the structure and the stresses at the boundaries in this model.

Weiss, Siegesmund, and Fuller Jr (2003) improved Royer-Carfagni's model taking into consideration a real microstructure in which the interaction of 59 grains was evaluated. The numerical model considered 80.000 triangular finite elements and a 'Griffith-like' failure criteria, then, the failure is reached when the strain energy of each element exceeds the surface energy required to propagate the crack. The microcrack patterns induced by thermal loads were directly related to the relationship between the fracture resistance energy of grain boundaries (γ_{ig}) and fracture energy surface of crystals (γ_{xtal}). For a ratio of 0.4 and isostatic restraint condition, cracks are still occurring inside the calcite. If the ratio of 0.1 is considered, almost no crack inside the grains occurs.

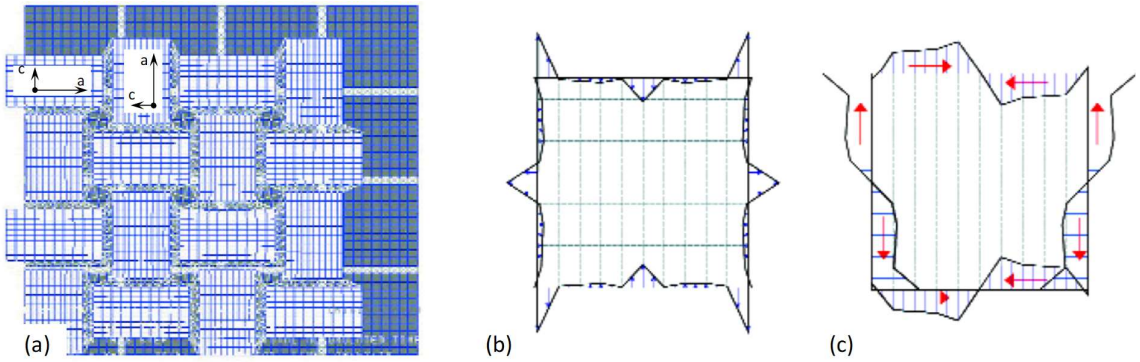

Figure 2.16 – Thermal action on calcite grains ΔT = -60°C (MARA, 2001)

(a) Chessboard-oriented grains (b) normal forces (c) shear forces

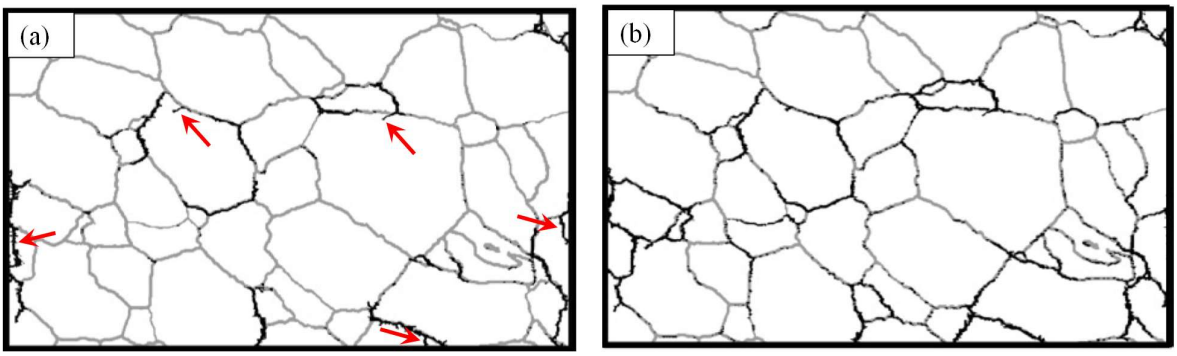

Figure 2.17 – Induced cracks on calcite crystals in FEM analysis:

(a) $\gamma_{ig} = 0.4\gamma_{xtal}$ (b) $\gamma_{ig} = 0.1\gamma_{xtal}$ (modified from WEISS; SIEGESMUND; FULLER JR, 2003)

2.5.2 Macromechanical effect

Ferrero, Migliazza, and Spagnoli (2009) presented a model based on the Euler-Bernoulli beam theory and linear elastic fracture mechanics to represent the deformation of bowed slabs in a Pescara building, in central Italy. The number of cycles required to achieve fixed increments of cracks was calculated according to Paris' law (Eq. 2.1). Increments of κ_I were calculated considering the elastic energy released for the plane stress state. Finally, the deflection of marble slabs could be calculates using Castigliano's theorem considering the deflection as a result of the derivative of strain energy concerning the load (GERE; GOODNO, 2012).

$$\frac{da}{dn} = C(\Delta\kappa_I)^m \longrightarrow \Delta n = \frac{\Delta a}{C(\Delta K_I)^m} \tag{2.1}$$

where

a: crack length

n: number of cycles

C, m: Paris constants

κ_I: stress intensity factor

The authors measured the deflection of bowed slabs at the Pescara building in October 2005 (after 9 years of the covering installation) to use as a reference state. In June 2007 another measurement was accomplished to calibrate the parameters, as indicated in Figure 2.18. A crack density parameter (n) is defined by the authors as a number equivalent to external edge cracks.

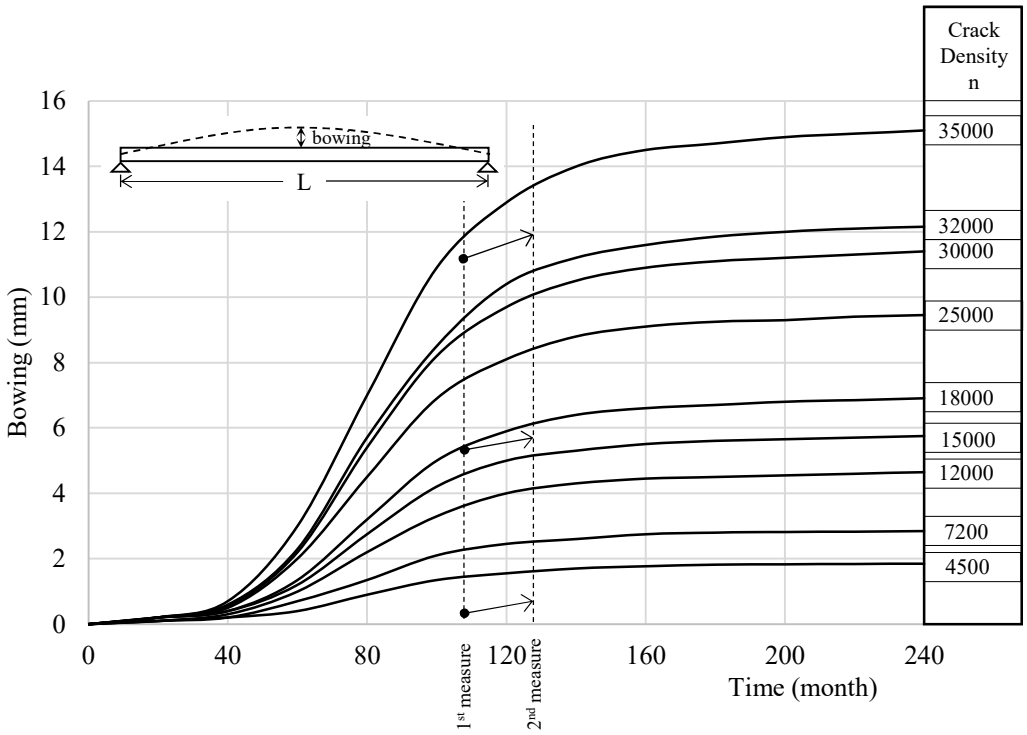

Figure 2.18 – Deflection vs thermal cycles (FERRERO; MIGLIAZZA; SPAGNOLI, 2009)

2.6 Some considerations about the literature on bowing

Open questions still remain on the key mechanisms of this phenomenon. One should consider that the panel restraint conditions could influence the deformation of slabs since the expansion of one slab affects the surrounding components, i.e., the deformation of a slab would be restrained by the deformation of the others around them and additional forces due to geometric nonlinearity could take place. It becomes clear if one recalls Figure 2.2 in which the boundary restraints act at the end of the slabs. In fact, Grelk *et al* (2004) verified this effect in some buildings where the contact stresses have squeezed out filling material between adjacent panels (Figure 2.19). The bowing concavity of each individual slab at Finlandia City Hall toward the same direction could also indicate the contribution of the fixing system as well, as pointed out by Hudson and Cosgrove (2019).

Figure 2.19 – Deformation in panels causing compaction of joint material (GELK et al, 2004)

In the literature about bowing there is no specific study on the influence of the rate of thermal exchanges between the stone panels and environment, however, it should also be considered as an important factor in this phenomenon. Meaningful results were presented by Bellopede and Marini (2016) through a 10-year natural aging test. According to those authors, GI specimen is one of the most likely kinds of marble susceptible to bowing because of the granoblastic texture with straight grain boundaries, AGA of 6.1, and almost even grain size. Therefore, after ten years of exposure, it should be expected deformation at least close to that one presented in real bowed panels after similar conditions (the Finlandia City Hall, e.g.). However, after 10-years, the GI specimen bowed 6 mm/m, far away from the deflection

measured in the marble slabs used in Finlandia City Hall (up to 35 mm/m) after 10 years. From Figure 2.20, it can be inferred that the average temperature rises faster during the spring in Helsinki than in Turin and the average temperature of the Italian city is almost 7°C higher than the one in the Finnish city. The high average relative humidity was a common characteristic in both cities. Then, no other great difference in the weather can be assumed instead of the differences in the instantaneous rate of thermal exchanges.

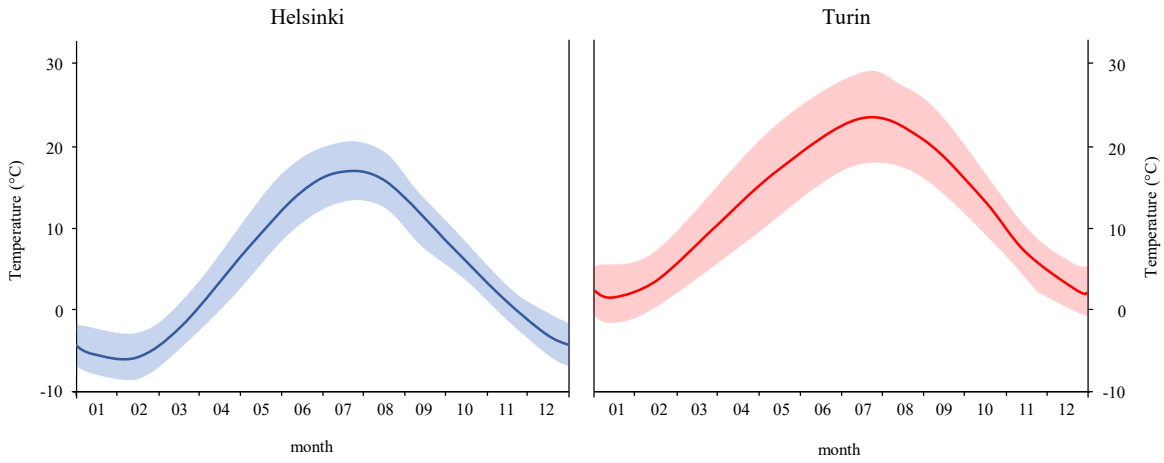

Figure 2.20 – Daily amplitude in Helsinki and Turin (modified from BELLOPEDE; CASTELLETTO; MARINI, 2016)

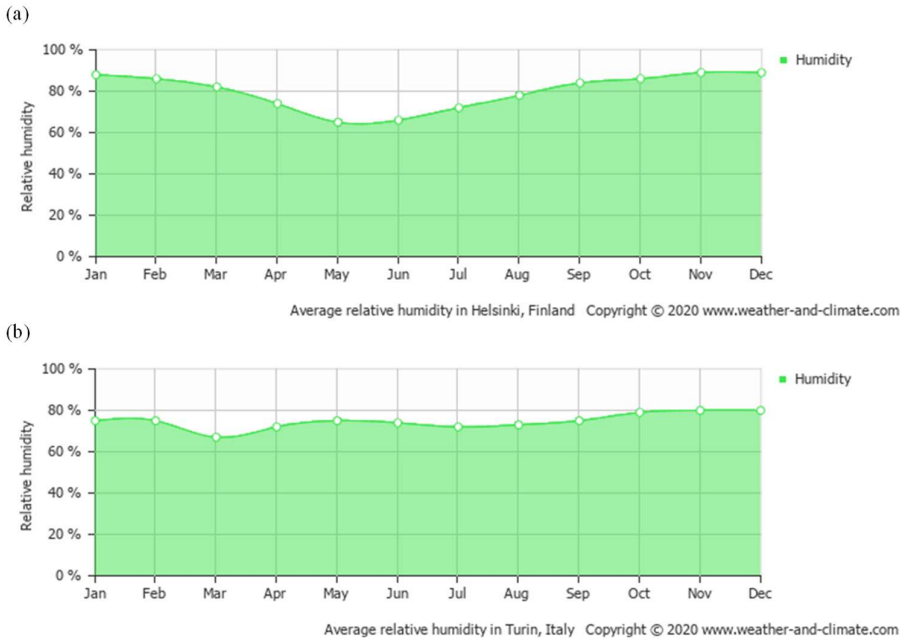

Figure 2.21 – Average relative humidity: (a) Helsinki (b) Turin

(WEATHER AND CLIMATE, 2021)

2.6.1 Assessment of transient problems in thermoelasticity

Previous studies have confirmed the influence of humidity and thermal loading on the decohesion of calcite grains in some kinds of marble, as reported by Grelk *et al* (2004), TEAM (2005), Grelk *et al* (2007), and others. However, there is a lot of unsolved questions about the induced stresses and the influence of humidity on bowing. This dissertation focuses on the theoretical aspects of thermal stresses on this pathology. Therefore, it is proposed to evaluate the stresses induced by thermal expansion/contraction and the influence of transient/stationary heat flux in ventilated stone panels with attention to the macro mechanical behavior since experimental tests and field observation have indicated the influence of the rate of thermal exchanges in this phenomenon. Surely pre-existing internal stresses are important on the thermal degradation of marble, but they will not be considered at this moment.

A variety of ways could be used to approach the problem, and one of them could consider the beam theories to model the phenomenon. Solution via Euler-Bernoulli beam is the most limited one because it assumes perpendicularity between the neutral axis and rigid cross-section, i.e., distortion due to shear stress is neglected in this stress-strain analysis. Linear and third-order approaches considering shear strain were proposed by Timoshenko and Reddy (REDDY, 1997), respectively, and they could have a better representation of the phenomenon. Deformed beams, as proposed by these theories, are presented in Figure 2.22 to illustrate the main differences in their assumptions.

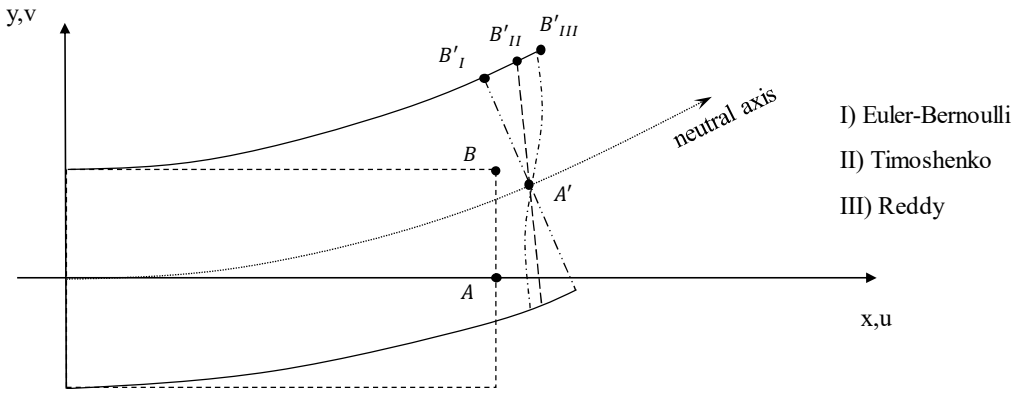

Figure 2.22 – Beam theories: (I) Euler-Bernoulli (II) Timoshenko (III) Reddy

A more sophisticated approach should evaluate the true deformed shape respecting the constitutive matrix in a continuum media and it was the one chosen in this work. Consideration

of the shear stresses along the slab might be an important contribution to the self-equilibrated stresses on the intergranular decohesion, for this reason, the stress-strain analysis will be computed with 2-D solid elements via the finite element analysis. This method should provide a better approach to the differential equations of equilibrium because no simplification is assumed to the deformed configuration. Moreover, the shear stresses developed along thickness can be assessed and quantified. Comparison between finite and small displacement theories are discussed and a novel formulation based on the exact solution is also proposed.

3 Numerical approach of thermal stresses in façades

Besides the economic problem caused by the cost of recladding a damaged façade due to bowing, countless losses might occur as the result of the degradation of monuments and historical heritages that undergo this decay. Degradation of the archaeological site of Hierapolis presented by Vettori et al (2019), trials to protect the byzantine marble sarcophagus discussed by Sassoni et al (2020), and the problems in contemporary architecture assessed by Gherardi et al (2019) and Chiu et al (2020) are a just few examples of reported cases that are related with the thermal degradation of marble. Taking into account the significance of the theme, a rigorous approach to assess thermal stress is proposed in this section.

Nonlinear mechanics theory has once been strictly applied in special problems in engineering, such as aeronautic or mechanical field, due to the high computational effort required in those analyses. Other areas have used the *small strain* approach because it could well represent the great majority of the problems adopting simplified hypotheses. However, the advances in technology have allowed widespread uses of nonlinear models in some areas where the *small strain* was predominant, such as geotechnical and rock engineering, where the assumption of *small deformations*, such as in landslides or underground excavation, might not be respected any more.

The infinitesimal stress-strain relationship assumes small displacements/deformation which could be approximated as infinitesimal without significant numerical errors once the safety and workability requirements of the great part of the ordinary structures in engineering do not allow large deformation. However, some specific cases, such that one experienced by a bowed marble slab, perhaps, should be faced with a more rigorous theory.

In accordance with this trend, it is proposed to evaluate the thermal stresses in stone panels using nonlinear concepts. It is known that daily variation of temperature induces thermal stresses in ventilated structures that are harmful enough to produce intergranular decohesion, even if these stresses are relatively small if they were compared to those in thermal machines, such as turbines or diesel engines. The finite displacement formulation was designed to consider large rotations and large displacements in a continuum media, then, even small displacements/strains can be assessed by that theory. When the deformation is small, the difference between both theories, linear and nonlinear, is minimal.

3.1 Finite displacement method

The finite displacement theory (FDT) is a solution for problems in continuum mechanics that corrects the non-exact assumptions done by small strain theory and even large rotations and/or large strains can be assessed.

In FDT the deformation gradient ($\mathbf{F}$) is used to represent the motion of a body in Lagrangian perspective, i.e., in this formulation, each particle of the body is evaluated as it deforms in time and space. **F** is a second-order tensor that describes the correlation between a current position x of the body with the reference or the undeformed configuration X. In other words, this tensor transforms a vector $d\boldsymbol{X}$ in an undeformed state into a deformed vector $d\boldsymbol{x}$ considering the rotation and stretch of this fiber. In plane strain analysis, as presented in this study, it can be represented by:

$$\mathbf{F} = \begin{bmatrix} \frac{\partial x}{\partial X} & \frac{\partial x}{\partial Y} \\ \frac{\partial y}{\partial X} & \frac{\partial y}{\partial Y} \end{bmatrix} \tag{3.1}$$

where

X, Y: coordinates in the initial configuration;

x, y: coordinates in the current configuration.

Each point in the current position can be expressed in terms of the initial configuration and a displacement vector, then, the tensor **F** can be rewritten as:

$$\mathbf{F} = \begin{bmatrix} \frac{\partial (X + \mathbf{u})}{\partial X} & \frac{\partial (X + \mathbf{u})}{\partial Y} \\ \frac{\partial (Y + \mathbf{v})}{\partial X} & \frac{\partial (Y + \mathbf{v})}{\partial Y} \end{bmatrix} = \text{Identity} + \begin{bmatrix} \frac{\partial \mathbf{u}}{\partial X} & \frac{\partial \mathbf{u}}{\partial Y} \\ \frac{\partial \mathbf{v}}{\partial X} & \frac{\partial \mathbf{v}}{\partial Y} \end{bmatrix} = \mathbf{I} + \mathbf{D} \tag{3.2}$$

where

$\mathbf{u}, \mathbf{v}$: displacement vector of a (X, Y) point

D: displacement gradient

Among all the definitions of strain, it will be used herein that one proposed by Green-Lagrange due to its simplicity in numerical implementation (BONET; WOOD, 2008; DILL,

2006). The Green-Lagrange strain tensor is a symmetric measure of deformation that considers not only the linear terms of deformation but also the quadratic variation of these vectors in the form:

$$\boldsymbol{\epsilon} = 0.5[\mathbf{F}^T\mathbf{F} - \mathbf{I}] \; or \begin{Bmatrix} \epsilon_{XX} \\ \epsilon_{YY} \\ 2\epsilon_{XY} \end{Bmatrix} = \begin{Bmatrix} \dfrac{\partial \mathbf{u}}{\partial X} \\ \dfrac{\partial \mathbf{v}}{\partial Y} \\ \dfrac{\partial \mathbf{u}}{\partial Y} + \dfrac{\partial \mathbf{v}}{\partial X} \end{Bmatrix} + \begin{Bmatrix} \frac{1}{2}\left(\dfrac{\partial \mathbf{u}}{\partial X}\right)^2 + \frac{1}{2}\left(\dfrac{\partial \mathbf{v}}{\partial X}\right)^2 \\ \frac{1}{2}\left(\dfrac{\partial \mathbf{u}}{\partial Y}\right)^2 + \frac{1}{2}\left(\dfrac{\partial \mathbf{v}}{\partial Y}\right)^2 \\ \dfrac{\partial \mathbf{u}}{\partial X}\dfrac{\partial \mathbf{u}}{\partial Y} + \dfrac{\partial \mathbf{v}}{\partial X}\dfrac{\partial \mathbf{v}}{\partial Y} \end{Bmatrix} \tag{3.3}$$

where

$\boldsymbol{\epsilon}$: Green strain tensor presented in matricial and Voigt notation

The energetic conjugate of Green strain is the second Piola-Kirchhoff stress tensor $\mathbf{S}_{PK2}$. This tensor does not have clear physical interpretation just as the Cauchy stress, but it is useful to compute nonlinear deformation and can be described in terms of Cauchy stresses $\boldsymbol{\sigma}$:

$$\mathbf{S}_{\mathrm{PK2}} = |\mathbf{F}|\, \mathbf{F}^{-1}\boldsymbol{\sigma}\, \mathbf{F}^{-\mathrm{T}} \tag{3.4}$$

The advantage of *large strain* over the *small strain* formulation becomes clear when it is written in terms of internal energy per unit volume. In *small strain* the deformed configuration (Ω) is unknown and it must be assumed equal to the initial one. On the other hand, the *large strain* formulation is already related to the initial configuration (i.e., known) and no simplification must be done. Similar reasoning might be applied to the rotation, in which each forward step is related to the previous one, and, in *small* strain, the rotation of the Cauchy stress tensor must be updated after each iteration. The $\mathbf{S}_{\mathrm{PK2}}$ tensor is related to the initial configuration, then, this correction is not necessary.

$$\frac{1}{v}\int_{\Omega} \boldsymbol{\sigma}\, \delta\boldsymbol{\varepsilon}\, d\Omega = \frac{1}{V}\int_{\Omega_0} \mathbf{S}_{\mathrm{PK2}}\, \delta\mathbf{E}_{\mathrm{Green}}\, \mathrm{d}\Omega_0 \tag{3.5}$$

3.1.1 Idealized mechanical behavior of a slab under thermal action

For sake of simplicity, one should consider a coarse discretization of a slab laid on the ground and subject to sunlight exposure on the external face, as illustrated in Figure 3.1. In this example, the deformation will be limited only to y-direction and a uniform increase of temperature inside each element is assumed. According to the classical elastic theory, for a generic material with a positive thermal expansion coefficient, the right-hand side element should present a larger expansion than the other. However, due to compatibility, the displacements of the nodes 3A–3B and 4A–4B must coincide, therefore, shear stresses on this interface would induce compressive stress at the upper element and tensile stresses at the lower. It is clear that the shear stress along the interface must not be constant once it should be zero at the boundary (nodes 3 and 4) and at the symmetry plane. The same concept can be applied to a more refined mesh and other directions.

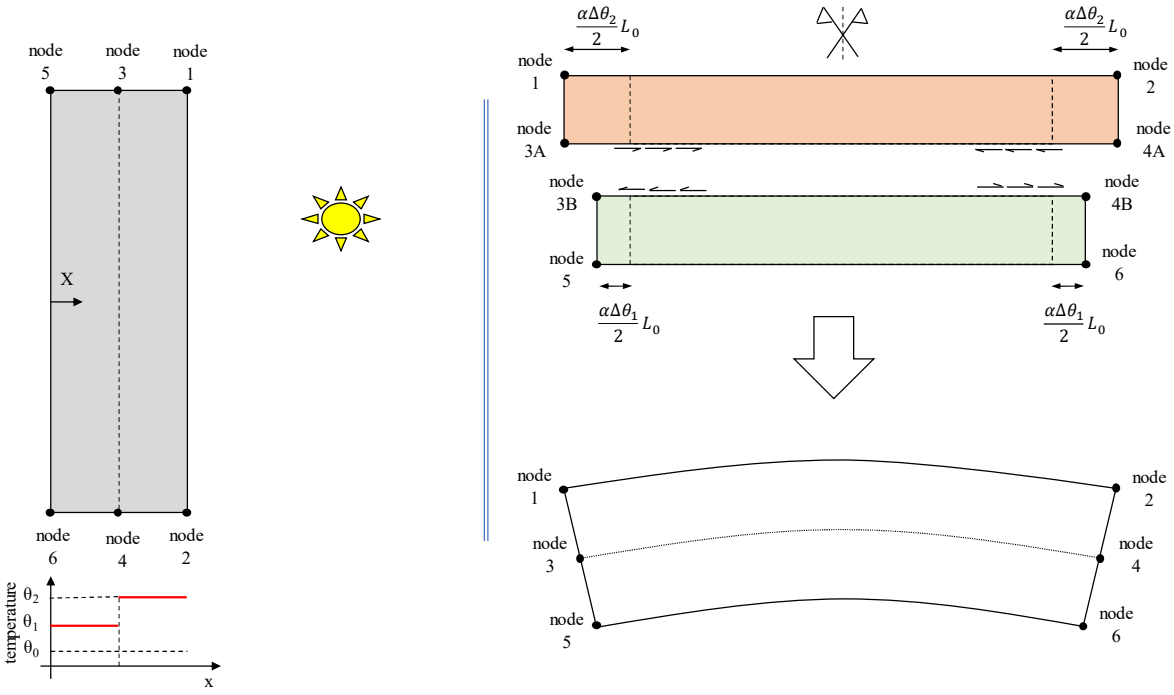

Figure 3.1 - Idealization of the deformation due to thermal loading in continuum media.

3.1.2 Constitutive model

According to the theory of elasticity, no stress should be induced in a continuous homogeneous isotropic material subject to uniform temperature increasing. Nonetheless, a gradient of temperature occurring in the inner part of a body would induce stresses due to differential strains (PRZEMIENIECKI, 1959; KERAMIDAS; TING, 1976; LAURA *et al*, 1978). In such analysis, the total strain could be decomposed into thermal and mechanical strain, in which the last one would be responsible for inducing internal stresses. If one deals with a small value of strain, the additive decomposition of Green-Lagrange strain tensor into elastic and plastic parts can be assumed (GREEN; NAGHDI, 1965; DENG; NEWMAN, 1999; PASCON; CODA, 2013). Since the daily variation of temperature in a ventilated stone panel is considered small, a similar assumption is done between the thermal and the elastic part of strain, and the total strain is given by:

$$\boldsymbol{\epsilon} = \boldsymbol{\epsilon}_{\theta} + \boldsymbol{\epsilon}_{\mathrm{mec}} \tag{3.6}$$

Assuming St. Venant-Kirchhoff nonlinear material, internal stresses in bowing could be calculated via the constitutive stress-strain relationship written in Equation 3.7:

$$\mathbf{S}_{\mathrm{PK2}} = \mathbb{C}\,\boldsymbol{\epsilon}_{\mathrm{mec}} = \mathbb{C}\,(\boldsymbol{\epsilon} - \boldsymbol{\epsilon}_{\theta}) \tag{3.7}$$

where

$$\mathbb{C} = A\begin{pmatrix} 1-\nu' & \nu & 0 \\ \nu' & 1-\nu' & 0 \\ 0 & 0 & \frac{1}{2}-\nu' \end{pmatrix},\quad A = \frac{E'}{(1-2\nu)(1+\nu)},\quad E' = \frac{E}{1-\nu^2},\quad \nu' = \frac{\nu}{1-\nu}$$

In continuum media, the stress-strain relationship could be solved for a displacement field that satisfies the equilibrium, compatibility, and constitutive relationship by the principle of virtual work. The variation of total potential energy can be described as presented in Equation 3.8, and the internal and external works as following in Equations 3.9 and 3.10, respectively.

$$\delta\Pi = \int_{\Omega_0} \delta\boldsymbol{\epsilon}_{\mathrm{v}}{}^{\mathrm{T}}\mathbb{C}\,\boldsymbol{\epsilon}_{mec}\,\mathrm{d}\Omega_0 - \int_{\Omega_0} \delta\mathbf{u}_{\mathrm{v}}^{\mathrm{T}}\,\boldsymbol{f}^{\mathrm{B}}\,\mathrm{d}\Omega_0 - \int_{\Gamma_0} \delta\mathbf{u}_{\mathrm{v}}^{\mathrm{T}}\,\boldsymbol{f}^{\mathrm{S}}\,d\Gamma_0 \tag{3.8}$$

$$\delta W_{\mathrm{int}} = \int_{\Omega_0} \delta\boldsymbol{\epsilon}_{\mathrm{v}}{}^{\mathrm{T}}\mathbb{C}\,\boldsymbol{\epsilon}_{mec}\,\mathrm{d}\Omega_0 \tag{3.9}$$

$$\delta W_{\mathrm{ext}} = \int_{\Omega_0} \delta\mathbf{u}_{\mathrm{v}}^{\mathrm{T}}\,\boldsymbol{f}^{b}\,\mathrm{d}\Omega_0 + \int_{\Gamma_0} \delta\boldsymbol{u}_{v}^{T}\,\boldsymbol{f}^{\mathrm{S}}\,\mathrm{d}\Gamma_0 \tag{3.10}$$

Assuming that only the mechanical part of the strain is responsible to induce stresses, the total strain can be isolated in Equation 3.8 and the solution is achieved using a numerical method. Then, the internal and external works could be expressed in terms of equivalent functions by rearranging the previous equations:

$$W_{internal,eq} = \int_{\Omega_0} \delta\boldsymbol{\epsilon}_{\mathrm{v}}{}^{\mathrm{T}}\mathbb{C}\,\boldsymbol{\epsilon}\,d\Omega_0 \tag{3.11}$$

$$W_{external,eq} = \int_{\Omega_0} \delta\boldsymbol{\epsilon}_{\mathrm{v}}{}^{T}\mathbb{C}\,\boldsymbol{\epsilon}_{\theta}\,\mathrm{d}\Omega_0 + \int_{\Omega_0} \delta u_{v}^{T}\,f^{B}\,\mathrm{d}\Omega_0 + \int_{\Gamma_0} \delta u_{v}^{T}\,f^{S}\,\mathrm{d}\Gamma_0 \tag{3.12}$$

According to the variational calculus, Equation 3.8 is solved for a displacement field in which the total potential energy reaches a stationary condition. Considering the incremental solution via the Newton-Raphson method, the internal work should be linearized and it must be updated in each iteration.

$${}^{t+\Delta t}\boldsymbol{\delta} W_{internal} = {}^{t}\boldsymbol{\delta} W_{internal} + {}^{t+\Delta t}\boldsymbol{\delta}(\boldsymbol{\delta} W_{internal}) \tag{3.13}$$

The linearization of internal virtual work is done using the product rule, as presented in Equation 3.14. The first term is composed of the linear and nonlinear part of the stiffness matrix and the second one is the geometric stiffness matrix associated with force changes due to rigid body rotation (BONET; WOOD, 2008):

$$\boldsymbol{\delta}(\boldsymbol{\delta} W_{internal}) = \int_{\Omega_0} \boldsymbol{\delta} E_v\;\boldsymbol{\delta} S_{2PK}\,\mathrm{d}\Omega_0 + \int_{V} S_{2PK}\;\boldsymbol{\delta}(\boldsymbol{\delta} E_v)\,\mathrm{d}\Omega_0 \tag{3.14}$$

After each iteration, the deviation between internal and external virtual work should reduce. Then, the solution could be approximated by successive iterations until it reaches a tolerable value:

$$ {}^{t}\boldsymbol{\delta}W_{internal} + {}^{t+\Delta t}\boldsymbol{\delta}(\delta W_{internal}) - \boldsymbol{\delta}W_{extenal,eq} = \text{error} \tag{3.15} $$

3.2 Discretization using the Finite Element Method

To solve the differential equation of equilibrium it will be used a discretization based on the well-known Finite Element Method (FEM). In this study was chosen a structured mesh formed by 6-node triangular finite elements, as shown in Figure 3.2.

The structured mesh fits well for this analysis since it is applied in a regular shape problem (rectangular slab) and the anisotropy can be well represented by the mesh. These reasons overcome the computational effort required to create an unstructured mesh.

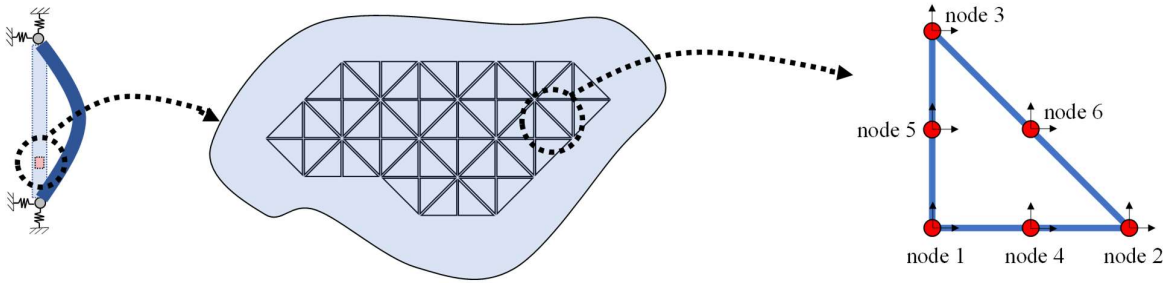

Figure 3.2 – Discretization via FEM

FEM approaches the variation in a continuum media by interpolating the variation of some specific points (nodes) in each element of this media using isoparametric shape functions, as described below.

$$ (X, Y) = \sum_{i=1}^{6} \mathrm{N}_i(\xi, \eta)(X_i, Y_i) \tag{3.16} $$

$$ (\mathbf{u}, \mathbf{v}) = \sum_{i=1}^{6} \mathrm{N}_i(\xi, \eta)(\mathbf{u}_i, \mathbf{v}_i) \tag{3.17} $$

where

(ξ, η): local coordinates;

N_i: shape function in local coordinates;

Local coordinates are used to simplify integration procedures since numerical integration is valid for a specific interval. Gauss-Legendre quadrature was chosen because of its higher efficiency over the Gauss-Lobato. Thus derivative functions with respect to local coordinates must be obtained using the Jacobian matrix J as follow:

$$\begin{bmatrix} \frac{\partial}{\partial \xi} \\ \frac{\partial}{\partial \eta} \end{bmatrix} = \begin{bmatrix} \frac{\partial X}{\partial \xi} & \frac{\partial Y}{\partial \xi} \\ \frac{\partial X}{\partial \eta} & \frac{\partial Y}{\partial \eta} \end{bmatrix} \begin{bmatrix} \frac{\partial}{\partial X} \\ \frac{\partial}{\partial Y} \end{bmatrix} = [J] \begin{bmatrix} \frac{\partial}{\partial X} \\ \frac{\partial}{\partial Y} \end{bmatrix} \tag{3.18}$$

where

j: jacobian matrix

One must recall that the discretization of the displacement gradient is related to reference coordinates, so, it might be represented as a function of the inverse Jacobian matrix J^{-1}:

$$\begin{aligned} \mathbf{\Lambda} &= \begin{bmatrix} J^{-1}(1,1)\frac{\partial N}{\partial \xi} + J^{-1}(1,2)\frac{\partial N}{\partial \eta} & 0 \\ J^{-1}(2,1)\frac{\partial N}{\partial \xi} + J^{-1}(2,2)\frac{\partial N}{\partial \eta} & 0 \\ 0 & J^{-1}(1,1)\frac{\partial N}{\partial \xi} + J^{-1}(1,2)\frac{\partial N}{\partial \eta} \\ 0 & J^{-1}(2,1)\frac{\partial N}{\partial \xi} + J^{-1}(2,2)\frac{\partial N}{\partial \eta} \end{bmatrix} \begin{Bmatrix} \mathbf{u} \\ \mathbf{v} \end{Bmatrix} \\ &= \mathbf{GU} \end{aligned} \tag{3.19}$$

where

$\mathbf{\Lambda}$: vectorized form of matrix $\mathbf{D}$

$\mathbf{G}$: matrix of derivative shape function in relation to reference coordinates

The strain tensor could be calculated as function of these derivative functions represented by the linear and nonlinear parts, as follows:

$$\{\epsilon\} = \left[\begin{bmatrix} 1 & 0 & 0 & 0 \\ 0 & 0 & 0 & 1 \\ 0 & 1 & 1 & 0 \end{bmatrix} + \frac{1}{2}\begin{bmatrix} \frac{\partial \mathbf{u}}{\partial X} & 0 & \frac{\partial \mathbf{v}}{\partial X} & 0 \\ 0 & \frac{\partial \mathbf{u}}{\partial Y} & 0 & \frac{\partial \mathbf{v}}{\partial Y} \\ \frac{\partial \mathbf{u}}{\partial Y} & \frac{\partial \mathbf{u}}{\partial X} & \frac{\partial \mathbf{v}}{\partial Y} & \frac{\partial \mathbf{v}}{\partial X} \end{bmatrix}\right] \begin{Bmatrix} \frac{\partial \mathbf{u}}{\partial X} \\ \frac{\partial \mathbf{u}}{\partial Y} \\ \frac{\partial \mathbf{v}}{\partial X} \\ \frac{\partial \mathbf{v}}{\partial Y} \end{Bmatrix} \tag{3.20}$$

$$= \left[\mathbf{H} + \frac{1}{2}\mathrm{A}(\Lambda)\right]\{\Lambda\}$$

where

$\mathbf{H}\{\Lambda\}$: linear part of Green-Lagrange strain tensor

$\mathrm{A}(\boldsymbol{\Lambda})\{\Lambda\}$: nonlinear part of Green-Lagrange strain tensor

As demonstrated by de Borst et al (2012), an infinitesimal variation in strain tensor is represented as:

$$\boldsymbol{\delta\epsilon} = [\mathbf{H} + \mathrm{A}(\boldsymbol{\Lambda})]\,\boldsymbol{\delta\Lambda} \tag{3.21}$$

3.2.1 Tangent stiffness matrix

For discretization of tangent stiffness matrix, one must recall that directional derivative of $\mathbf{F}$ in $\mathbf{U}_v$ direction can be represented as:

$$\lim_{\mathbf{U}_v \to 0}\left(\frac{\mathbf{F}(x + \mathbf{U}_v) - \mathbf{F}(x) - \boldsymbol{\nabla}\mathbf{F}(x)\cdot\mathbf{U}_v}{\|\mathbf{U}_v\|}\right) = 0 \tag{3.22}$$

or

$$\boldsymbol{\delta}\mathbf{F}_{\mathrm{v}} = \boldsymbol{\delta}\mathbf{D}_{\mathrm{v}} \tag{3.23}$$

where

$\boldsymbol{\nabla}\mathbf{F}(\boldsymbol{x})\cdot\mathbf{U}_{\mathrm{v}}$ *or* $\delta\mathbf{F}_{\mathrm{v}}$: directional derivative of $\mathbf{F}$ in $\mathbf{U}_{\mathrm{v}}$ (a virtual displacement)

$\delta\mathbf{D}_v$: infinitesimal variation in the displacement gradient

Recalling that internal energy is described as a function of infinitesimal increment in virtual strain in an arbitrary direction, it is represented by:

$$\delta\boldsymbol{\epsilon}_v = 0.5(\boldsymbol{\delta}\mathbf{F}_v^T\,\mathbf{F} + \mathbf{F}^T\boldsymbol{\delta}\mathbf{F}_v) \tag{3.24}$$

Now, the solution by Newton-Raphson is approached considering infinitesimal increments related to the real displacement. Since the virtual displacement is arbitrary, it might be considered constant in the directional derivative of an infinitesimal variation in virtual strain tensor in $\vec{u}_r$ direction:

$$\delta(\delta\boldsymbol{\epsilon}_v) = 0.5(\boldsymbol{\delta}\mathbf{F}_v^T\,\boldsymbol{\delta}\mathbf{F}_r + \boldsymbol{\delta}\mathbf{F}_r^T\boldsymbol{\delta}\mathbf{F}_v) \tag{3.25}$$

Then, the tangent stiffness matrix is obtained by linearization of internal virtual work using the product rule. The discretized form of Eq 3.11 is described in Eq 3.26 in which both nonlinear and geometric stiffness matrix are presented:

$$\begin{aligned}\delta U_v^T\,(\mathbf{K}_{NL} + \mathbf{K}_\sigma)\,\delta U_r \\ = \delta U_v\Bigg(\int_V \left[\left(\mathbf{H} + \frac{1}{2}\mathrm{A}(\boldsymbol{\Lambda})\right)\mathbf{G}\right]^T \mathbb{C}\left(\mathbf{H}\right. \\ \left. + \frac{1}{2}\mathrm{A}(\boldsymbol{\Lambda})\right)\mathbf{G}\,dV + \mathbf{G}\mathbf{S}_{PK2}\mathbf{G}\Bigg)\delta U_r\end{aligned} \tag{3.26}$$

3.2.2 Thermal component

3.2.2.1 Temperature function

Since the variation of equivalent external work is a function of temperature it was necessary to calculate the temperature field through Fourier's law. It was considered heat flow in 1-D direction with fixed boundary conditions (Equation 3.27):

$$\frac{\partial \theta}{\partial t} = \alpha \frac{\partial^2 \theta}{\partial x^2} \tag{3.27}$$

Dimensionless functions were assumed as a solution to the previous equation, then, the dimensionless Fourier's law could be written as presented in Equation 3.29:

$$\Theta = \frac{\theta(x,t)}{\theta_0}\ , \quad \chi = \frac{\boldsymbol{x}}{\boldsymbol{X}_0} \quad and \quad \mathrm{T} = \frac{\alpha\, t}{{\boldsymbol{X}_0}^2} \tag{3.28}$$

$$\frac{\partial \Theta}{\partial \mathrm{T}} = \frac{\partial^2 \Theta}{\partial \chi^2} \tag{3.29}$$

Using the concept of separation of variables and assuming that each function will individually satisfy the boundary condition, it is possible to rewrite a multivariable function as a sum of the product of these functions. Then, the dimensionless temperature function could be rewritten as:

$$\Theta(\mathrm{T},\chi) = \sum c_i T_i(\mathrm{T}) \chi_i(\chi) \tag{3.30}$$

Substituting Equation 3.30 into Equation 3.29 one gets that each equation is related as:

$$\dot{\mathrm{T}}_i\, \chi_i = \mathrm{T}_i\, \ddot{\chi}_i \tag{3.31}$$

Previous equality could be represented by a constant value as given in Equation 3.32 just rearranging Equation 3.31 since dimensionless time function is not related with dimensionless position function and vice-versa:

$$\frac{\dot{\mathrm{T}}_i}{\mathrm{T}_i} = \frac{\ddot{\chi}_i}{\chi_i} = -M_i^2 \tag{3.32}$$

Equations 3.33 and 3.34 can be assumed as solutions that satisfy Equation 3.32:

$$\mathrm{T}_i = C_i e^{-\mathrm{M}_i^2 \mathrm{T}} \tag{3.33}$$

$$\chi_i = A_i \cos(M_i \chi) + B_i \sin(M_i \chi) \tag{3.34}$$

Substituting Equations 3.33 and 3.34 into Equation 3.30 and applying the boundary restraint conditions for a nontrivial solution one can find the first unknown coefficient:

$$\Theta(T,\chi) = \sum e^{-M_i^2 T}[A'_i \cos(M_i\chi) + B'_i \sin(M_i\chi)] \tag{3.35}$$

$$\Theta(T=0,\chi=0) = 0 \rightarrow A'_i = 0 \tag{3.36}$$

$$\sin(M_i \cdot 1) = 0 \rightarrow M_i = n \cdot \pi \tag{3.37}$$

The other coefficient can be calculated considering the boundary conditions at the initial configuration:

$$\Theta(T=0,\chi) = \sum B'_i \sin(M_i\chi) \tag{3.38}$$

$$\begin{aligned}\int_0^1 \Theta(T=0,\chi)\sin(M_j\chi)d\chi &= B'_i \int_0^1 \sin(M_i\chi)\sin(M_j\chi)d\chi \\ &= B'_i \frac{X_0}{2}\end{aligned} \tag{3.39}$$

$$B'_i = \frac{2}{X_0}\int_0^1 \Theta(T=0,\chi)\sin(M_j\chi)\,d\chi \tag{3.40}$$

To determine the coefficient B'_i, the solution of the conduction problem is posed as the sum of a stationary solution θ_s and a transient solution θ_t:

$$\theta(X,T) = \theta_s(X) + \theta_t(Z,T) \tag{3.41}$$

Assuming the initial condition:

$$\theta(X,T=0) = \theta_0 \tag{3.42}$$

and the stationary solution:

$$\theta_s(X) = \theta_0 + \theta_1 Z \tag{3.43}$$

Then, the transient solution at $T = 0$:

$$\theta_t(X, T=0) = \theta(X, T=0) - \theta_s(X) \tag{3.44}$$

$$= -\theta_1 X \tag{3.45}$$

The dimensionless transient function is given by:

$$\Theta_t(X, T=0) = -X \tag{3.46}$$

Similarly as given in Equations 3.35 – 3.37,

$$\Theta_t(T=0, \chi) = \sum B_i \sin(M_i X) \tag{3.47}$$

$$M_i = n \cdot \pi \tag{3.48}$$

the integral of series expansion at $T = 0$ is written as:

$$\int_0^1 \sin(M_j X)\ \Theta_t(X, T=0)\, dX$$

$$= \int_0^1 \sin(M_j X) \sum_{i=1}^{\infty} B'_i \sin(M_i X)\, e^{(-M_i T)}\Big|_{T=0} dX \tag{3.49}$$

that is,

$$-\int_0^1 \sin(M_j X)\, X\, dX = \sum_{i=1}^{\infty} B_i \int_0^1 \sin(M_j X) \sin(M_i X)\, dX \tag{3.50}$$

The left-hand side of the equation is calculated via integration by parts:

$$\int_0^1 \sin(M_j X)\, X\, dX = -\frac{\cos(M_j X)}{M_j} X\Big|_0^1 - \int_0^1 -\frac{\cos(M_j X)}{M_j}\, dX$$

$$= -\frac{\cos(M_j X)}{M_j} X + -\frac{\sin(M_j X)}{M_j^2} X\Big|_0^1$$

$$= \frac{(-1)^{i+1}}{M_j} \tag{3.51}$$

The right hand side is calculated by the trigonometric formula for arc sum:

$$\int_0^1 \sin(M_j X)\sin(M_i X)\,dX =$$

$$\frac{1}{2}\int_0^1 \cos\left[\left(M_j - M_i\right)X\right] - \cos\left[\left(M_j + M_i\right)X\right]\,dX \tag{3.52}$$

For $M_j \neq M_i$, one has:

$$\int_0^1 \sin(M_j X)\sin(M_i X)\,dX =$$

$$\frac{1}{2}\left\{\frac{\sin\left[\left(M_j - M_i\right)X\right]}{M_j - M_i} - \frac{\sin\left[\left(M_j + M_i\right)X\right]}{M_j + M_i}\right\}_0^1 = 0 \tag{3.53}$$

For $M_j = M_i$, one has:

$$\int_0^1 \sin^2(M_i X)\,dX = \int_0^1 \frac{1}{2}[1 - \cos(2M_i X)]\,dX$$

$$= \frac{1}{2}\left[X - \frac{\sin(2M_i X)}{2M_i}\right]\Bigg|_0^1$$

$$= \frac{1}{2} \tag{3.54}$$

So, one has

$$-\frac{(-1)^{i+1}}{M_j} = \frac{B_i}{2} \rightarrow B_i = \frac{2(-1)^i}{M_i} = \frac{2(-1)^i}{\pi\, i} \tag{3.55}$$

3.2.2.2 Thermal strain

The temperature is calculated in each integration point just by recalling the Equation 3.28. Considering known the temperature distribution at each time t, the deformation gradient due to thermal expansion could be calculated as:

$$\mathbf{F}_\theta = \alpha \cdot \Delta\theta \cdot \mathbf{I} + \mathbf{I} \tag{3.56}$$

In this work the slabs in external facades are considered isostatic structures, then, no contributions of external forces will take place. Accordingly, the equivalent external work can be represented as a function only of the thermal actions:

$$\delta W_{external,eq} = \int \delta\epsilon_{IJ} S(\theta)_{IJ}\, d\Omega_0 \tag{3.57}$$

4 Thermal stresses in façades based on an exact solution

Temporal and spatial variation of temperature in a ventilated structure is associated with meteorological conditions, such as sunlight exposure or the influence of wind and rainfall. At a first glance, it could be considered a random or unpredictable phenomenon. However, the variation of temperature in these structures tends to be almost periodic whether on a large or small scale, i.e., the variation of the average temperature of these structures in a year or its instantaneous variation in a day can be represented by periodic functions. Considering the cycle of 24 hours, the temperature in these structures rises due to sunlight exposure, it reaches a peak, and then it cools down at the sunset or when wind gusts or rain occur.

Several studies measured this oscillation to approach the thermal comfort problem in the building environment and the almost periodic behavior was verified (LI; WEI; LI, 2019; NABONI *et al*, 2020; STAZI *et al*, 2020 and others). For this reason, the variation of temperature in the ventilated facade is represented herein by periodic functions.

The analytical solution proposed in this work was developed from the law of heat conduction, also known as the heat equation, represented by:

$$\frac{\partial \mathrm{T}}{\partial t} = \alpha_t \frac{\partial^2 \mathrm{T}}{\partial x^2} \tag{4.1}$$

where

$$\alpha_t = \frac{\kappa_t}{\rho c_p} \tag{4.2}$$

stands for the thermal diffusivity.

Even considering that the theoretical distribution of temperature is periodic, the real one is not exactly periodic. The temperature measured in two consecutive days at the same time rarely overlaps which means that there is a gap between these two temperatures at the beginning of each cycle. For instance, in Figure 4.1 it is presented the temperature on the external surface

at the Pescara Justice Court's façade in which the gap between the temperature at 0:00h on August 10th and at 0:00h on August 11th is indicated.

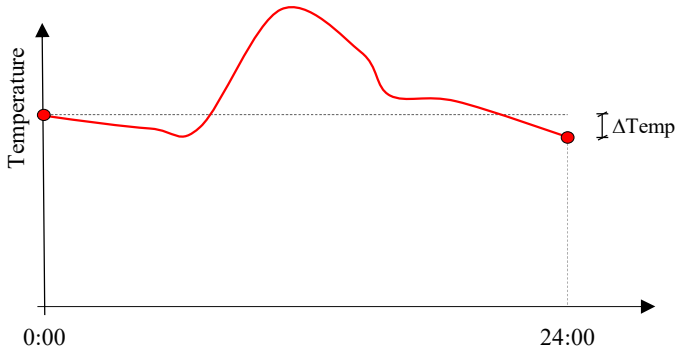

Figure 4.1 – Variation of temperature on August 10th 2007 (ROLLI and ANGELINI, 2007)

Fourier series allows us to model any function as the sum of trigonometric series. In discontinuous functions, however, there are overestimated values close to the jump discontinuity, known as the Gibbs's phenomenon (ARFKEN; WEBER; HARRIS, 2012), and the direct approach of discontinuous problems using Fourier series would induce errors if one calculates the thermal stresses and temperature without any correction. To overcome the Gibbs' phenomenon, it was proposed to split the solution into two parts: a periodic and a polynomial one. Consequently, the temperature distribution inside a slab would be the sum of these two functions, and the Fourier series could be applied to the periodic solution avoiding the Gibbs' phenomenon mentioned previously. An example of this decomposition was applied to the measured temperature values on August 10th, as presented in Figure 4.2.

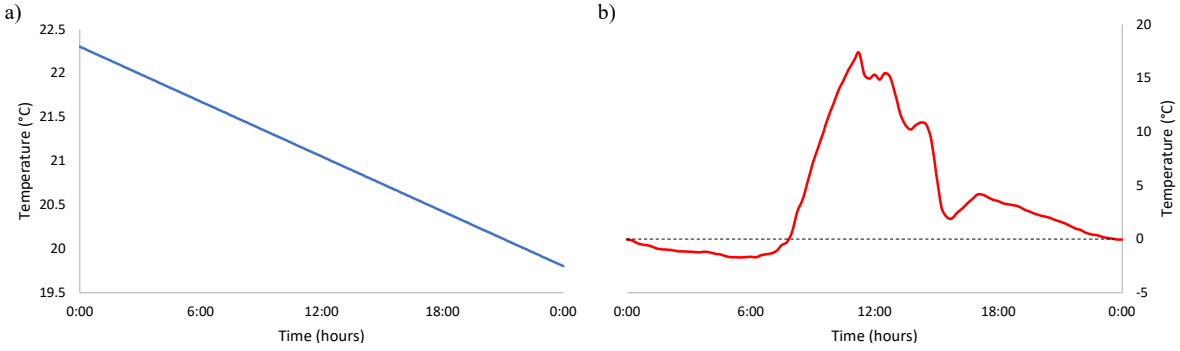

Figure 4.2 – Polynomial and periodic solutions

For convenience, it is defined beforehand four contractions of the trigonometric and hyperbolic functions that are used in the analytical solution:

$$\mathrm{ChC_n}(x) = \cosh(\varpi_n x)\cos(\varpi_n x) \tag{4.3}$$

$$\mathrm{ChS_n}(x) = \cosh(\varpi_n x)\sin(\varpi_n x) \tag{4.4}$$

$$\mathrm{ShC_n}(x) = \sinh(\varpi_n x)\cos(\varpi_n x) \tag{4.5}$$

$$\mathrm{ShS_n}(x) = \sinh(\varpi_n x)\sin(\varpi_n x) \tag{4.6}$$

$$\varpi_n = \sqrt{\frac{\omega_n}{2\alpha_t}} \tag{4.7}$$

and ω_0 stands for the fundamental angular frequency

$$\omega_n = n \cdot \omega_0 = \frac{2\pi \cdot n}{T} \tag{4.8}$$

4.1 Heat flux formulation in ventilated facades

The heat exchange between the surrounding air and the slab is calculated assuming Newton's law of cooling through the convective heat transfer coefficient. In the present formulation, the surrounding equivalent temperature ($T_{int,\infty}$ and $T_{ext,\infty}$) are assumed as the equivalent temperature necessary to induce the same heat flux of that one considering all the thermal exchanges between the slab and the environment in a similar way as the Sol-air temperature, described by Kuehn, Ramsey, and Threlkeld (1998).

The temperature inside the slab is calculated considering the Fourier law in which $\mathrm{T}(x = 0, t)$ and $\mathrm{T}(x = L, t)$ represent the temperature at the internal and external surfaces, respectively, as represented in Figure 4.3.

$$q = h_o(T_1 - T_2) \tag{4.9}$$

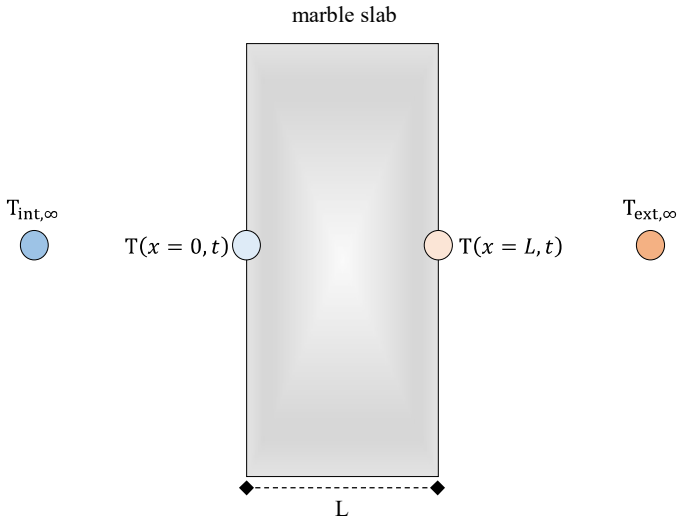

Figure 4.3 – Model of heat flux considered in this work

4.1.1 Thermal boundary conditions

The temperature at the boundaries of a slab can be described by Sol-air temperature or in situ measures and both can be written using the harmonics of Fourier series as given by equations below:

$$T_e = T_{e,0} + \sum_{n=1}^{\infty} M_n \cos(\omega_n t) + N_n \sin(\omega_n t) \tag{4.10}$$

$$T_i = T_{i,0} + \sum_{n=1}^{\infty} O_n \cos(\omega_n t) + P_n \sin(\omega_n t) \tag{4.11}$$

4.1.2 Periodic component

The periodic component was assumed as the sum of trigonometric functions:

$$T_p(x,t) = \sum_{n=1}^{\infty} \sum_{i=1}^{4} X_n^{(i)} T_n^{(i)}(x,t) \tag{4.12}$$

The general solution of the periodic function used herein was developed by Alford *et al* (1939). Those authors did not present the development of their analytic solution, but their equations produce the same results of the equations from the present work. To ensure the orthogonality between the components, two initial conditions were assumed:

For $\mathrm{T_n}(x = 0, t) = 0$ the general solution is given by Equation 4.13. The ω_n stands for the angular velocity and Ψ_n stands for the time lag of each general solution.

$$\begin{aligned} T_n &= \sinh(\varpi \cdot x)\cos(\omega_n t + \Psi_n)\cos(\varpi \cdot x) \\ &\quad - \cosh(\varpi \cdot x)\sin(\omega_n t + \Psi_n)\sin(\varpi \cdot x) \\ &\equiv \mathrm{ShC}(x)\cos(\omega_n t + \Psi_n) - \mathrm{ChS}(x)\sin(\omega_n t + \Psi_n) \end{aligned} \tag{4.13}$$

if $\Psi_n = 0$, Equation 4.13 can be written as:

$$T_n^{(1)} = \mathrm{ShC}(x)\cos(\omega_n t) - \mathrm{ChS}(x)\sin(\omega_n t) \tag{4.14}$$

otherwise, for $\Psi_n = -\pi/2$, it is given by:

$$T_n^{(2)} = \mathrm{ShC}(x)\sin(\omega_n t) + \mathrm{ChS}(x)\cos(\omega_n t) \tag{4.15}$$

The other general solution arises from the assumption of $\frac{\partial T}{\partial x}(x = 0, t) = 0$:

$$\begin{aligned} T_n &= \cosh(\varpi_n \cdot x)\cos(\omega_n t + \Psi_n)\cos(\varpi_n \cdot x) \\ &\quad - \sinh\left(\sqrt{\frac{\omega_n}{2\alpha}} \cdot x\right)\sin(\omega_n t + \Psi_n)\sin\left(\sqrt{\frac{\omega_n}{2\alpha}} \cdot x\right) \\ &\equiv \mathrm{ChC}(x)\cos(\omega_n t + \Psi_n) - \mathrm{ShS}(x)\sin(\omega_n t + \Psi_n) \end{aligned} \tag{4.16}$$

for $\Psi_n = 0$, one gets

$$T_n^{(3)} = \mathrm{ChC}(x)\cos(\omega_n t) - \mathrm{ShS}(x)\sin(\omega_n t) \tag{4.17}$$

while for $\Psi_n = -\pi/2$,

$$T_n^{(4)} = \mathrm{ChC}(x)\sin(\omega_n t) + \mathrm{ShS}(x)\cos(\omega_n t) \tag{4.18}$$

The derivative functions in relation to position x are described by:

$$\frac{\partial T_n^{(1)}}{\partial x} = \sqrt{\frac{\omega_n}{2\alpha}}\cos(\omega_n t)\,[ChC(x) - ShS(x)] + \sqrt{\frac{\omega_n}{2\alpha}}\sin(\omega_n t)\,[-ShS(x) - ChC(x)] \tag{4.19}$$

$$\frac{\partial T_n^{(2)}}{\partial x} = \sqrt{\frac{\omega_n}{2\alpha}}\sin(\omega_n t)\,[ChC(x) - ShS(x)] + \sqrt{\frac{\omega_n}{2\alpha}}\cos(\omega_n t)\,[ShS(x) + ChC(x)] \tag{4.20}$$

$$\frac{\partial T_n^{(3)}}{\partial x} = \sqrt{\frac{\omega_n}{2\alpha}}\cos(\omega_n t)\,[ShC(x) - ChS(x)] + \sqrt{\frac{\omega_n}{2\alpha}}\sin(\omega_n t)\,[-ChS(x) - ShC(x)] \tag{4.21}$$

$$\frac{\partial T_n^{(4)}}{\partial x} = \sqrt{\frac{\omega_n}{2\alpha}}\sin(\omega_n t)\,[ShC(x) - ChS(x)] + \sqrt{\frac{\omega_n}{2\alpha}}\cos(\omega_n t)\,[ChS(x) + ShC(x)] \tag{4.22}$$

and the multiplicative coefficients are solved recalling Equation 4.9, which describes the external boundary conditions,

$$q_{e,net,n} = h_e\big[T_{e,n} - T_n(0,t)\big] = -k\frac{\partial T_i}{\partial x}(0,t) \tag{4.23}$$

that is described in a rearranged form as:

$$-h_e T_i(0,t) + k\frac{\partial T_i}{\partial x}(0,t) = -h_e T_{e,i} \tag{4.24}$$

$$
\begin{aligned}
-h_e T_n = &+\cos(\omega_n t)\,[-h_e ShC(x)]X_n^{(1)} \\
&+\cos(\omega_n t)\,[-h_e ChS(x)]X_n^{(2)} \\
&+\cos(\omega_n t)\,[-h_e ChC(x)]X_n^{(3)} \\
&+\cos(\omega_n t)\,[-h_e ShS(x)]X_n^{(4)} \\
&+\sin(\omega_n t)\,[+h_e ChS(x)]X_n^{(1)} \\
&+\sin(\omega_n t)\,[-h_e ShC(x)]X_n^{(2)} \\
&+\sin(\omega_n t)\,[+h_e ShS(x)]X_n^{(3)} \\
&+\sin(\omega_n t)\,[-h_e ChC(x)]X_n^{(4)}
\end{aligned} \tag{4.25}
$$

$$
\begin{aligned}
k\frac{\partial T_n}{\partial x} = &+\cos(\omega_n t)\,k\sqrt{\frac{\omega_n}{2\alpha}}\,[+ChC(x) - ShS(x)]X_n^{(1)} \\
&+\cos(\omega_n t)\,k\sqrt{\frac{\omega_n}{2\alpha}}\,[+ShS(x) + ChC(x)]X_n^{(2)} \\
&+\cos(\omega_n t)k\sqrt{\frac{\omega_n}{2\alpha}}\,[+ShC(x) - ChS(x)]X_n^{(3)} \\
&+\cos(\omega_n t)k\sqrt{\frac{\omega_n}{2\alpha}}\,[+ChS(x) + ShC(x)]X_n^{(4)} \\
&+\sin(\omega_n t)\,k\sqrt{\frac{\omega_n}{2\alpha}}\,[-ShS(x) - ChC(x)]X_n^{(1)} \\
&+\sin(\omega_n t)\,k\sqrt{\frac{\omega_n}{2\alpha}}\,[+ChC(x) - ShS(x)]X_n^{(2)} \\
&+\sin(\omega_n t)\,k\sqrt{\frac{\omega_n}{2\alpha}}\,[-ChS(x) - ShC(x)]X_n^{(3)} \\
&+\sin(\omega_n t)\,k\sqrt{\frac{\omega_n}{2\alpha}}\,[+ShC(x) - ChS(x)]X_n^{(4)}
\end{aligned} \tag{4.26}
$$

To determine the multiplicative coefficients $X_n^{(i)}$, their terms are aggrouped to produce two linear equations. The first one is obtained by collecting the $\cos(\omega_n t)$

components of external wall temperatures for $x = 0$ and the $\cos(\omega_n t)$ of external environment temperatures:

$$\left\{-h_e ShC(0) + k\sqrt{\frac{\omega_n}{2\alpha}}[+ChC(0) - ShS(0)]\right\} X_n^{(1)}$$
$$+\left\{-h_e ChS(0) + k\sqrt{\frac{\omega_n}{2\alpha}}[+ShS(0) + ChC(0)]\right\} X_n^{(2)}$$
$$+\left\{-h_e ChC(0) + k\sqrt{\frac{\omega_n}{2\alpha}}[+ShC(0) - ChS(0)]\right\} X_n^{(3)}$$
$$+\left\{-h_e ShS(0) + k\sqrt{\frac{\omega_n}{2\alpha}}[+ChS(0) + ShC(0)]\right\} X_n^{(4)} = -h_e M_n \qquad (4.27)$$

The second equation is obtained by collecting the $\sin(\omega_n t)$ components of external wall temperatures for $x = 0$ and the $\sin(\omega_n t)$ of external environment temperatures:

$$\left\{+h_e ChS(0) + k\sqrt{\frac{\omega_n}{2\alpha}}[-ShS(0) - ChC(0)]\right\} X_n^{(1)}$$
$$+\left\{-h_e ShC(0) + k\sqrt{\frac{\omega_n}{2\alpha}}[+ChC(0) - ShS(0)]\right\} X_n^{(2)}$$
$$+\left\{+h_e ShS(0) + k\sqrt{\frac{\omega_n}{2\alpha}}[-ChS(0) - ShC(0)]\right\} X_n^{(3)}$$
$$+\left\{-h_e ChC(0) + k\sqrt{\frac{\omega_n}{2\alpha}}[+ShC(0) - ChS(0)]\right\} X_n^{(4)} = -h_e N_n \qquad (4.28)$$

The same procedure can be performed for the boundary condition of the internal side of the slab. The third equation is obtained by collecting the $\cos(\omega_n t)$ components of internal wall temperatures for $x = 0$ and the $\cos(\omega_n t)$ of internal environment temperatures:

$$\left\{+h_i ShC(L) + k\sqrt{\frac{\omega_n}{2\alpha}}[+ChC(L) - ShS(L)]\right\} X_n^{(1)}$$
$$+\left\{+h_i ChS(L) + k\sqrt{\frac{\omega_n}{2\alpha}}[+ShS(L) + ChC(L)]\right\} X_n^{(2)}$$

$$+\left\{+h_i ChC(L)+k\sqrt{\frac{\omega_n}{2\alpha}}[+ShC\ (L)-ChS(L)]\right\}X_n^{(3)}$$

$$+\left\{+h_i ShS(L)+k\sqrt{\frac{\omega_n}{2\alpha}}[+ChS(L)+ShC(L)]\right\}X_n^{(4)}=h_i O_n \tag{4.29}$$

The fourth equation is obtained by collecting the $\sin(\omega_n t)$ components of internal wall temperatures for $x=0$ and the $\sin(\omega_n t)$ of internal environment temperatures:

$$\left\{-h_i ChS(L)+k\sqrt{\frac{\omega_n}{2\alpha}}[-ShS(L)-ChC(L)]\right\}X_n^{(1)}$$

$$+\left\{+h_i ShC(L)+k\sqrt{\frac{\omega_n}{2\alpha}}[+ChC(L)-ShS(L)]\right\}X_n^{(2)}$$

$$+\left\{-h_i ShS(L)+k\sqrt{\frac{\omega_n}{2\alpha}}[-ChS\ (L)-ShC(L)]\right\}X_n^{(3)}$$

$$+\left\{+h_i ChC(L)+k\sqrt{\frac{\omega_n}{2\alpha}}[+ShC(L)-ChS(L)]\right\}X_n^{(4)}=h_i P_n \tag{4.30}$$

Finally, the multiplicative coefficients are reached by solving the linear system given by Equation 4.31:

$$\mathbf{A}\boldsymbol{x}=\boldsymbol{b} \tag{4.31}$$

4.1.3 Polynomial component

For the polynomial part of the function, it was assumed the simplest polynomial (linear in time and third order in space) that satisfies the Fourier law:

$$T_L(x,t)=(a_0+a_1\ t)x^3+(b_0+b_1 t)x^2+(c_0+c_1 t)x+(d_0+d_1 t) \tag{4.32}$$

The coefficients of the equation above are obtained substituting Equation 4.32 into the Fourier law and by comparison between the left and right hand-side. The equations 4.33 and

4.34 represent each term of the time derivative function and the second order position derivative function, respectively:

$$\frac{\partial T_L}{\partial t}(x,t) = a_1 x^3 + b_1 x^2 + c_1 x + d_1 \tag{4.33}$$

$$\alpha \frac{\partial^2 T_L}{\partial x^2}(x,t) = \alpha(a_0 + a_1\, t)6x + \alpha(b_0 + b_1 t)2 \tag{4.34}$$

Since the temperature at the boundaries is known, the coefficients are calculated as:

$$a_0 = \frac{T_{f,L} - T_{f,0} - T_{i,L} + T_{i,0}}{6\alpha L \Delta T} \tag{4.35}$$

$$a_1 = 0 \tag{4.36}$$

$$b_0 = \frac{T_{f,0} - T_{i,0}}{2\alpha \Delta T} \tag{4.37}$$

$$b_1 = 0 \tag{4.38}$$

$$c_0 = \frac{T_{i,L} - a_0 L^3 - b_0 L^2 + T_{i,0}}{L} \tag{4.39}$$

$$c_1 = \frac{T_{f,L} - T_{i,L} - d_1 \Delta T}{L \Delta T} \tag{4.40}$$

$$d_0 = T_{i,0} \tag{4.41}$$

$$d_1 = \frac{T_{f,0} - T_{i,0}}{\Delta T} \tag{4.42}$$

4.2 Thermal stresses

Thermal stresses in infinitely long and unrestrained slabs could be calculated by adding the thermal component to the Airy stress function (JOHNS, 1965; TIMOSHENKO; GOODIER, 1970) which, in rectangular slab and plane strain analysis, could be given by Equation 4.43. Since the slab is considered in this work as an isostatic structure, it is free to expand and no stress is expected at the borders; hence the second term of Equation 4.43 corresponds to suppression of internal stresses generated due to thermal expansion (first term). The third term is related to equilibrium because asymmetric thermal distribution could result in eccentric load.

$$\sigma = \frac{\alpha E}{1-\nu}\left\{-\theta + \frac{1}{L}\int_0^L \theta\, dx + \frac{12}{L^3}\left(x - \frac{L}{2}\right)\int_0^L \left[\theta\left(x - \frac{L}{2}\right)\right] dx\right\} \tag{4.43}$$

One must recall that the temperature function is composed of periodic and polynomial components and both must be considered in thermal stress calculation.

4.2.1 Periodic component of thermal stress

The periodic function of temperature is responsible for part of the thermal stresses induced in the slab. The integrals of the trigonometric terms of each general solution must be previously calculated to get to the thermal component of the periodic solution. Then, some contractions are defined:

$$I_{ChC,n} = \int_0^L ChC_n(x)\, dx = \frac{1}{2\sigma_n}[ChS_n(x) + ShC_n(x)]|_0^L \tag{4.44}$$

$$I_{ChS,n} = \int_0^L ChS_n(x)\, dx = \frac{1}{2\sigma_n}[ShS_n(x) - ChC_n(x)]|_0^L \tag{4.45}$$

$$I_{ShC,n} = \int_0^L ShC_n(x)\, dx = \frac{1}{2\sigma_n}[ShC(x) + ChC_n(x)]|_0^L \tag{4.46}$$

$$I_{ShS,n} = \int_0^L ShS_n(x)\, dx = \frac{1}{2\sigma_n}[ChS_n(x) - ShC_n(x)]|_0^L \tag{4.47}$$

$$I_{xChC,n} = \int_0^L x\, ChC_n(x)\, dx$$

$$= \frac{1}{2\sigma_n^2}\{\sigma_n x[ShC_n(x) + ChS_n(x)] - ShS_n(x)\}|_0^L \tag{4.48}$$

$$I_{xChS,n} = \int_0^L x\, ChS_n(x)\, dx$$

$$= \frac{1}{2\sigma_n^2}\{\sigma_n x[ShS_n(x) - ChC_n(x)] + ShC_n(x)\}|_0^L \tag{4.49}$$

$$I_{xShC,n} = \int_0^L x\, ShC_n(x)\, dx$$

$$\frac{1}{2\sigma_n^2}\{\sigma_n x[ChC(x) + ShS_n(x)] - ChS_n(x)\}|_0^L \tag{4.50}$$

$$I_{xShS,n} = \int_0^L x\, ShS_n(x)\, dx$$

$$= \frac{1}{2\sigma_n^2}\{\sigma_n x[ChS_n(x) - ShC_n(x)] + ChC_n(x)\}|_0^L \tag{4.51}$$

The sum of the three integrals of Equation 4.43 is written as:

$$TChC_n(x) = ChC_n(x) - \frac{I_{ChC,n}}{L} - \frac{12}{L^3}\left[I_{xChC,n} - \frac{I_{ChC,n}\ \cdot\ L}{2}\right]\left(x - \frac{L}{2}\right) \tag{4.52}$$

$$TChS_n(x) = ChS_n(x) - \frac{I_{ChS,n}}{L} - \frac{12}{L^3}\left[I_{xChS,n} - \frac{I_{ChS,n}\ \cdot\ L}{2}\right]\left(x - \frac{L}{2}\right) \tag{4.53}$$

$$TShC_n(x) = ShC_n(x) - \frac{I_{ShC,n}}{L} - \frac{12}{L^3}\left[I_{xShC,n} - \frac{I_{ShC,n}\ \cdot\ L}{2}\right]\left(x - \frac{L}{2}\right) \tag{4.54}$$

$$TShS_n(x) = ShS_n(x) - \frac{I_{ShS,n}}{L} - \frac{12}{L^3}\left[I_{xShS,n} - \frac{I_{ShS,n}\ \cdot\ L}{2}\right]\left(x - \frac{L}{2}\right) \tag{4.55}$$

Finally, the contribution of stress due to the periodic function is represented by:

$$\sigma(x,t) = -\frac{\alpha\, E}{1-\nu}\left\{\sum_{n=1}^{\infty} T_n^1\ [TShC_n(x)\cos(\omega_n t) - TChS_n(x)\sin(\omega_n t)]\right.$$

$$\sum_{n=1}^{\infty} T_n^2\ [TShC_n(x)\sin(\omega_n t) + TChS_n(x)\cos(\omega_n t)]$$

$$\left.\sum_{n=1}^{\infty} T_n^3\ [TChC_n(x)\cos(\omega_n t) - TShS_n(x)\sin(\omega_n t)]\right.$$

$$\sum_{n=1}^{\infty} T_n^4 \left[TChC_n(x)\sin(\omega_n t) - TShS_n(x)\cos(\omega_n t)\right]\Bigg\} \tag{4.56}$$

4.2.2 Polynomial component of thermal stress

The contribution of the polynomial function into the thermal stresses are obtained directly by the integration of Equation 4.32:

$$\sigma = (a_0 + a_1 t)\left(x^3 - \frac{9}{10}L^2 x + \frac{1}{5}L^3\right) + (b_0 + b_1 t)\left(x^2 - Lx + \frac{1}{6}L^2\right) \tag{4.57}$$

5 Results and Discussion

The numerical formulation and the exact solution discussed in this section have a special focus on the thermoelasticity applied to bowing problems. The different approaches of each subsection represent the evolution during the development of this dissertation. In the first part, it is presented the preliminary results discussing the influence of three anchoring systems on the deformation due to thermal load. Afterward, a comparison between stress distribution in linear and nonlinear models is evaluated in parametric analysis assuming fixed thermal boundary conditions. Lastly, the real case of the Pescara Justice Court's façade is approached by the exact solution presented in the previous chapter.

The results presented herein were already submitted, or in the process to be submitted, to specific journals and congress in order to be peer-reviewed. The list of publications can be found in the Appendix section.

5.1 Preliminary results

5.1.1 Influence of the anchoring systems into the deflection due to thermal loading

The results presented in this subsection were previously submitted to the *14th International Congress on Rock Mechanics and Rock Engineering* in the *modeling and computational rock engineering* section. This work evaluated the influence of the anchoring systems on the deflection due to thermal loading.

For a homogeneous slab without imposed restraint conditions, the thermal action due to sunlight exposure produces an expansion of vertical fibers that enlarge from internal toward the external side, as presented in Figure 5.1. In this analysis, a slab of 60 cm length and 3 cm thickness was considered, but, due to symmetry, only the lower half of the slab (30 of 60 cm) was used to compute the displacement. Since the goal was to verify the deformed shape and the influence of anchoring systems, some assumptions were done about indirectly related topics. The thermal

gradient along marble width, for instance, was linearly interpolated and a fixed gradient of 20°C was assumed for this introductory work.

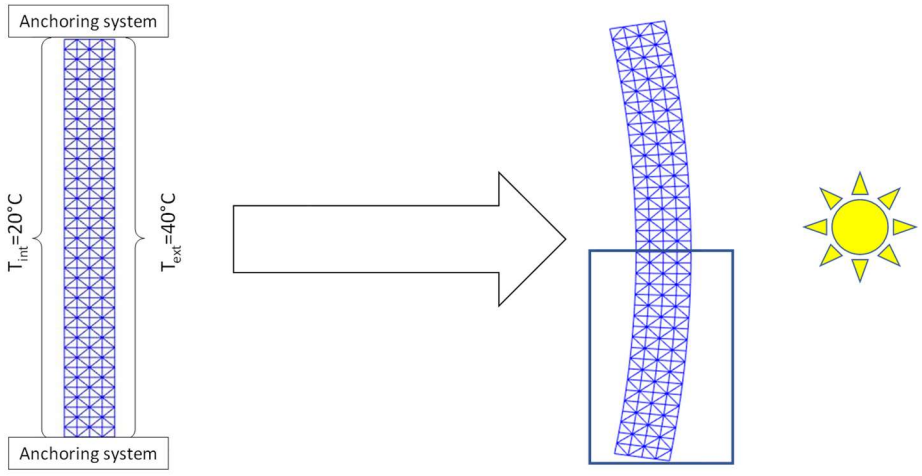

Figure 5.1 – Deformed marble slab due to thermal action

Taking into consideration the deformation and the stress in marble slabs are directly correlated with the forces at the anchoring system, some different conditions were considered, as presented in Figure 5.2. The undercut support was assuming restricting the rotations and displacements. The kerf support restricts partially the displacements at the bottom and the top, and the dowel restricts displacements just locally.

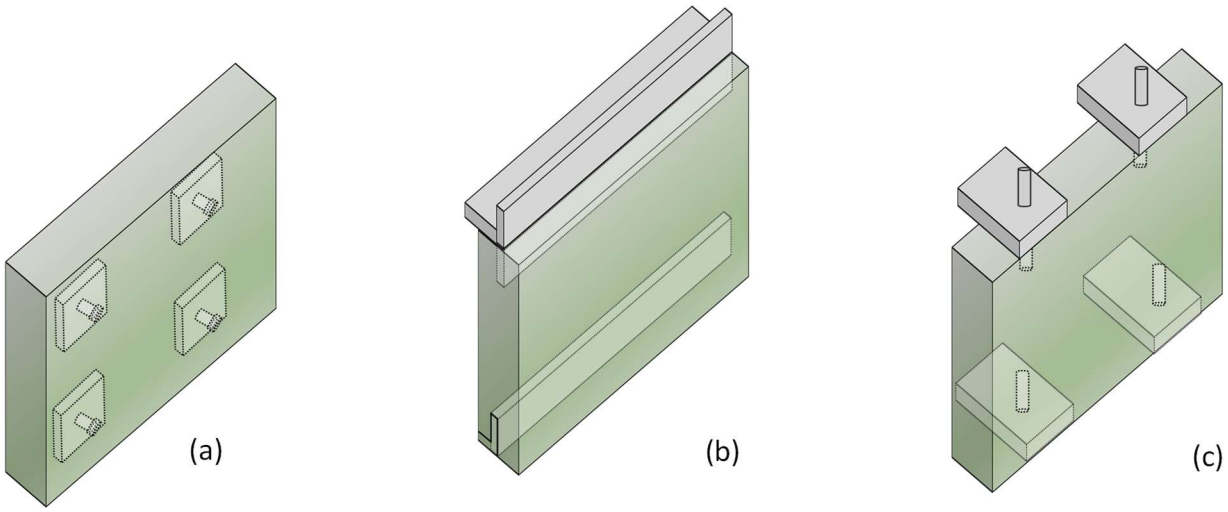

Figure 5.2 – Restraint conditions: (a) undercut (b) kerf (c) dowel

To evaluate the effect of thermal stresses it was considered no free space between adjacent slabs and the anchoring systems. This statement is reasonable if were considered the expansion of weathered marble or even errors in design and installation procedures since they represent the major problems in the natural stone cladding (NETO; BRITO, 2012).

In Figure 5.3, it is presented the coordinates (x, y) of the external surface deformed by thermal actions using linear and nonlinear concepts. To clarify the previous information about the displacement, the deformed meshes with displacements magnified by a factor scale of 600 were presented in Figure 5.4. It is clear that the deformation along the slab is inversely proportional to the increase of boundary restrain conditions. So, the bowing effect should be more evident in those façades with anchoring system using dowel instead of those with undercut support.

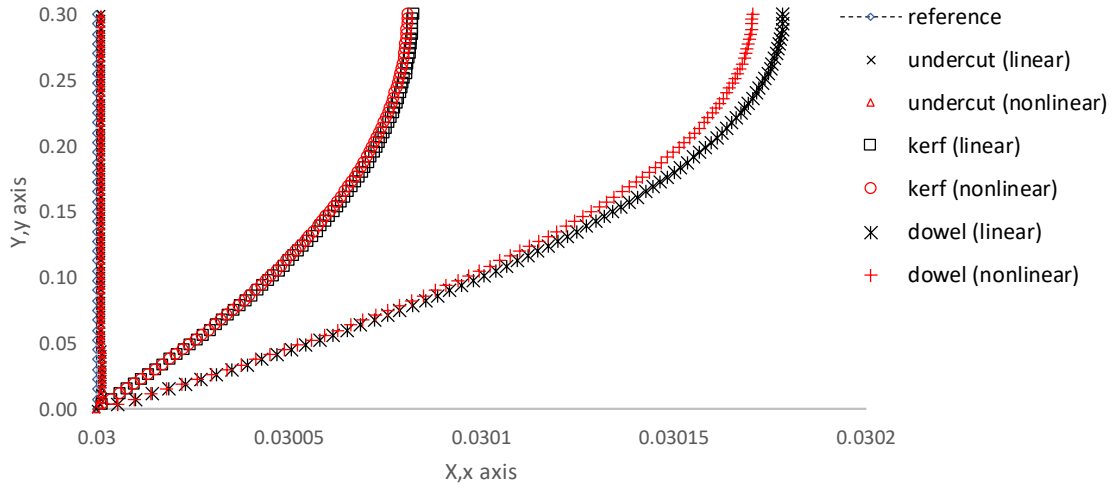

Figure 5.3 – Displacements of the deformed surfaces (linear and nonlinear models)

According to these results, the deformation in the nonlinear model was slightly lower than the other mainly because of the effect of the quadratic term of the Green-Lagrange deformation. The influence of the boundary restraint conditions was clearly identified in these theoretical analyses, however, the same effect was not found in experimental results accomplished by TEAM (2005). The unexpected result of the experimental test can be explained by the influence of the adjacent structures that increase the rigidity of the anchoring systems and it was not considered by those authors since just one type of each anchoring system was evaluated by TEAM (2005). Obviously, a single line of kerf or dowel anchoring system is not enough to provide the rigidity to

avoid the displacement as assumed in the theoretical analysis. It would be more realistic if a real façade of several rows were considered. Even though, the kerf and dowel systems presented higher deformation due to bowing.

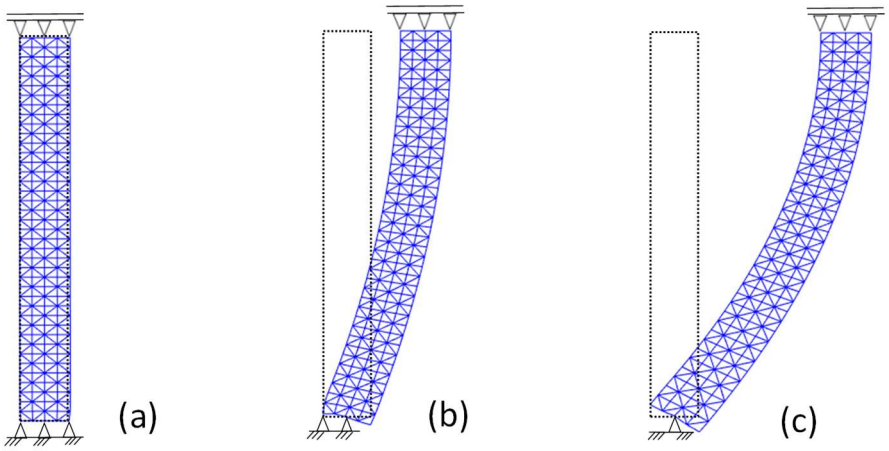

Figure 5.4 - Deformed meshes: (a) undercut (b) kerf (c) dowel

5.2 Numerical analysis of thermal stresses

The formulation in this subsection was submitted to the *MATERIALS* in the *advances in structural mechanics modeled with FEM* special issue.

5.2.1 Validation

Initially, the verification of numerical formulation with simple analytical solutions to verify the accuracy is presented, then, a comparison with results in the literature is proposed. Since the evaluation of nonlinear concepts is discussed, no direct analytical solution is available to verify the formulation, thus, the validation tests were accomplished in two steps: one to evaluate the convergence of the nonlinear model and the other to verify the numerical formulation of thermal loading.

The nonlinear numerical model was verified considering mechanical loads applied on a beam. Since finite displacements are assumed, the external loads used in this example are not

constant, as indicated in Equation 3.7, because they will vary according to geometry changes. A way to solve them could be expressing the follower loads in terms of parametric variables which will be updated according to the current geometry, as indicated in Equation 5.1. The linearization of these surface forces must also be considered when the tangent stiffness matrix is calculated, as explained by Bonet and Wood (2008).

An example with a built-in beam with bending moment applied at the end is now considered. Since the bending moment is constant along the beam, rotated Cauchy stresses (recall Equation 3.4) must remain invariant in perpendicular sections along this beam, as indicated in Figure 5.5.

$$\delta W_{ext} = \int \mathrm{N}_a \, \bar{\mathrm{p}} \left(\frac{\partial \boldsymbol{x}}{\partial \xi} \times \boldsymbol{e}_3 \right) d\xi \tag{5.1}$$

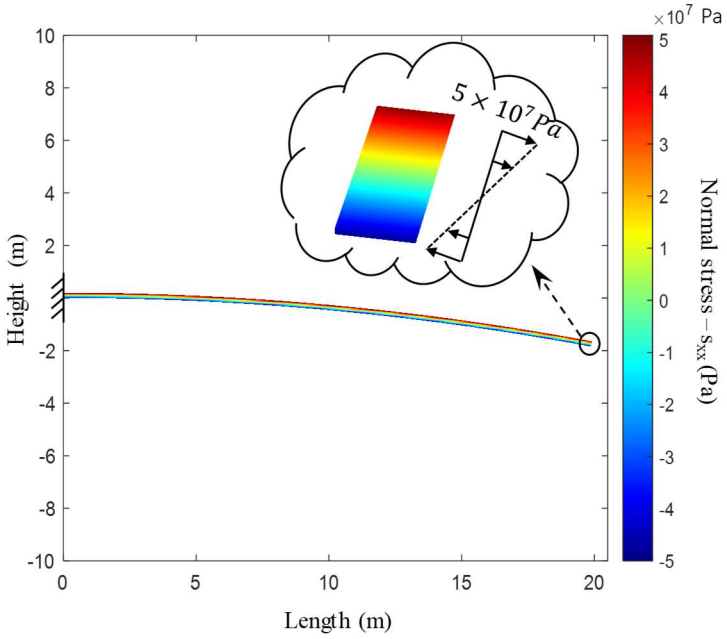

Figure 5.5 - Normal stress induced by bending moment applied at the end of a built-in beam.

Henceforth the numerical formulation of thermal stresses is considered. Firstly, the nonlinear stress-strain measures of the numerical code were substituted by engineering strain and Cauchy stresses. After that, the numerical integration of the temperature function presented in Chapter 3

was converted into an exact solution using the integral of the Fourier series. To do so, Equation 4.43 was rewritten in dimensionless form:

$$\sigma = \frac{E\alpha\theta_0}{(1-\nu)}\left[-\Theta + \int_0^1 \Theta\, dZ + 12\left(Z-\frac{1}{2}\right)\int_0^1 \Theta\left(Z-\frac{1}{2}\right)dZ\right] \tag{5.2}$$

recalling that

$$\int_0^1 \sin(M_i Z)\, dZ = -\frac{1}{M_i}\cos(M_i Z)\Big|_0^1 = \begin{cases} \dfrac{2}{M_i} \text{ if } i \text{ is odd} \\ 0 \text{ if } i \text{ is even} \end{cases} \tag{5.3}$$

In these analyses, the transient heat flux was calculated considering fixed boundaries conditions. The temperature on the exposed face was assumed as 50 °C along the whole surface; for the internal side, it was assumed 20 °C. The thermal and mechanical properties of marble were assumed the same as used in Ferrero, Migliazza, and Spagnoli (2009), as indicated in Figure 5.6. Transient heat flux was calculated to four elapsed times (5 s, 10 s, 25 s, and 50 s) and a good correlation was achieved between linear and analytical solution, as presented in Figure 5.7.

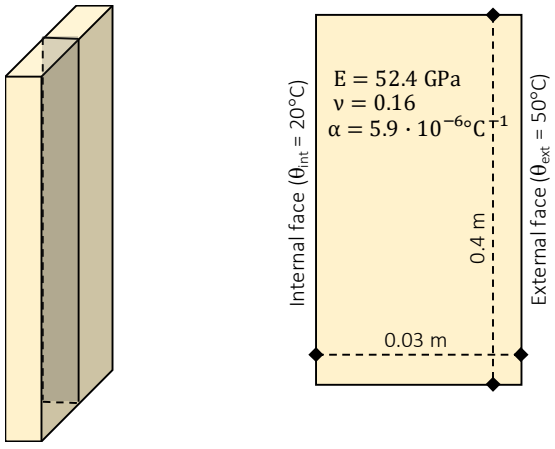

Figure 5.6 - Model used in validation test.

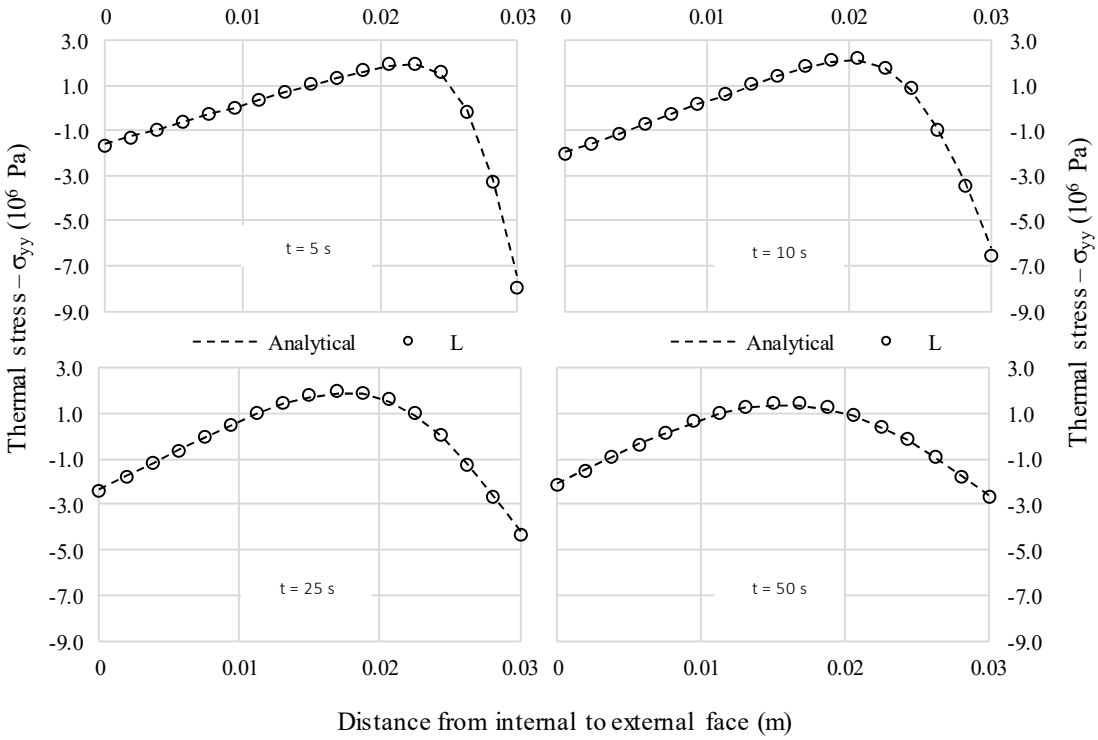

Figure 5.7 - Comparison between analytical and numerical (linear) solution for several elapsed times. (t = 5 s, t = 10 s, t = 25 s, t = 50 s).

5.2.2 Numerical approach using the Pescara Justice Court's data

Ferrero, Migliazza, and Spagnoli (2009) monitored the temperature of the internal and external face of a ventilated façade at the Pescara's building for six days in 2007. An automatic system recorded the temperatures at each 15 min and the highest gradient of temperature was 4.7 °C which induced about 0.04 MPa in tensile stresses according to that model. Similar analyses were performed using the formulation presented in Chapter 3 for several elapsed times to evaluate the differences between stress distribution in a linear and nonlinear model in continuum media. Transient heat flux with fixed boundary conditions was used.

Figures 5.8 - 5.10 present the thermal stresses for each analysis. Normal stress distributions were considered at the symmetric planes and the shear stresses were represented in two orthogonal planes. The results show that internal stress distribution is different from the one usually found in classical beam theories undergoing mechanical loads, where the traction and compression stresses belong to opposite sides of the neutral axis. Nevertheless, considering the theoretical formulation

presented in the previous section it would be expected to find such distribution because the fibers on the external face, where the thermal expansion is greater, would try to expand, but they will be constrained by the adjacent fibers in which the thermal deformations are smaller. Then, the external fibers should be under compression and those on the left side would be under tensile stresses. Symmetric behavior is expected on the left-hand side.

It must be noted that internal stresses are greater at the initial instant of the transient regime and they reduce until it becomes constant when stationary condition takes place. The results are consistent with those expected if the shape of the internal temperature curve in the transient regime is considered. In the beginning, only those fibers close to the right-hand side are deformed by thermal expansion, thus, a greater amount of stress will be induced to counterpoise these unbalanced loads. Nonetheless, when the transient gradient approaches stationary conditions these unbalanced loads reduce. The greater stresses developed in the transient analysis at the beginning could explain why the intergranular decohesion in thermally treated marble is higher close to the exposed surface, as identified by Bellopede, Castelletto, and Marini (2016) and Bellopede, Zichella, and Marini (2020). This phenomenon can also be related to the increase of bowing with the height of buildings related by Siegesmund, Ruedrich, and Koch (2008) since the thermal exchanges could increase according to elevation due to wind action.

Shear stresses and normal stresses in x direction were concentrated at the ends of the slab. Similar results were found by Carpinteri and Paggi (2008) in nonhomogeneous beams using the classical beam's theory; however, in that formulation, the shear stresses tend to infinity when they approach the boundaries. In the numerical formulation proposed in this study, the shear stresses at the boundaries in simply supported slabs tend to zero just as expected for the isostatic condition.

The shear stress distribution is consistent with the theory of long thin beams, in which most of its length follows a strain profile almost translation-symmetric. At the slab edges, in which the translation-symmetry cited does not hold, there are other bidimensional deformation modes that dissipate the energy induced by thermal strains in a more efficient way. These edge deformation modes explain why the stress calculated by the finite element method does not fit exactly to the analytical solution in Figure 5.7.

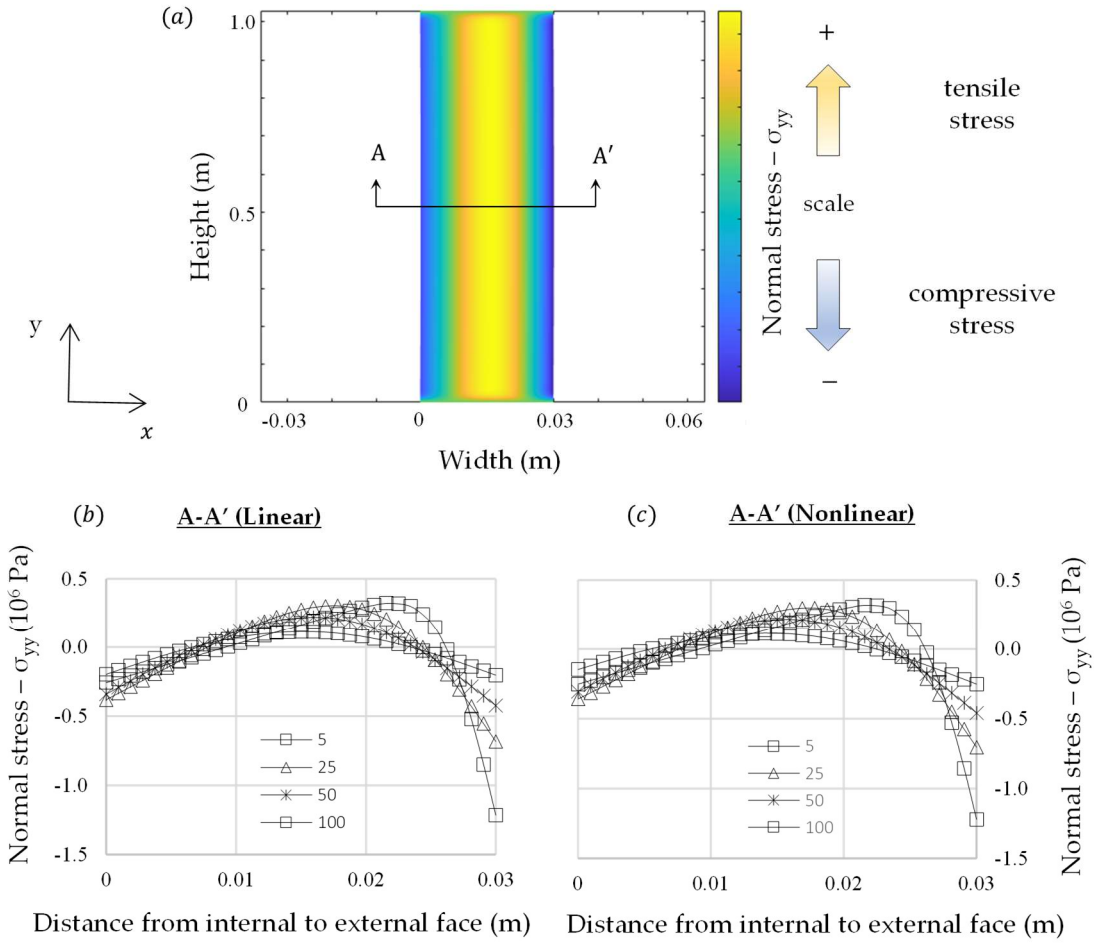

Figure 5.8 - Comparison between linear and nonlinear numerical analysis of δ_{yy}: (***a***) Representation of a generic normal stress distribution (***b***) linear analysis (***c***) nonlinear analysis.

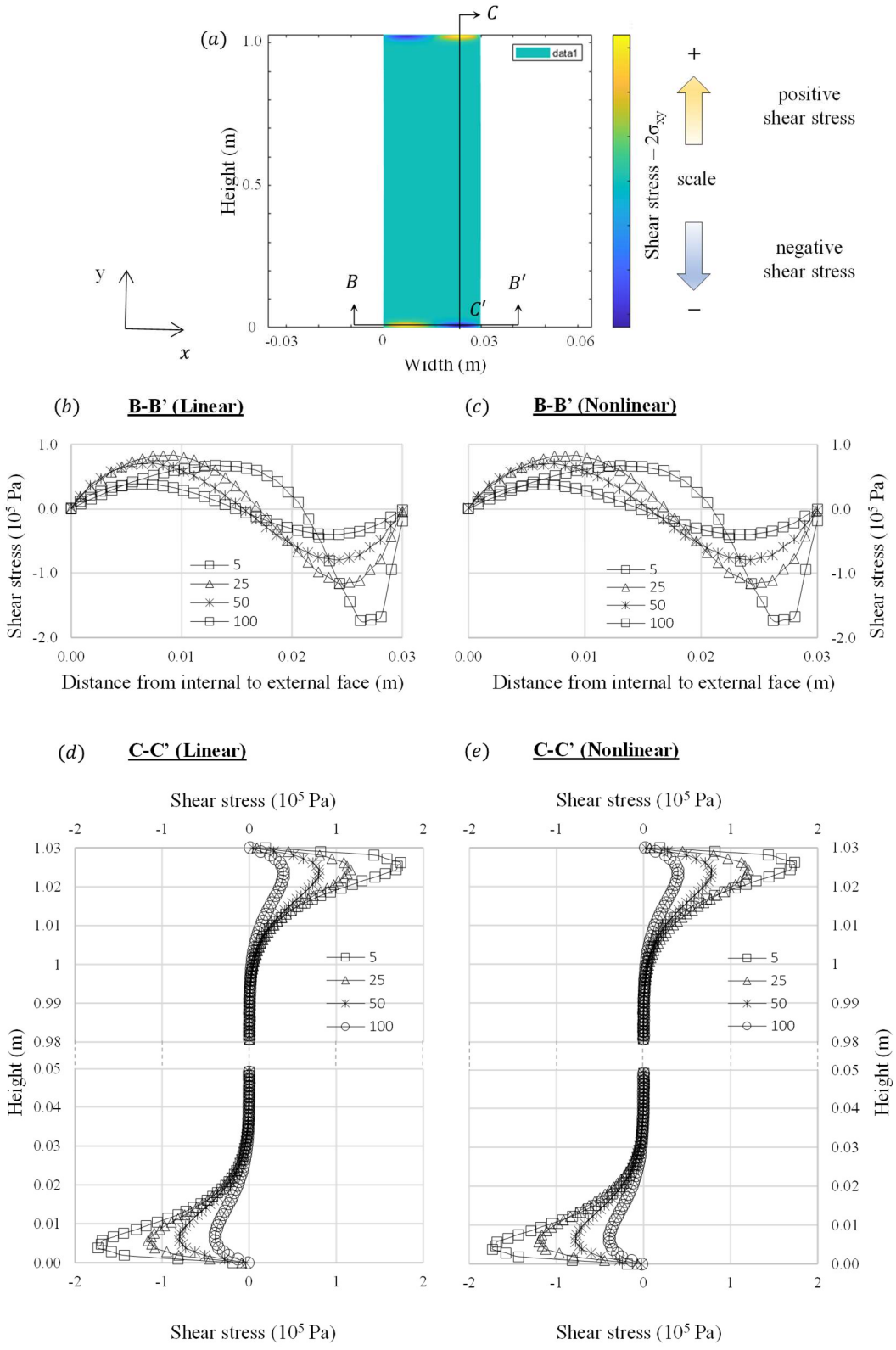

Figure 5.9 - Comparison between linear and nonlinear numerical analysis of $2\delta t_{xy}$: (a) generic shear stress distribution, (b,d): linear analysis, (c,e): nonlinear analysis.

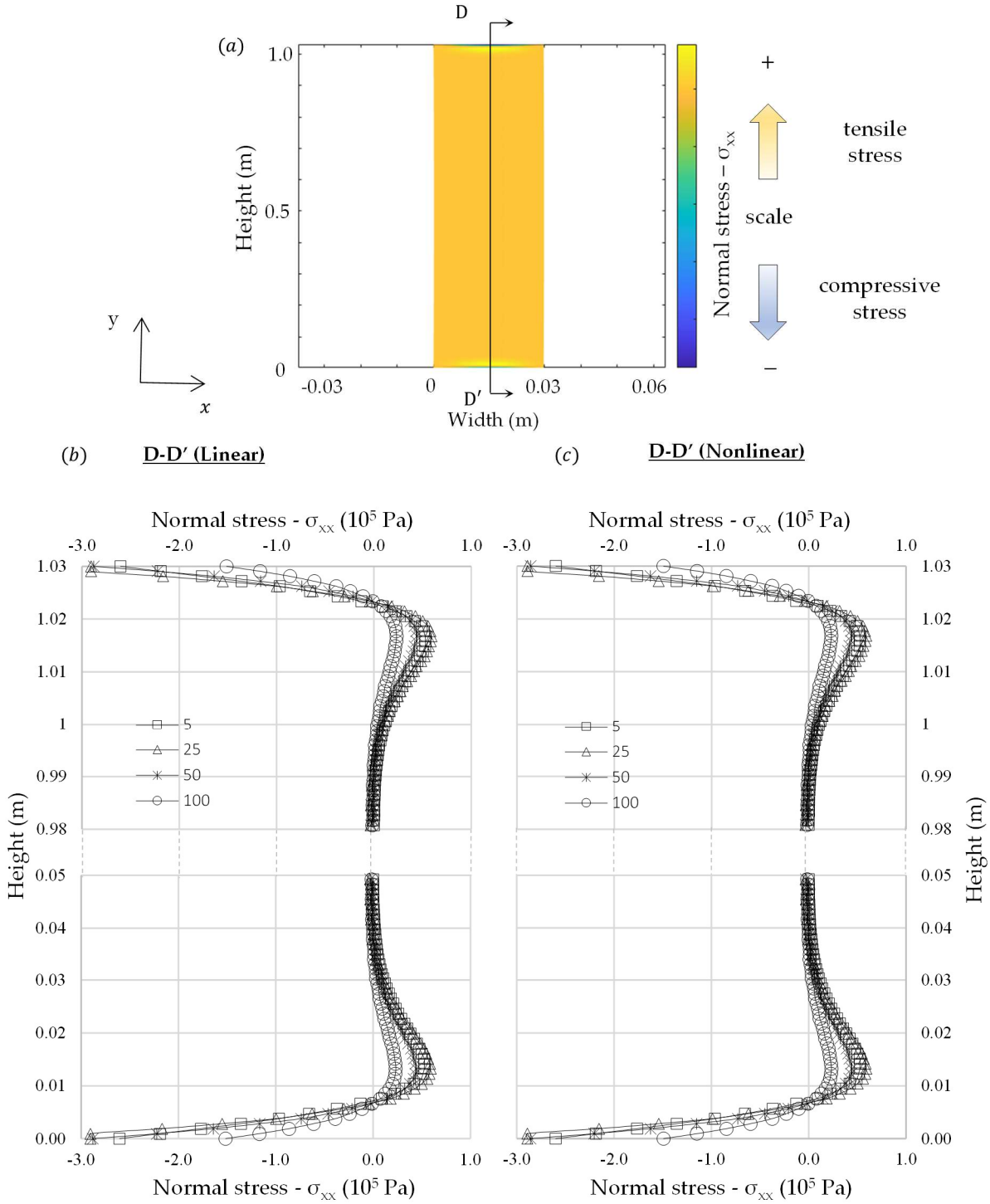

Figure 5.10 - Comparison between linear and nonlinear numerical analysis of δ_{xx}: (a) representation of a generic normal stress distribution (b) linear analysis (c) nonlinear analysis.

In transient conditions, the difference between stress distribution in the linear and nonlinear analysis is minimal, a foreseeable outcome due to the magnitude of the deformation. However, for stationary conditions, the internal stresses completely vanish over the entire body in the linear analysis just as expected by the analytical solution if one recalls Equation 5.2 considering the linear distribution of temperature through width. While, in nonlinear analysis, residual stresses still remain, as indicated in Figure 5.11.

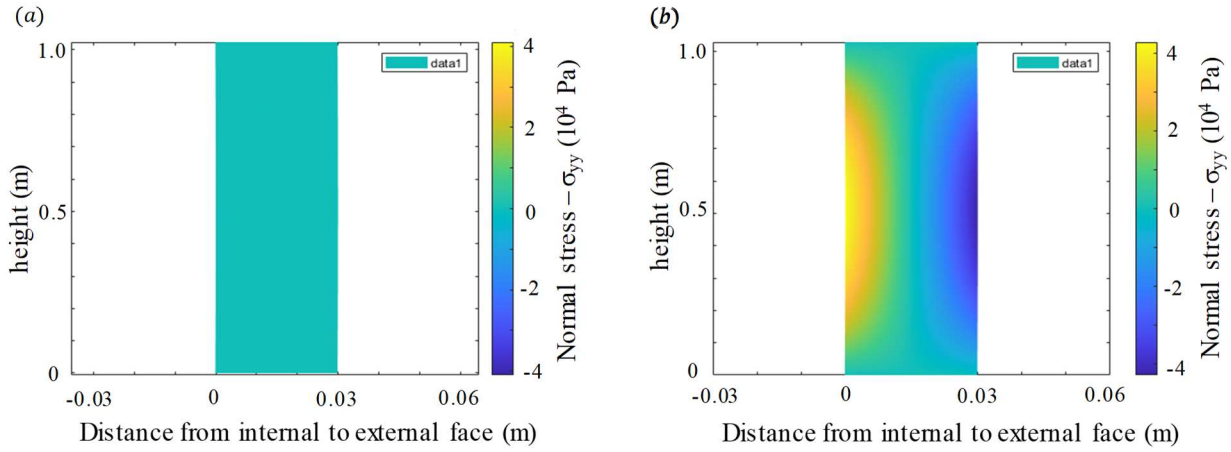

Figure 5.11 - Evaluation of normal stress distribution (σ_{yy}) in steady heat flux ($t \rightarrow \infty$)

(a) linear (b) nonlinear

5.3 Exact solution applied at the Pescara Justice Court's facade

The previous section has demonstrated differences between linear and nonlinear formulations, even considering that these differences are not so expressive if the daily variation of temperature in a slab is considered. For this reason, the exact solution considering small strain concepts could be used to evaluate the problem without major errors. The formulation in this section was used in the paper submitted to *Applied Sciences* in the *Effects of temperature on rock and rock masses* special issue.

The temperature measured on the external façade at the Pescara Justice Court was used to evaluate the thermal stresses induced by heat exchanges between the building and the environment, however, the periodic oscillation of temperature was considered this time.

5.3.1 Periodic functions of temperature

As previously described, the temperature at both sides of the Pescara Justice Court's facade was measured every fifteen minutes between August 8-13 2007. Therefore, the first step needed to compute the thermal stresses was transforming these discrete functions into continuous in order to be possible to integrate the temperature function over time to calculate the stresses.

Periodic functions of period t equal 24 hours were assumed starting from 0:00 h. Then, the historical series measured at the Pescara Justice Court was reduced from 0:00h on August 9 until 0:00h on August 12. For each period a pair of periodic functions were calculated using the Fourier series to represent the variation of temperature at the hidden (internal) and the exposed (external) surfaces. Then, the functions were represented by:

$$T_{int}^{i}(x,t) = \frac{a_{0,int}}{2} + \sum_{n=1}^{\infty}\left[a_{n,int}\cos(\omega_n x) + b_{n,int}\sin(\omega_n x)\right] \tag{5.4}$$

$$T_{ext}^{i}(x,t) = \frac{a_{0,ext}}{2} + \sum_{n=1}^{\infty}\left[a_{n,ext}\cos(\omega_n x) + b_{n,ext}\sin(\omega_n x)\right] \tag{5.5}$$

where the coefficients are defined by

$$a_0 = \frac{2}{T}\int_0^T f(x)\,dx \tag{5.6}$$

$$a_n = \frac{2}{T}\int_0^T f(x)\cos(n\,\omega_0 x)\,dx \tag{5.7}$$

$$b_n = \frac{2}{T}\int_0^T f(x)\sin(n\,\omega_0 x)\,dx \tag{5.8}$$

In the Appendix section, it is presented the comparison between the periodic functions (theoretical) and the temperature measured on the external and the internal surfaces for each period of 24 hours between August 9-12. Once previous analyses have shown the greater importance of

the rate of temperature changes rather than the absolute value of the thermal gradient, the analyses presented in this section were focused on the interval that higher rates were found.

The higher rate of temperature change between 9-12 was measured on August 10th and it was chosen to be evaluated by the exact solution proposed in this dissertation. The theoretical temperature on August 10th, as well as the temperature measured on the façade, are presented in Figure 5.12. Between 14:30 until 15:30 the temperature variation reached the minimum of -0.125°C/min. This rate is smaller (considering absolute value) than the one adopted for the maximum rate of heating (0.35°C/min) in standard bowing tests (BS16306).

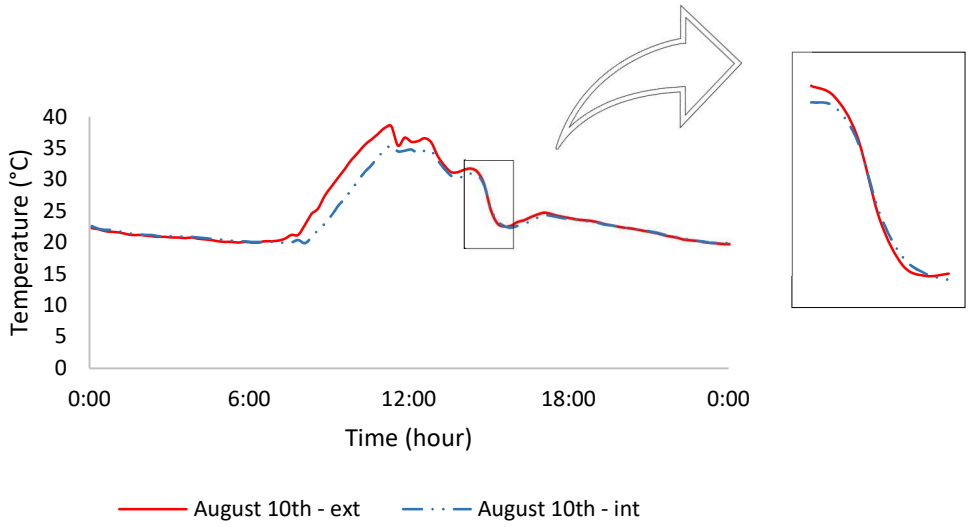

Figure 5.12 – Gradient of temperature between external and internal surface

5.3.2 Thermal stresses

5.3.2.1 Temperature distribution measured on August 10th

The thermal stresses were calculated according to the formulation presented in Chapter 4. To comprise the singularities of the distribution of thermal stresses along the whole cycle, it was chosen the key points in which the stresses could be affected by the temperature changing, for instance:

1. 06:00: when the minimum gradient of temperature was measured;
2. 08:00: just after the inflection point when the temperature of both sides start to rise;

3. 09:00: when the gradient of temperature between both sides rise at the same rate;
4. 11:00: just after the highest gradient of temperature is reached when also occurs another inflection point;
5. 12:15: when the temperature of both sides start to fall;
6. 14:00: at the inflection point during the cooling cycle;
7. 15:00: when the lowest rate of temperature changing occurs;
8. 15:45: at the inflection point when the temperature of both sides falls until a minimum and starts to rise.

These key points in the stress distribution were split into three graphics (Figures 5.13 - 5.15). Firstly, the singularities at the beginning of the cycle from when the marble slab starts to get the sunlight until the end of the heating step. Afterward, the singularities during the cooling step are presented. Then, the sections in which the temperature rises/declines at an almost constant rate.

Between the sunset and the sunrise, the gradient of temperature between both sides of a slab is almost null, therefore, zero or almost zero stress act in the slab. Just after the sunrise, at 08:00, the exposed surface starts to heat while the hidden side slowly gains heat. When the temperature reaches the maximum, there is another inflection point and the internal stresses reduce.

Just after the temperature in a slab reaches the maximum, it starts to decrease until sunset. On August 10th, 2007, it was verified some inflection points during the decrease of temperature which was assumed to be linked with wind gusts that were measured at the Pescara Airport and they probably reached the façade of the Pescara Justice Court (Ito et al, 2021).

The highest values of stresses were calculated at 09:00 and 15:00 when the peaks of compressive and tensile stresses were, respectively, achieved. The thermal stress distribution along the August 10th is presented in Figure 5.16. It is worthwhile to highlight that the peak of stresses was achieved while the slab was heating up or cooling down. It indicates that, until those points, the differential strains due to thermal expansion into the slab were increasing. After that, the heat flux approaches to steady-state, and the thermal stresses (and differential strains) reduce until close to null stress.

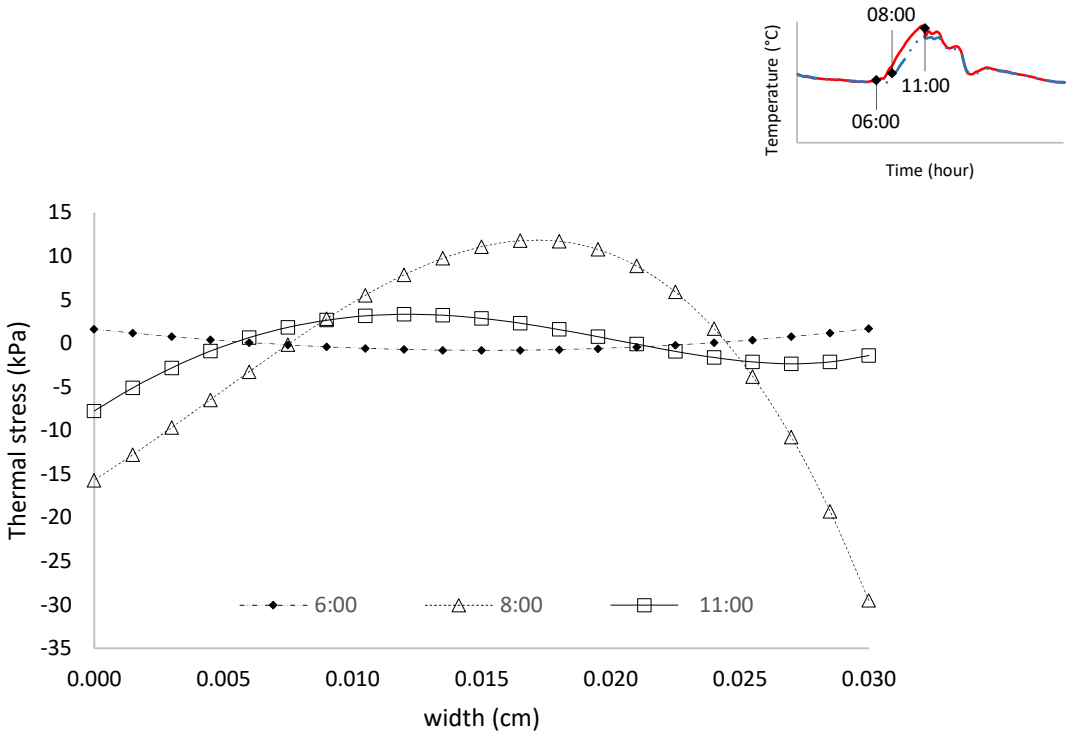

Figure 5.13 – Thermal stresses during the heat step

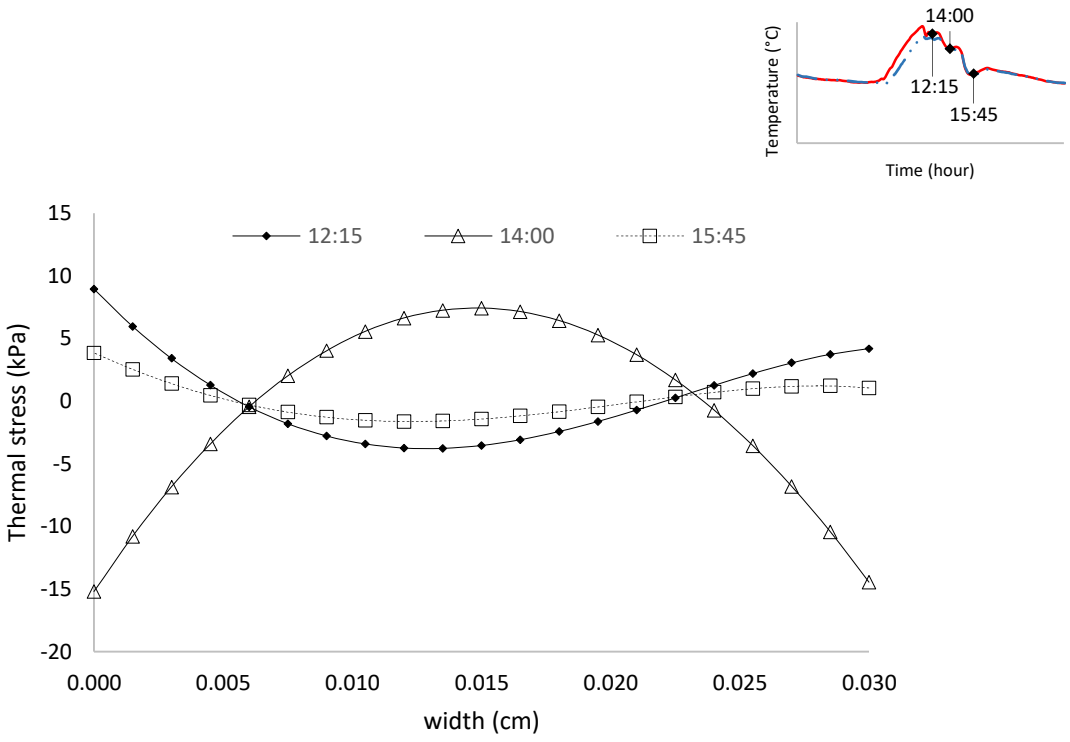

Figure 5.14 – Thermal stresses during the cooling step

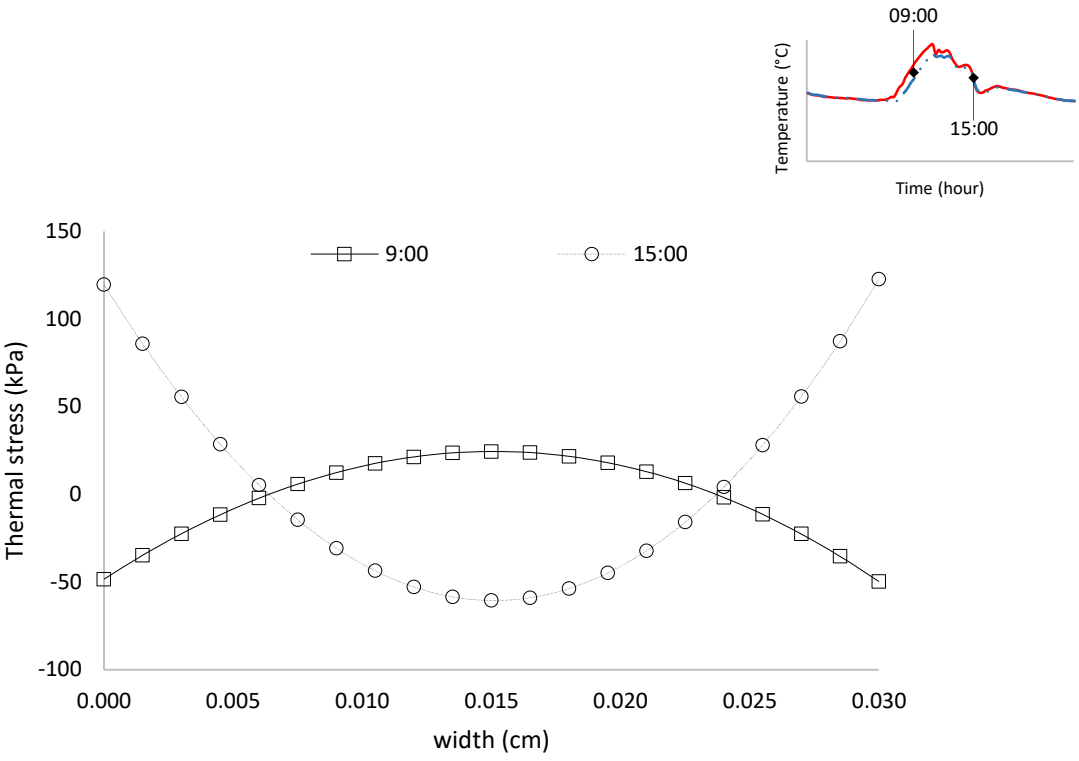

Figure 5.15 – Highest and lowest values of thermal stresses on August 10th

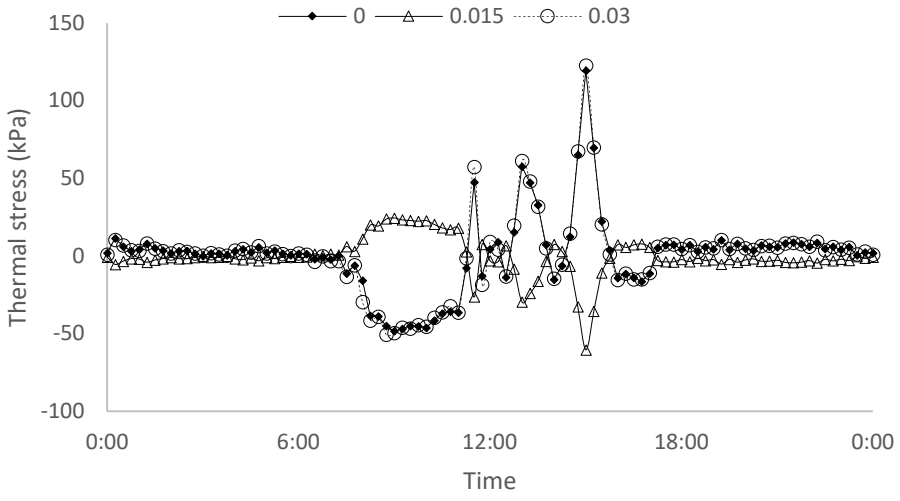

Figure 5.16 – Thermal stresses on August 10th in three different positions

The shape of the thermal distributions along the width is also related to the heat flux condition. As discussed in the previous subsection, the highest level of stress is achieved at the beginning of the transient heat flux. Due to the thickness of the material used in covering systems (3~5 cm) and the thermal resistance, the transient condition turns almost stationary after some minutes, and the stress distribution change from asymmetric to symmetric after one or two minutes. Since the rate of temperature changes and the gradient itself are small, the symmetric condition takes place almost the entire period.

At the inflection points, when the temperature is rising and it suddenly decreases, or vice-versa, the transient condition and the asymmetric distribution of thermal stresses are evidenced.

5.3.2.2 Sudden temperature decrease (hypothetical cases)

Two hypothetical cases in which the temperature sudden decreases were also evaluated. In this analyses the dimensionless time function was assumed:

$$T = \frac{\text{elapsed time} \times \text{thermal diffusion coefficient}}{\text{thickness}^2} \tag{5.9}$$

In the first simulation, presented in Figure 5.17, the temperature at the external surface suddenly decreased by 1°C while the temperature at the internal surface was kept constant. This analysis could represent the cold wind gust hitting the façade on a sunny day. The other simulation, in Figure 5.18, admit that the temperature at both sides (internal and external) suddenly decreases by 1°C.

The peaks of stress in both analyses are the same, but the internal stress distribution in the first case presents higher asymmetry and it would be the worst for the deformation of marble slabs in cyclic condition because the decohesion would be accentuated at the external side due to this higher asymmetry.

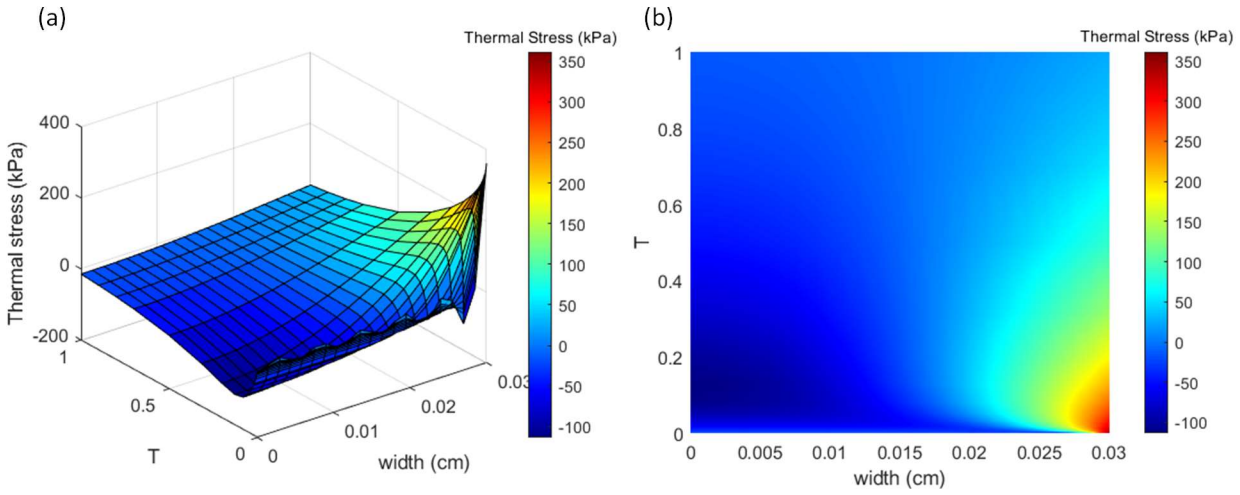

Figure 5.17 – Thermal stress along the width considering the variation of temperature at the external surface: (a) 3-D graphic (b) 2-D graphic

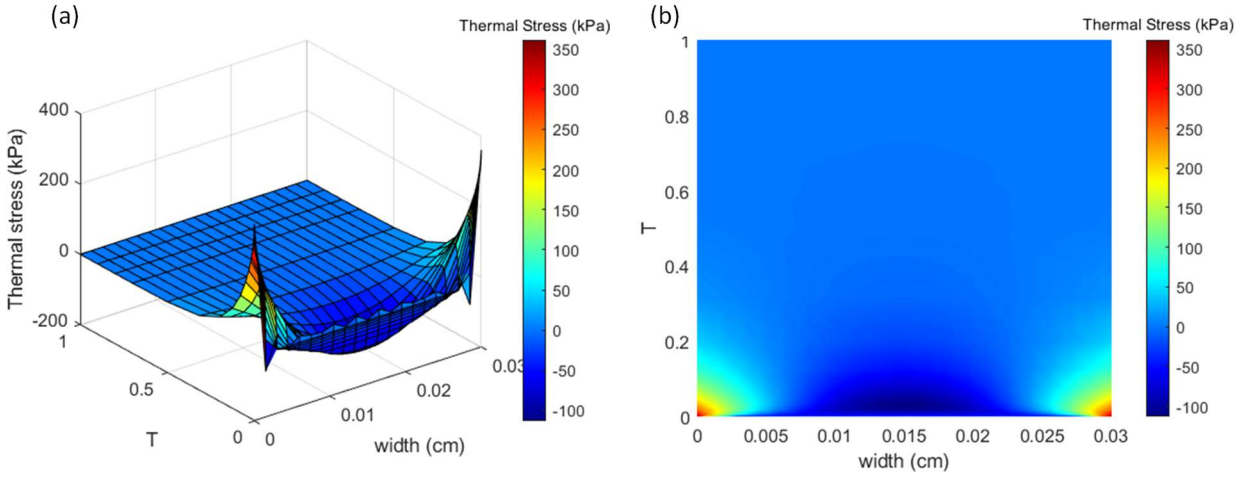

Figure 5.18 – Thermal stress along the width considering the variation of temperature at the external surface: (a) 3-D graphic (b) 2-D graphic

6 Final remarks

6.1 Summary

In this dissertation, the thermoelastic problem in external facades due to daily variation of temperature is approached aiming to improve the understanding of a specific pathology in natural stones known as bowing. A numerical approach considering the influence of nonlinear stress-strain measures and an exact solution was developed. Temperature measured on the ventilated façade at the Pescara Justice Court, in Central Italy, was used in these analyses, and comparison with results in literature was also addressed.

Firstly, it is presented the state of art about the problem of bowing in marble slabs, and comments about previous studies are presented. This pathology has affected numerous building covering systems worldwide, but most of them were located in the North hemisphere because of the elevated value of these building materials and their costs as covering systems. Previous studies identified some of the key mechanisms linked with bowing, such as the influence of:

1. Temperature;
2. Moisture;
3. Microstructure,
4. Anchorage system;
5. Geological stress release, and others.

Due to the thermal anisotropy of calcite grains, earlier studies have focused on the microstructural behavior of marble undergoing thermal loads (Royer-Carfagni, Ferrero, Weiss, and others). The great achievement of these publications has helped to clarify the results of laboratory tests. However, the macrostructural behavior and the determination of shear stresses were slightly approached and this lack of information was fulfilled by the analyses in this thesis.

The numerical formulation considered the nonlinear stress-strain measured, given by the second Piola-Kirchhoff stress and Green-Lagrange strain tensors, in a continuum media under thermal loading with fixed boundary conditions in finite element analysis. The consideration of continuum media provided the real deformed shape instead of the hypothetical configuration

assumed by the classic beam theory. Due to the magnitude of the loads, in which the highest thermal gradient was assumed as 4.7°C, no great differences between linear and nonlinear analysis were found; but, in a steady-state condition, the nonlinear model showed residual stresses while in the linear formulation these stresses completely vanished. Another outcome of the numerical analysis was the determination of shear stresses which were located at the boundaries if unidirectional heat flux through width is considered. Therefore, in macroscale, the shear stresses should not influence the intergranular decohesion if homogeneous material is considered. It would be resulting from the induced tensile stresses only.

An additional formulation was presented to evaluate the thermal stresses in ventilated facades given by an exact solution. The input data of temperature was the same used in numerical analysis, but the real oscillation of temperature in the slab was considered. Therefore, the real thermal stresses induced by that variation were calculated. The exact solution corroborated the results achieved by the numerical analysis, in which the higher influence of the variation of thermal gradient over the absolute value of the variation of temperature is verified. During the heating cycle, compressive thermal stresses were induced at the boundaries while tensile stresses were concentrated at the inner part of the slab. For the cooling cycle, tensile thermal stresses acted at the boundaries and compressive at the inner part. The physical meaning of the highest stress due to the rapid decrease in temperature can be understood by the non-gradual deformation from the external to the internal surface of the slab. Internal stresses are induced to counterpoise these unbalanced deformations to maintain the integrity of the body.

The stress distribution verified in the exact and numerical solutions helps the understanding of the experimental test accomplished by Bellopede et al (2020) in which the increase in porosity at the boundaries was greater than the one inside the slab.

6.2 Suggestions for future studies

The influence of the variation of thermal gradient was exhaustively evaluated in this dissertation for a homogenous continuum media and it has supported the understanding of some experimental tests which were slightly discussed by previous authors. However, the effect of combined action of thermal load and the environmental humidity needs further studies since the effect of thermal loading in dry specimens has proven that the intergranular decohesion occurs,

but it reaches a plateau after some cycles. On the other hand, in a wet environment, the decohesion increases continuously.

Future studies could verify the influence of additional forces induced by the compression of capillary water in the voids caused by intergranular decohesion due to thermal loads, in a similar way as the concept of pore pressure introduced by Terzaghi in soil mechanics. The water would penetrate inside the marble by the narrow channels, then, during the next heat and cooling cycles, the intergranular water would induce additional tensile stresses until the intergranular contact bonding failure. In this case, the orthotropy of calcite could also be considered.

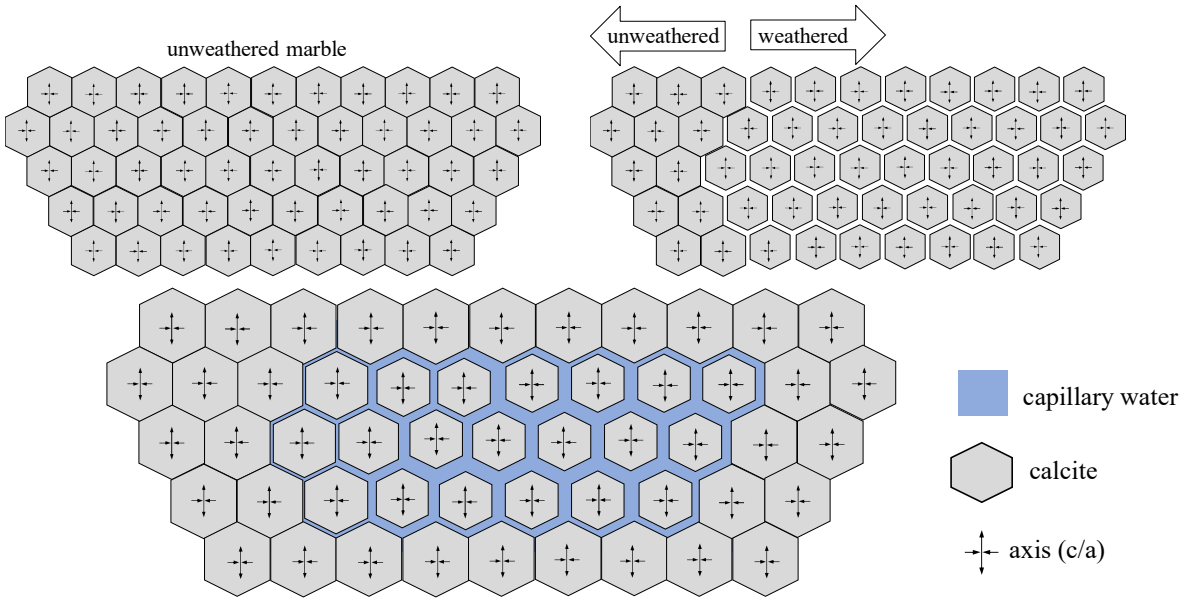

Figure 6.1 – Idealization of pore pressure induced by capillary water

Lastly, the influence of geological stress release due to exploitation of these natural stones could be evaluated considering the temperature and pressure in which the calcite grains of the marble were recrystallized after the metamorphism. Then, thermal stresses could be acting even without the influence of insolation (which would be an extra load).

References

AMERICAN SOCIETY FOR TESTING AND MATERIALS. **ASTM C1242:2019** Standard Guide for Selection, Design, and Installation of Dimension Stone Attachment Systems. Pennsylvania, 2019.

ALENKA, M.; TADEJA, M.; ANA, M. 3D visualization and quantification of bowing marble microstructure. **Construction and Building Materials**, v. 23, p. 2380-2385, 2009. DOI: 10.1016/j.conbuildmat.2008.10.009

ALFORD, J. S.; MASS, L.; RYAN, J. E.; SCHENECTADY, N.Y.; URBAN, F. O; BLOOMFIELD, N. J. Effect of heat storage and variation in outdoor temperature and solar intensity on heat transfer through walls. **Heating, Piping, and Air Conditioning**, v. 11, p. 369-396, 1939.

AKESSON, U.; LINDQVIST, J. E.; SCHOUENBORG, B.; GRELK, B. Relationship between microstructure and bowing properties of calcite marble claddings. **Bulletin of Engineering Geology and the Environment,** v. 65, p. 73-79, 2005. DOI: 10.1007/s10064-005-0026-x

ARFKEN, G. B.; WEBER, H. J.; HARRIS, F. E. **Mathematical methods for physicists: a comprehensive guide**. San Diego: Academic Press, 2012. 1220 p.

BELLOPEDE, R.; CASTELLETTO, E.; MARINI, P. Ten years of natural ageing of calcareous stones. **Engineering Geology.** v. 211, p. 19-26, 2016. DOI: 10.1016/j.enggeo.2016.06.015

BELLOPEDE, R.; CASTELLETTO, E.; SCHOUENBORG, B.; MARINI, P. Assessment of the European Standard for the determination of resistence of marbleto thermal and moisture cycles: recommendations for improvements. **Environ. Earth Sci.** v. 75, 946, 2016. DOI: 10.1007/s12665-016-5748-5

BELLOPEDE, R.; ZICHELLA, L.; MARINI, P. Marble durability assessment by means of total optical porosity and adjacent grain analysis. **Key Engineering Materials**. v. 848, p. 35-47, 2020. DOI: 10.4028/www.scientific.net/KEM.848.35

BENJELLOUN, Y.; SIGOYER, J.; DESSALES, H.; GARAMBOIS, S.; SAHIM, M. Construction history of the aqueduct of Nicaea (Iznik, NW Turkey) and its on-fault deformation viewed from archaeological and geophysical investigations. **Journal of Archaeological Science: Reports.** v. 21, p. 389-400, 2018. DOI: 10.1016/j.jasrep.2018.08.010

BERTAGNINI, A.; FRANZINI, M.; GRATZIU, C.; SPAMPINATO, M. Weathered marbles in nature and monuments (in Italian). **Italian Society of Mineralogy and Petrology.** v. 39, p. 39-46, 1984.

BONET, J.; WOOD, R. D. **Nonlinear continuum mechanics for finite element analysis**. 2nd Edition. New York: Cambridge Press, 2008. 318 p.

BRITISH STANDARD INSTITUTION. **BS 8298:2010** Code of practice for the design and installation of natural stone cladding and lining. London, 2010.

BRITISH STANDARD INSTITUTION. **BS 16306:2013** Natural stone test method - Determination of resistance of marble to thermal and moisture cycles. London, 2013.

CAMPOSINHOS, R. S.; CAMPOSINHOS, R. P. A. Dimension-stone cladding design with dowel anchorage. **Construction Materials.** v 162, p. 95-104, 2008. DOI: 10.1680/coma.2009.162.3.95

CAMPOSINHOS, R. S.; CAMPOSINHOS, R. P. A. Dimension stone design- kerf anchorage in limestone and marble. **Construction Materials.** v 165, p. 161-175, 2009. DOI: 10.1680/coma.8.00052

CARMIGNANI, L.; CONTI, P.; CORNAMUSINI, G.; MACCHERI, M. The internal Northern Apennines, the Northern Tyrrhenian sea and the Sardinia-Corsica block. **Italian Geological Society.** v 32, p. 59-77, 2004.

CARPINTERI, A.; PAGGI, M. Thermo-elastic mismatch in nonhomogeneous beams. **Journal of Engineering Mathematics**. v 61, p. 371-384, 2008. DOI: 10.1007/s10665-008-9212-8

CHEN, B.; YANG, Y.; ZHOU, J; ZHUANG, Y.; MCFARLAND, M. Damage detection of underwater foundation of a Chinese ancient stone arch bridge via sonar-based techniques. **Measurement.** v. 169, 108283, 2021. DOI: 10.1016/j.measurement.2020.108283

CHIU, Y. C.; CHEN, P. H.; LIAO, W. C. Impact of subtropical island climate on the appearance and aesthetics of white marble buildings. **Journal of Building Engineering**, v 31, 101334, 2020. DOI: 10.1016/j.jobe.2020.101334

DE BORST, R.; CRISFIELD, M.A.; REMMERS, J.J.C.; VERHOOSEL, C.V. **Nonlinear finite element analysis of solids and structures.** 2nd Edition. West Sussex: Wiley, 2012.

DENG, X.; NEWMAN JR, J. C. Implementation and application of a large-rotation finite element formulation in NASA code ZIP2DL. In: FAA-NASA SYMPOSIUM ON THE CONTINUED AIRWORTHINESS OF AIRCRAFT STRUCTURES, 1997, Georgia.

DILL, E. H. **Continuum mechanics**: Elasticity, Plasticity, Viscoelasticity. 1st Edition. New York: CRC Press, 2006. 368 p.

FERRERO, A. M.; MARINI, P. Experimental studies on the mechanical behavior of two thermal cracked marbles. **Rock Mechanics and Rock Engineering**. v 34, p. 57-66, 2001. DOI: 10.1007/s006030170026

FERRERO, A. M.; MIGLIAZZA, M.; SPAGNOLI, A. Theoretical modelling of bowing in cracked marble slabs under cyclic thermal loading. **Construction and Building Materials.** v 23, p. 2151-2159, 2009. DOI: 10.1016/j.conbuildmat.2008.12.015

FERRERO, A. M.; MIGLIAZZA, M.; SPAGNOLI, A. Micromechanics of intergranular cracking due to anisotropic thermal expansion in calcite marbles. **Engineering Fracture Mechanics.** v 130, p. 42-52, 2014. DOI: 10.1016/j.engfracmech.2014.01.004

GAMBINO, F.; BORGHI, A.; ATRI, A.; GALLO, L. M.; GHIRALDI, L.; GIARDINO, M.; MARTIRE, L.; PALOMBA, M.; PEROTTI, L.; MACADAM, J. Tourinstones: a free mobile application for promoting geological heritage in the city of Torino. **Geoheritage**, v 11, p. 3-17, 2019. DOI: 10.1007/s12371-017-0277-5

GARZONIO, C. A.; FRATINI, F.; MANGANELLI, C.; GIOVANNINI, P.; BLASI, C. Analyses of geomechanical decay phenomena on marbles employed in historical monuments in Tuscany. **Mechanics of jointed and faulted rock**, p. 259-263, 1995.

GERE, J. M.; GOODNO, B. J. **Mechanics of materials.** 8th Edition. Toronto: Cengage, 2012.

GHERARDI, F.; KAPRIDAKI, C.; ROVERI, M.; GULOTTA, D.; MARAVELAKI, P. N.; TONIOLO, L. The deterioration of Apuan white marble in contemporary architectural context. **Journal of Cultural Heritage**, v 35, p. 297-306, 2019. DOI: 10.1016/j.culher.2018.06.008

GREEN, A. E.; NAGHDI, P. M. A general theory of an elastic-plastic continuum. **Archive for Rational Mechanics and Analysis.** v. 18, p. 251-281, 1965. DOI: 10.1007/BF00251666

GRELK, B., CHRISTIANSEN, C., SCHOUENBORG, B., MALAGA, K. Durability of marble cladding - A comprehensive literature review. **Journal of ASTM International**, v 4, n 4, p. 1-19, 2007. DOI: 10.1520/JAI100857

GRELK, B.; GOLTERMANN, P.; SCHOUENBORG, B.; KOCH, A.; ALNAES, L. The laboratory testing of potential bowing and expansion of marble. **Dimension stones.** Taylor & Francis Group, London, p. 253-260, 2004.

HUDSON, J. A.; COSGROVE, J. W. **Understanding building stones and stone buildings.** 1st Edition. Leiden: CRC Press, 2019.

ITO, W. H.; FERRERO, A. M.; VAGNON, F., MIGLIAZZA, M. R.; DE QUEIROZ, P. I. B. Thermomechanical numerical analysis of bowing in marble slabs. In: 14th International Congress on Rock Mechanics and Rock Engineering, 2019. **Proceedings in Earth and Geosciences,** v 6, 2019, p. 2649-2656.

JOHNS, D. J. **Thermal stress analysis**. 1st Edition. London: Pergamon Press, 1965. 211 p.

KERAMIDAS, G. A.; TING, E. C. A finite element formulation for thermal stress analysis. Part I: variational formulation. **Nuclear Engineering and Design.** v 39, p. 267-275, 1976. DOI: 10.1016/0029-5493(76)90075-3

KLEIN, C.; PHILPOTTS, A. **Introduction to mineralogy and petrology.** 2nd ed. New York: Cambridge University Press, 2016.

KOCH, A.; SIEGESMUND, S. Bowing of marble panels: on-site damage analysis from the Oeconomicum Building at Gottingen (Germany). **Natural stone, Weathering Phenomena, Conservation Strategies and Case studies.** v. 205, 2002. DOI: 10.1144/GSL.SP.2002.205.01.22

KOCH, A.; SIEGESMUND, S. The combined effect of moisture and temperature on the anomalous expansion behaviour of marble. **Environmental Geology.** v. 46, p. 350-363, 2004. DOI: 10.1007/s00254-004-1037-9

KUEHN, T. H.; RAMSEY, J. W.;THRELKELD, J. L. **Thermal environmental engineering**. New Jersey: Prenticel Hall, 1998. 740 p.

LAURA, P. A. A.; GUTIERREZ, R. H.; SANCHEZ SARMIENTO, G.; BASOMBBRIO, F. G. Thermal stresses in rectangular plates: variational and finite element solutions. **Nuclear Engineering and Design.** v 47, p. 297-303, 1978. DOI: 10.1016/0029-5493(78)90073-0

LI, C.; WEI, J.; LI, C. Influence of foliage thickness on thermal performance of green façades in hot and humid climate. **Energy and Buildings.** v. 199, p. 72–87, 2019. DOI: 10.1016/j.enbuild.2019.06.045

LIVINGSTON, R. A. Acid rain attack on outdoor sculpture in perspective. **Atmospheric Environment.** v 146, p. 332-345, 2016. DOI: 10.1016/j.atmosenv.2016.08.029

MUSTONEN, J. Finlandia-Talon julkisivujen korjaus.Raken-nusinsinőőri-päivät. ***RIL K160-1993***, p. 61-68, 1993.

MACCHERI, M.; MOLLI, G.; CONTI, P. The Carrara marble: a geological and economical updated review. **Zeitschrift der Deutschen Gesellschaft für Geowissenschaften.** v. 158, p. 719-736, 2007. DOI: 10.1127/1860-1804/2007/0158-0719

MALAGA, K; SCHOUENBORG, B.; GRELK, B. Bowing and expansion of natural stone panels: marble and limestone testing and assessment. **Materiales de Construccion**, v. 58, p. 97-112, 2008. DOI: 10.3989/mc.2008.v58.i289-290.84

MARINI, P., BELLOPEDE, R. Bowing of marble slabs: Evolution and correlation with mechanical decay. **Construction and Building Materials.** v. 23, p. 2599–2605, 2009. DOI: 10.1016/j.conbuildmat.2009.02.010

MARMI-CARRARA. **Marmi di Carrara**. 2021. Available at: http://www.marmidicarrara.com/index.html. Acessed on: 05 Jan. 2021.

MURRU, A.; FREIRE-LISTA, D. M.; FORT, R.; VARAS-MURIEL, M. J.; MELONI, P. Evaluation of post-thermal shock effects in Carrara marble and Santa Caterina di Pittinuri limestone. **Construction and Building Materials**, v. 186, p. 1200-1211, 2018. DOI: 10.1016/j.conbuildmat.2018.08.034

MARA EC Project. **Developing long-term durability of marble façades**. 2001. Unpublished.

NABONI, E.; MILELLA, A.; VADALA, R.; FIORITO, F. On the localised climate change mitigation potential of building façades. **Energy and Buildings.** v. 224, 110284, 2020. DOI: 10.1016/j.enbuild.2020.110284

NETO, N.; BRITO, J. Validation of an inspection and diagnosis system for anormalies in natural stone cladding (NSC). **Construction and Building Materials**. v. 30, p. 224-236, 2012. DOI: 10.1016/j.conbuildmat.2011.12.032

ORTLOFF, C. The Pont du Garde aqueduct and castellum: Insight into Roman hydraulic engineering practice. **Journal of Archaeological Science: Reports.** v. 20, p. 808-817, 2018. DOI: 10.1016/j.jasrep.2018.05.021

PASCON, J. P.; CODA, H. B. Large deformation analysis of elastoplastic homogeneous materials via high order tetrahedral finite elements. **Finite Elements in Analysis and Design**, v. 76, p. 21-38, 2013. DOI: 10.1016/j.finel.2013.08.006

PRZEMIENIECKI, J. S. Thermal stresses in rectangular plates. **Aeronautical Quarterly**, v. 10, p. 65-78, 1959. DOI: 10.1017/S0001925900001438

REDDY, J. N. On locking-free shear deformable beam finite elements. **Computer methods in applied mechanics and engineering**, v. 149, p. 113-132, 1997. DOI: 10.1016/S0045-7825(97)00075-3

RODRÍGUEZ, P.; ARAB, P. B.; CELESTINO, T. B. Characterization of rock cracking patterns in diametral compression test by acoustic emission and petrographic analysis. **International Journal of Rock Mechanics and Mining Sciences**, v. 83, p. 73-85, 2016. DOI: 10.1016/j.ijrmms.2015.12.017

RODRÍGUEZ, P.; CELESTINO, T. B. Application of acoustic emission monitoring and signal analysis to the qualitative and quantitative characterization of the fracturing process in rocks. **Engineering Fracture Mechanics,** V. 210, p. 54-69, 2019. DOI: 10.1016/j.engfracmech.2018.06.027

ROLLI, Y.; ANGELINI, V. **Temperature survey of the ventilated stone cladding at the Pescara Justice Court** (in Italian). Pescara, 2007. 17 p. (Test Report R/073/0042)

RONG, G.; PENGA, J.; YAOA, M.; JIANGC, Q.; WONG, L. N. Y. Effects of specimen size and thermal-damage on physical and mechanical behavior of a fine-grained marble. **Engineering Geology,** v. 232, p. 46-55, 2018. DOI: 10.1016/j.enggeo.2017.11.011

ROYER-CARFAGNI, G. Some considerations on the warping of marble façades: the example of Alvar Aalto's Finland Hall in Helsinki. **Construction and Building Materials,** v. 13, p. 449-457, 1999. DOI: 10.1016/S0950-0618(99)00036-7

ROYER-CARFAGNI, G. On the thermal degradation of marble. **International Journal of Rock Mechanics and Mining Sciences,** v. 36, p. 119-126, 1999. DOI: 10.1016/S0148-9062(98)00169-7

SASSONI, E.; UGOLOTTI, G.; PAGANI, M. Nanolime, nanosilica or ammonium phosphate? Laboratory and field study on consolidation of a byzantine marble sarcophagus. **Construction and Building Materials**, v 262, 120784, 2020. DOI: 10.1016/j.conbuildmat.2020.120784

SCHOUENBORG, B.; GRELK, B.; MALAGA, K. Testing and assessment of marble and limestone (TEAM) – important results from a large European research project on cladding panels. **Journal of ASTM International,** v. 4, p. 1-14, 2007. DOI: 10.1520/JAI100855

SIEGESMUND, S; RUEDRICH, J.; KOCH, A. Marble bowing: comparative studies of three different public building façades. **Environmental Geology**, v. 56, p. 473-494, 2008. DOI: 10.1007/s00254-008-1307-z

STAZI, F.; ULPIANI, G.; PERGOLINI, M.; PERNA, C. The role of wall layers properties on the thermal performance of ventilated façades: Experimental investigation on narrow-cavity design. **Energy and Buildings.** v. 209, 109622, 2020. DOI: 10.1016/j.enbuild.2019.109622

TEAM EC Project. **Final report Testing and assessment of marble and limestone** (**GRD1-1999-10735**). Sweden: Swedish National Testing and Research Institute, 2005. Available at: http://buildingteam.extweb.sp.se/PDF/TEAM%20Final%20Report.pdf. Accessed in Oct/2018.

TIMOSHENKO, S. P.; GOODIER, J. N. **Theory of elasticity**. 3rd Edition. New York: McGraw Hill, 1970. 608 p.

VAGNON, F.; COLOMBERO, C.; COLOMBO, F.; COMINA, C.; FERRERO, A. M.; MANDRONE, G.; VINCIGUERRA, S. C. Effects of thermal treatment on physical and mechanical properties of Valdieri marble - NW Italy. **International Journal of Rock Mechanics and Mining Sciences,** v. 116, p. 75-86, 2019. DOI: 10.1016/j.ijrmms.2019.03.006

VETTORI, S.; CABASSI, J.; CANTISANI, E.; RIMINESI, C. Environmental impact assessment on the stone decay in the archaeological site of Hierapolis (Denizli, Turkey). **Science of The Total Environment**, v 650, p. 2962-2973, 2019. DOI: 10.1016/j.scitotenv.2018.10.038

WEISS, T.; SIEGESMUND, S.; FULLER JR, E. R. Thermal degradation of marble: indications from finite-element modelling. **Building and Environment,** v. 38, p. 1251-1260, 2003. DOI: 10.1016/S0360-1323(03)00082-9

WILCZEK, I. The layers of history: New architecture interventions in castle ruins. **Frontiers of Architectural Research.** *in press*, 2020. DOI: 10.1016/j.foar.2020.12.001

WINKLER, E. M. Properties of marble as building veneer. **International Journal of Rock Mechanics Mining Sciences and Geomechanics Abstracts,** v. 33, p. 215-218, 1996. DOI: 10.1016/0148-9062(95)00050-X

WEATHER AND CLIMATE. Available in: https://weather-and-climate.com. Accessed 13 Feb 2021.

Appendix A

A.1 Temperature measured on August 9 2007

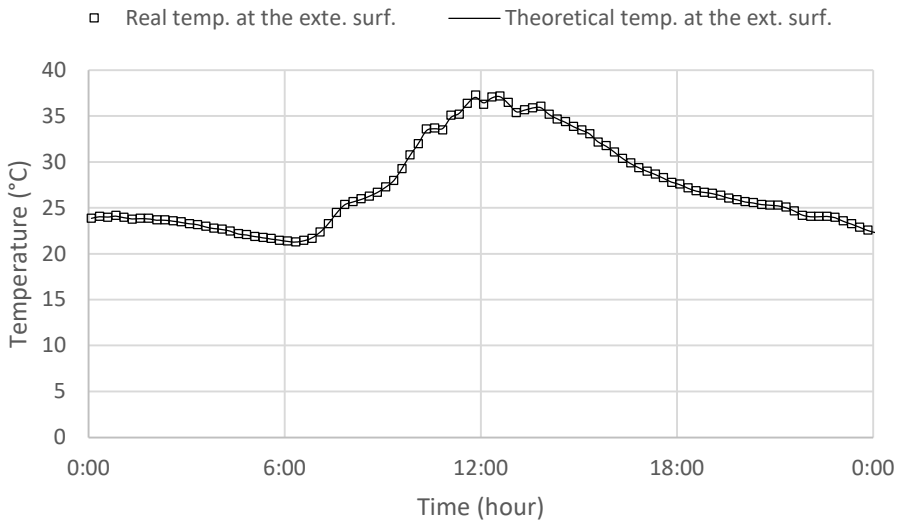

Figure A.1 – Comparison between real and theoretical temperature at the external surface

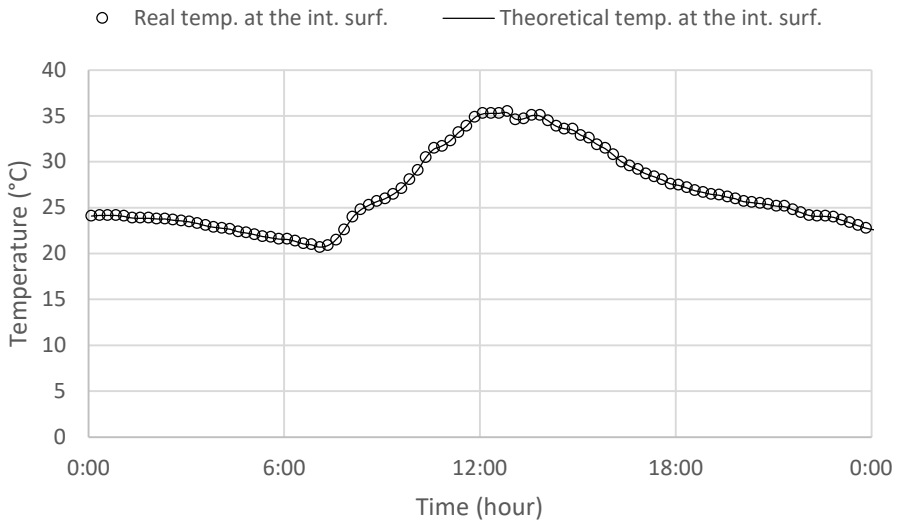

Figure A.2 - Comparison between real and theoretical temperature at the internal surface

Table A.1 – Coefficients M_i, N_i, O_i, and P_i for August 9 2007

i	External surface		Internal surface	
	$M_{i,ext}$	$N_{i,ext}$	$O_{i,int}$	$P_{i,int}$
1	-5.47777	-3.29035	-4.49117	-3.58231
2	2.67275	0.74534	2.35947	1.19938
3	-0.92329	0.10951	-0.98271	-0.11024
4	-0.07484	-0.10048	-0.06077	-0.10651
5	-0.13466	0.00192	0.01389	-0.01037
6	0.12713	-0.11998	0.06135	0.05155
7	-0.10061	0.16744	-0.2055	0.00228
8	-0.07869	-0.11404	0.11139	-0.10856
9	0.05967	-0.08347	0.02777	0.08205
10	-0.01112	0.13649	-0.11662	0.0109
11	-0.16398	-0.10185	0.00937	-0.10518
12	0.10254	-0.00449	0.04703	0.09599
13	-0.14408	0.05753	-0.16996	-0.01803
14	0.02549	0.02756	0.06149	0.00757
15	-0.03795	0.0105	-0.0475	0.01748
16	0.01871	0.02082	0.01017	0.03872
17	0.01052	0.01354	-0.01017	-0.01872
18	-0.03358	-0.0165	0.01223	0.01011
19	0.06926	0.01061	-0.00612	0.01079
20	-0.08188	-0.02004	-0.02462	-0.02551
21	0.05407	-0.01013	0.03967	0.02125
22	-0.05236	-0.03147	-0.03277	-0.04359
23	0.01389	0.02478	0.01217	0.01858

24	-0.02649	-0.02504	-0.00041	-0.02461
25	0.0207	0.02249	-0.0208	0.02046
26	0.00002	-0.02404	0.01169	-0.00696
27	-0.00648	0.01308	-0.01072	-0.00741
28	0.02148	-0.02012	0.0121	0.00929
29	-0.01408	0.0267	-0.01099	-0.00605
30	0.02073	-0.021	0.01911	0.00595
31	-0.01959	0.03027	-0.02835	-0.00781
32	-0.0046	-0.0189	0.01042	0.01196
33	0.00409	0.03587	-0.01255	0.0052
34	-0.01432	-0.04093	0.00875	-0.00529
35	0.00792	0.0466	-0.0127	0.00211
36	-0.018	-0.02816	0.00885	0.01195
37	0.01195	0.01847	-0.00684	-0.01073
38	-0.02354	-0.00518	-0.00585	-0.00862
39	0.01611	-0.00563	0.01211	-0.00043
40	-0.01361	0.00222	-0.01192	0.00169
41	0.01694	-0.00533	0.00423	0.00048
42	-0.01766	-0.00246	-0.00217	-0.00315
43	0.0068	-0.00906	-0.00247	0.00046
44	-0.00942	0.00445	-0.00067	0.00567
45	0.0071	-0.0029	0.00838	-0.0017
46	-0.0152	-0.00537	-0.00528	-0.0046
47	0.00524	0.00141	0.00618	0.00377
48	-0.00591	-0.01024	-0.00697	-0.01207

A.2 Temperature measured on August 10 2007

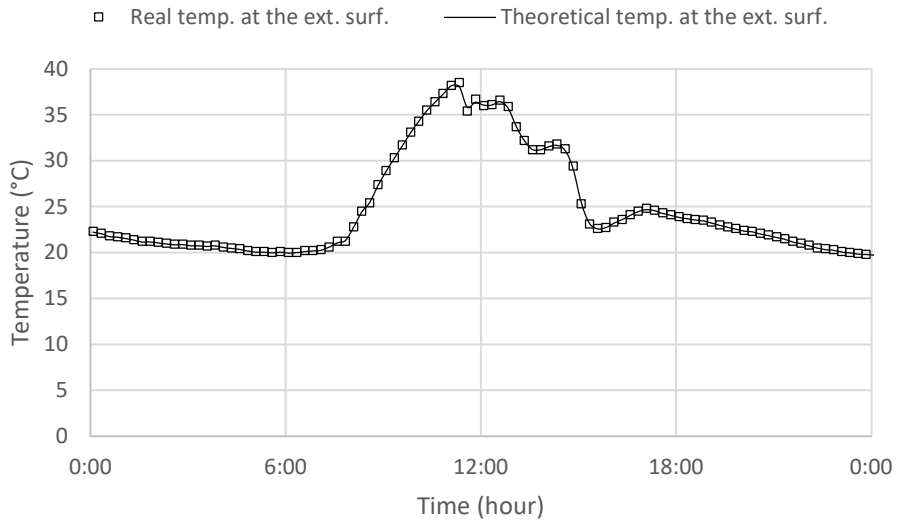

Figure A.3 – Comparison between real and theoretical temperature at the external surface

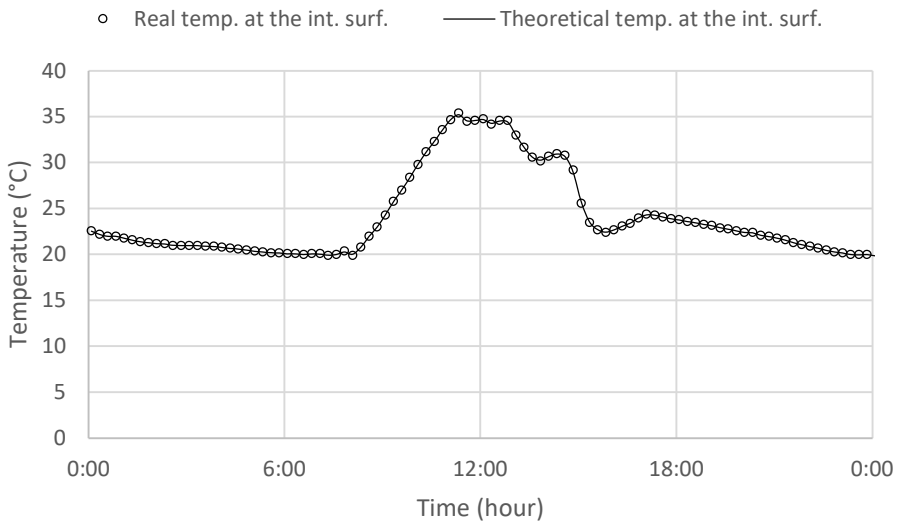

Figure A.4 - Comparison between real and theoretical temperature at the internal surface

Table A.2 - Coefficients M_i, N_i, O_i, and P_i for August 10 2007

i	External surface		Internal surface	
	$M_{i,ext}$	$N_{i,ext}$	$O_{i,int}$	$P_{i,int}$
1	-6.26823	-1.64552	-4.92359	-2.22415
2	3.73653	-0.86415	3.24056	0.00972
3	-2.06271	1.03852	-2.18377	0.26247
4	0.55802	-0.43617	0.89376	-0.1571
5	0.31646	-0.01535	0.07065	0.06145
6	-0.48788	0.03733	-0.37795	-0.14607
7	0.34936	0.19449	0.31923	0.31208
8	0.07216	-0.2781	0.09238	-0.24965
9	-0.26673	0.18395	-0.28286	0.09174
10	0.24506	0.06476	0.25379	0.10174
11	-0.0339	-0.29948	-0.02988	-0.2213
12	-0.15368	0.32797	-0.16034	0.19622
13	0.25287	-0.21524	0.24964	-0.11165
14	-0.24358	0.10147	-0.20754	0.02104
15	0.20231	0.01685	0.1552	0.04812
16	-0.13057	-0.07729	-0.06516	-0.10426
17	0.05037	0.05891	0.00808	0.08871
18	0.0144	0.01091	0.03704	-0.0519
19	-0.01276	-0.05918	-0.01696	-0.02822
20	-0.0029	0.0727	0.00341	0.04279
21	0.0439	-0.04723	0.03267	-0.04639
22	-0.03915	0.00931	-0.00984	0.00429
23	0.02454	0.0148	0.00597	0.01923

24	0.02883	-0.00773	0.02282	-0.02095
25	-0.04846	-0.00147	-0.00889	0.01271
26	0.07486	0.00614	0.03173	0.01111
27	-0.06218	0.01307	-0.04079	-0.02477
28	0.03587	0.0011	0.0562	0.01502
29	-0.02002	-0.0116	-0.02977	-0.00916
30	0.0114	0.01584	0.0074	-0.01048
31	-0.04446	0.00806	0.00997	0.01414
32	0.05694	-0.02685	0.0124	0.00074
33	-0.05312	0.05317	-0.0296	-0.0022
34	0.03562	-0.03254	0.04844	0.00717
35	-0.02746	0.01325	-0.03768	-0.00754
36	0.02527	-0.00149	0.01072	0.00669
37	-0.01777	0.00178	-0.00075	-0.008
38	0.02103	-0.01062	-0.00124	0.01465
39	-0.0134	0.03309	-0.00219	-0.00527
40	0.00453	-0.0411	0.00831	-0.00311
41	-0.00202	0.02919	-0.00869	0.00356
42	0.0027	-0.01694	0.00168	-0.00389
43	-0.00417	0.01182	-0.00372	0.0079
44	0.00148	-0.01408	0.00268	0.00783
45	0.00771	0.02544	0.00017	-0.00081
46	-0.01395	-0.0239	0.00065	-0.00304
47	0.01	0.02314	-0.0015	0.00974
48	-0.01414	-0.0245	-0.00697	-0.01207

A.3 Temperature measured on August 11 2007

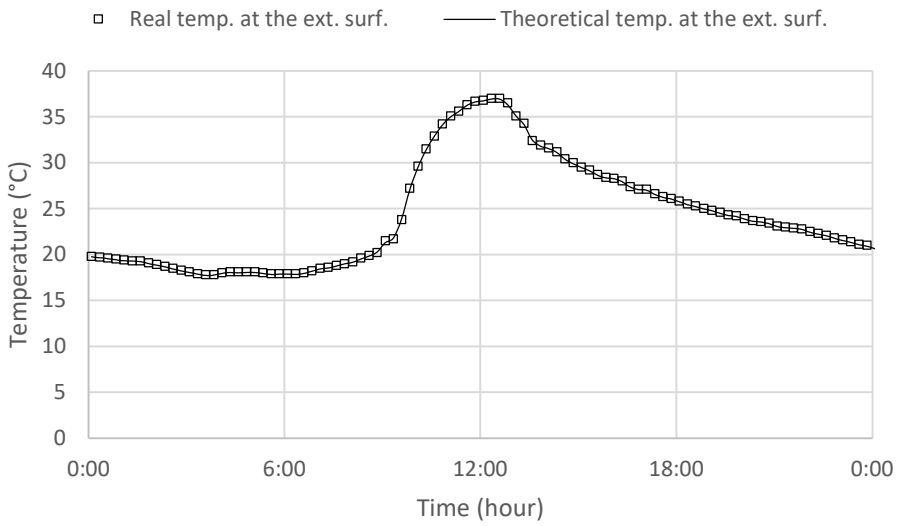

Figure A.5 – Comparison between real and theoretical temperature at the external surface

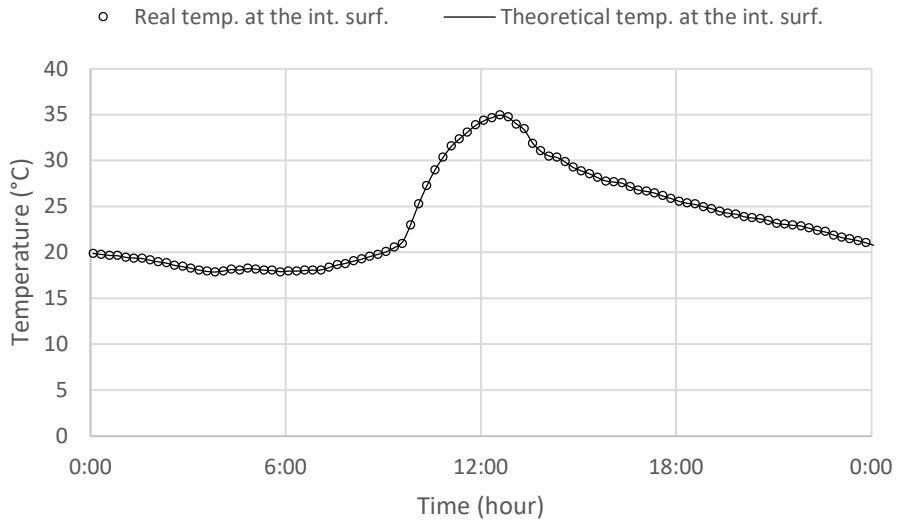

Figure A.6 - Comparison between real and theoretical temperature at the internal surface

Table A.3 - Coefficients M_i, N_i, O_i, and P_i for August 11 2007

i	External surface		Internal surface	
	$M_{i,ext}$	$N_{i,ext}$	$O_{i,int}$	$P_{i,int}$
1	-5.87944	-3.89997	-4.72519	-4.02693
2	3.30348	0.66641	2.61956	1.00477
3	-1.96157	0.09483	-1.62831	-0.35643
4	1.13349	-0.42488	1.02481	-0.00959
5	-0.56834	0.4497	-0.61972	0.13121
6	0.11239	-0.25543	0.2263	-0.08701
7	0.00496	0.15794	-0.12713	0.12599
8	-0.2146	0.00157	-0.11674	-0.08148
9	0.13895	-0.17628	0.13998	-0.04846
10	-0.0511	0.18445	-0.11408	0.09686
11	0.02647	-0.16496	0.10063	-0.11246
12	0.02054	0.13964	-0.06321	0.1236
13	-0.03136	-0.07871	0.01897	-0.07535
14	0.01409	0.00519	0.00603	0.00938
15	0.00598	0.02907	-0.00207	-0.00002
16	-0.0247	-0.07377	0.01543	-0.04516
17	0.04344	0.06564	-0.02961	0.04903
18	-0.04806	-0.02826	0.00312	-0.0365
19	0.02925	0.01641	0.00652	0.01946
20	-0.02437	0.0105	-0.02073	-0.00413
21	-0.00028	-0.01095	-0.00474	-0.0138
22	0.02701	0.00796	0.01926	0.01771
23	-0.03869	-0.02595	-0.00317	-0.03885

24	0.03755	0.01095	-0.01044	0.0164
25	-0.01781	0.00103	-0.00289	-0.01244
26	-0.02134	-0.02867	-0.00216	-0.0134
27	0.0211	0.03543	-0.01261	0.02325
28	-0.01664	-0.02417	0.00891	-0.02348
29	0.02838	0.00864	0.00929	0.01319
30	-0.01804	0.00681	-0.00464	-0.00622
31	0.01345	-0.00618	0.00548	0.00542
32	0.01145	-0.00811	0.00183	-0.00329
33	-0.02708	0.00961	-0.00511	0.00416
34	0.02591	-0.01082	0.01549	0.00513
35	-0.005	0.0157	-0.00371	0.0059
36	-0.00343	-0.01704	0.00913	-0.00244
37	0.00701	-0.00446	-0.02109	0.00275
38	-0.011	0.01035	0.00227	-0.01291
39	0.00031	-0.02164	0.00368	-0.00363
40	0.00174	0.01432	-0.00125	0.00461
41	-0.00464	-0.01258	-0.00214	-0.01171
42	0.00395	0.00316	-0.00844	0.00837
43	-0.00164	-0.00415	-0.00032	-0.00954
44	-0.00828	0.00117	-0.0026	0.00773
45	0.01598	-0.00067	0.00372	0.00308
46	-0.01286	-0.00409	-0.00753	-0.00366
47	0.00994	0.00009	0.00315	0.00474
48	-0.00317	-0.00548	-0.00401	-0.00695

A.4 Temperature measured on August 12 2007

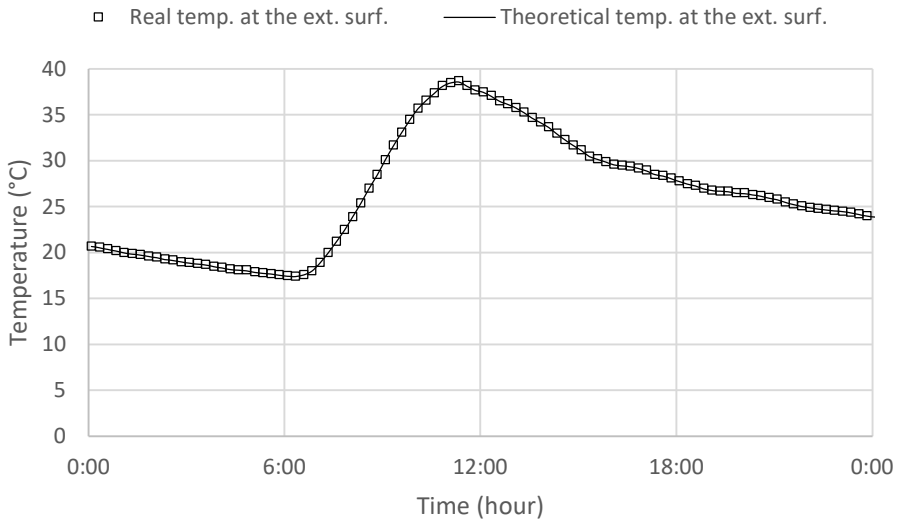

Figure A.7 – Comparison between real and theoretical temperature at the external surface

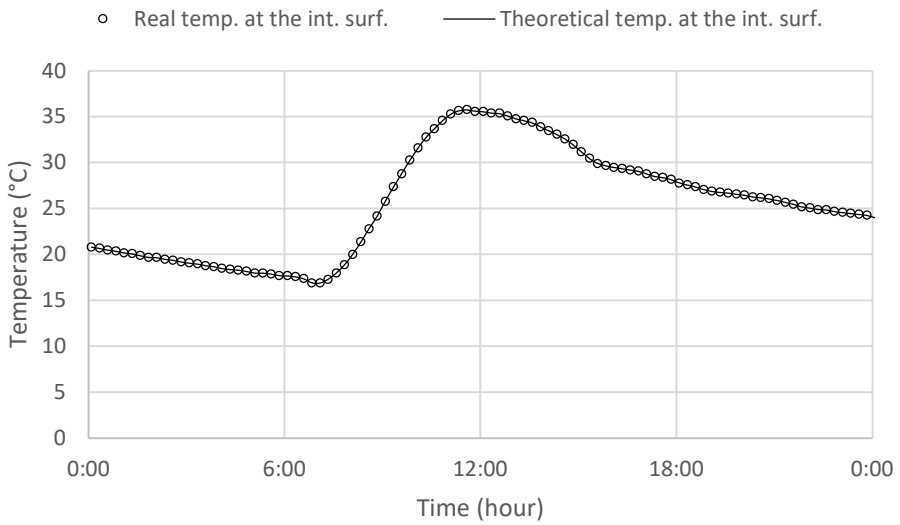

Figure A.8 - Comparison between real and theoretical temperature at the internal surface

Table A.4 - Coefficients M_i, N_i, O_i, and P_i for August 12 2007

i	External surface		Internal surface	
	$M_{i,ext}$	$N_{i,ext}$	$O_{i,int}$	$P_{i,int}$
1	-6.78157	-3.16293	-5.43087	-3.98705
2	3.7658	-0.78645	3.40752	0.31112
3	-1.21492	1.37071	-1.4968	0.71525
4	-0.04421	-0.73937	0.252	-0.66042
5	0.24629	0.10619	0.25675	0.24345
6	-0.07161	0.11183	-0.24406	0.06074
7	0.0702	0.03675	0.107	-0.03217
8	-0.04374	-0.15707	0.06251	-0.10954
9	0.05291	0.04182	-0.02238	0.09328
10	-0.02954	0.00539	-0.02348	-0.03555
11	-0.02404	-0.00503	0.0092	-0.04227
12	-0.00601	-0.01764	0.00212	0.03348
13	0.03922	0.01825	0.0053	0.00489
14	-0.03052	0.00391	-0.03818	-0.03222
15	0.0062	0.00167	0.02775	0.01997
16	-0.00239	0.01489	0.00277	0.00626
17	0.01223	0.00083	-0.00965	-0.00949
18	-0.0233	0.00437	0.00229	-0.00823
19	0.00367	-0.00964	0.01907	-0.01525
20	0.00588	0.01627	-0.01574	0.00875
21	-0.00855	-0.00121	0.00562	-0.0144
22	-0.00107	0.01274	-0.00141	0.00053
23	-0.00442	-0.00684	0.01566	0.00741

24	0.00416	0.0063	-0.01654	-0.00175
25	-0.01396	-0.01103	-0.00783	-0.01122
26	0.00359	0.0188	0.00656	0.00558
27	0.0005	-0.01063	-0.0025	0.00724
28	-0.00706	0.00103	-0.00745	-0.01268
29	0.00336	-0.0016	-0.0066	0.0042
30	-0.00171	0.00865	0.00744	-0.00143
31	0.00572	0.00142	0.00413	-0.00406
32	0.00032	0.00295	-0.00137	-0.00169
33	-0.00344	-0.01164	-0.00739	-0.00237
34	0.00379	0.01034	0.00449	0.00321
35	0.00097	-0.00832	0.00014	-0.00304
36	0.00097	0.00491	0.00409	0.0006
37	-0.00208	0.00601	0.00294	0.00197
38	0.00263	-0.00023	-0.00107	0.00287
39	-0.00522	-0.00597	-0.00077	-0.0063
40	0.00064	0.00472	-0.00193	0.00178
41	0.00002	0.00299	-0.00606	-0.00143
42	-0.00094	0.00009	-0.00455	-0.00322
43	-0.00112	-0.00126	-0.00676	-0.00645
44	0.00153	-0.00478	0.00511	0.00007
45	0.0018	0.0009	-0.00653	-0.00173
46	-0.00187	-0.00668	-0.00083	0.00291
47	-0.00183	0.00464	0.00048	-0.00034
48	0.00253	0.00439	0.00042	0.00073

Appendix B

B.1 List of publications

The main results achieved during my Ph.D. course were split by topics and submitted for publication (or are in preparation for submission) in specific journals and congress on this topic. If necessary, one can use the following references:

ITO, W.H.; FERRERO, A.M.; VAGNON, F.; MIGLIAZZA, M.R.; DE QUEIROZ, P.I.B. Thermomechanical numerical analysis of bowing in marble slabs. **14th International Congress on Rock Mechanics and Rock Engineering**, p. 2649-2657, 2019. EID: 2-s2.0-85063602937

ITO, W.H.; FERRERO, A.M.; DE QUEIROZ, P.I.B. Numerical analysis of bowing phenomenon due to thermal stresses in marble slabs. **Materials**, v. 13, 4367, 2020. DOI: 10.3390/ma13194367

ITO, W.H.; SCUSSIATO, T.; VAGNON, F.; FERRERO, A.M.; MIGLIAZZA, M.R.; RAMIS, J.; DE QUEIROZ, P.I.B. On the thermal stresses and natural weathering in ornamental stones. **Applied Sciences,** v. 11, 1188, 2021. DOI: 10.3390/app11031188

ITO, W.H.; SCUSSIATO, T.; UMILI, G.; VAGNON, F.; FERRERO, A.M.; MIGLIAZZA, M.R.; RAMIS, J.; DE QUEIROZ, P.I.B. Exact solution of thermal stresses due to natural weathering in ventilated facades. **International Journal of Engineering Science** (in prep.)